Statistical Tools and Methodologies for URLLC - A Tutorial

Onel L. A. López, *Member, IEEE*, Nurul H. Mahmood, *Member, IEEE*, Mohammad Shehab, *Member, IEEE*, Hirley Alves, *Member, IEEE*, Osmel M. Rosabal, *Student Member, IEEE*, Leatile Marata, *Member, IEEE*, and Matti Latva-aho, *Senior Member, IEEE*

Abstract—Ultra-reliable low-latency communication (URLLC) constitutes a key service class of the fifth generation and beyond cellular networks. Notably, designing and supporting URLLC poses a herculean task due to the fundamental need of identifying and accurately characterizing the underlying statistical models in which the system operates, e.g., interference statistics, channel conditions, and the behavior of protocols. In general, multi-layer end-to-end approaches considering all the potential delay and error sources and proper statistical tools and methodologies are inevitably required for providing strong reliability and latency guarantees. This paper contributes to the body of knowledge in the latter aspect by providing a tutorial on several statistical tools and methodologies that are useful for designing and analyzing URLLC systems. Specifically, we overview the frameworks related to i) reliability theory, ii) short packet communications, iii) inequalities, distribution bounds, tail approximations, and risk-assessment tools, iv) rare events simulation, v) large-scale tools such as stochastic geometry, clustering, compressed sensing, and mean-field games, vi) queuing theory and information freshness, and vii) machine learning. Throughout the paper, we briefly review the stateof-the-art works using the addressed tools and methodologies, and their link to URLLC systems. Moreover, we discuss novel application examples focused on physical and medium access control layers. Finally, key research challenges and directions are highlighted to elucidate how URLLC analysis/design research may evolve in the coming years.

Index Terms—age of information, clustering, compressed sensing, extreme value theory, finite blocklength, inequalities and distribution bounds, machine learning, meta distribution, queuing theory, rare event simulations, reliability theory, risk assessment, URLLC.

I. INTRODUCTION

LTRA-reliable low-latency communication (URLLC) aims to support wireless connectivity with wired-grade reliability and latency performance, and constitutes a key service class of the fifth generation (5G) and beyond cellular networks. The potential applications of URLLC, also referred to as critical machine-type communication (MTC), are indeed numerous and include smart grid, professional audio, intelligent transport systems, industrial and process

This research has been supported by the Academy of Finland, 6G Flagship program under Grant 346208, and the Finish Foundation for Technology Promotion.

Authors are with Centre for Wireless Communications (CWC), University of Oulu, FIN-90014 Oulu, Finland. (e-mail: {onel.alcarazlopez, nurul-huda.mahmood, mohammad.shehab, hirley.alves, osmel.martinezrosabal, leatile.marata, matti.latva-aho}@oulu.fi).

This work has been submitted to the IEEE for possible publication. Copyright may be transferred without notice, after which this version may no longer be accessible.

automation, augmented reality, entertainment industry, ehealth, Tactile Internet, as well as yet many unforeseen use cases [1]–[8].

In URLLC, reliability is often defined as the probability that a data unit is successfully transferred within a certain time period¹. Noteworthy, although reliability and latency are inherently tied by definition, the technological enablers of URLLC can be often classified as delay-reducing or reliability-promoting [12]. For instance, latency figures can be mainly improved by leveraging short codes and transmission time intervals [1], [5], [13], [14], edge caching/computing/slicing [2], [6], [12], [15], limitedoverhead protocols [2], [4], [16]-[18], and non-orthogonal multiple-access (NOMA) [2], [5], [19], [20]. Meanwhile, high reliability levels can be attained by exploiting diversity techniques as in multi-connectivity [4], [5], [21]-[24], data replication [17], [25], automatic repeat request protocols [5], [26], and multiple-input multiple-output (MIMO) systems [4], [5], [18], [27], as well as efficient network coding and relaying [12], [28]–[30] and space-time block codes [12], [13], [27]. A robust URLLC design may inevitably exploit several of the above technologies so that both latency and reliability metrics perform at the desired levels.

Remarkably, designing and supporting URLLC poses a herculean task due to the fundamental need of identifying and accurately characterizing the underlying statistical models in which the URLLC system operates, e.g., interference statistics, channel conditions, the behavior of protocols, etc [3], [4], as this is required for ultimately providing strong quality-of-service (QoS) guarantees. This inevitably requires multi-layer end-to-end approaches considering all the potential delay and error sources [4]–[8]², and proper statistical tools and methodologies [12], [14], [31]–[33]. This paper contributes to the body of knowledge in the latter aspect by providing a tutorial on several statistical tools and methodologies that are useful for designing and analyzing

¹The data unit (and also reliability/latency figures) in question can be application-dependent or pre-specified. A well-known example of the latter is the layer 2 protocol data unit of 32 bytes, as considered by the third generation partnership project (3GPP) [9], but one can find alternative proposals as well, e.g., [10]. See Section II-A for a more detailed definition of "reliability", especially within the context of reliability theory [11].

²Among sources of delay, we can mention link establishment, signal propagation, waiting times between transmissions, network queues, backhauling, random backoff times, inter/intra-layer processing and computing tasks, whereas relatively low signal-to-interference-plus-noise ratio (SINR), energy shortage, hardware component failure, and multi-user access collision classify as error sources.

TABLE I
REPRESENTATIVE SURVEY/OVERVIEW/TUTORIAL PAPERS RELATED TO TOOLS AND METHODOLOGIES FOR DESIGNING/ANALYZING URLLC WIRELESS SYSTEMS

Ref.	Main Contributions	Tools/Methodologies
[14]	Overview of FBL theoretical and protocolar principles	i) FBL Coding Theory, ii) Short Packet Protocols
[12]	Discussion about URLLC enablers and overview of techniques and methodologies for the design of URLLC systems	i) Risk Analysis/Optimization Tools, ii) EVT, iii) Effective Bandwidth, iv) SNC, v) Meta Distribution, vi) MF Game Theory
[31]	Revision of the security aspects of compressed sensing and applications to secure wireless communications	i) Compressed Sensing, ii) Security Tools
[32]	Discussion of requirements and challenges in URLLC vehicular networks, and overview of frameworks to enable them	i) FBL Coding Theory, $ii)$ Effective Bandwidth, $iii)$ SNC, $iv)$ Lyapunov Optimization, $v)$ Markov Decision Process
[33]	Review promising network architectures and DL frameworks for $6G\ URLLC$	i) DL Frameworks, ii) FBL Coding Theory, iii) Queuing Theory Tools, iv) Stochastic Geometry for Delay Analysis
this work	Comprehensive overview and exemplification of tools and methodologies for the analysis and design of URLLC systems	i) Reliability Theory, ii) Inequalities and Distribution Bounds, iii) EVT, iv) Risk-assessment Tools, v) Rare Events Simulation Tools, vi) FBL Coding Theory, vii) Short Packet Protocols, viii) Effective Capacity, ix) SNC, x) AoI, xi) Meta Distribution, xii) Clustering, xiii) Compressed Sensing, xiv) MF Game Theory, xv) ML

URLLC systems. We specifically focus on physical and medium access control layer perspectives.

A. State-of-the-Art Tutorials

There are already some survey, tutorial, and overview papers on tools and methodologies for designing and analyzing URLLC systems in the literature. Table I collects those that cover at least two tools/methodologies³, and summarizes their main contributions. Next, we discuss the scope and contributions of such works in more detail.

In 2016, Durisi *et al.* [14] overviewed the main theoretical principles for the design and performance analysis of short packet communications, which are a key component in URLLC. Specifically, they delved into the structure of a data packet, finite blocklength (FBL) error characterization, and proper communication protocols. They discussed three exemplary scenarios, i.e., *i*) the two-way channel, *ii*) the downlink broadcast channel, and *iii*) the uplink random access channel, and illustrated how the transmission of control information can be optimized for short packets. The main conveyed message was that it is crucial to consider all the communication resources that are invested in the transmission of metadata when data messages are short.

In 2018, Benis *et al.* [12] discussed definitions of latency and reliability, examined various enablers of URLLC and their inherent tradeoffs, and overviewed a wide variety of techniques and methodologies for URLLC. The latter included risk analysis and optimization tools, extreme value theory (EVT), effective bandwidth, stochastic network calculus (SNC), the meta distribution, and mean-field (MF) game theory. Moreover, via four selected use cases related to *i*) ultrareliable millimeter-wave communication, *ii*) virtual reality, *iii*) mobile edge computing, and *iv*) multiconnectivity for ultra dense networks, the authors showed how such tools provide a principled and clean-slate framework for

modeling and optimizing URLLC-centric problems at the network level. The authors agreed that URLLC mandates a departure from expected utility-based approaches relying on average quantities to taming risk and distribution tails.

In 2019, Zhang *et al.* [31] reviewed the state-of-the-art of compressed sensing -based secure wireless communications. For this, they first studied the security aspects of compressed sensing according to different types of random measurement matrices such as Gaussian matrix, circulant matrix, and other special random matrices. Meanwhile, applications such as the wireless wiretap channel, wireless sensor network, Internet of Things, crowdsensing, smart grid, and wireless body area networks were thoroughly discussed immediately after.

In 2020, Yang *et al.* [32] investigated the challenges and solutions for enabling URLLC for vehicular networks. Specifically, the underlying application scenarios exploiting vehicle-to-vehicle/infrastructure/network/pedestrian communications were overviewed, together with the corresponding URLLC requirements and potential challenges. Moreover, the authors highlighted some frameworks for optimizing latency and/or reliability and discussed a few case studies. The optimization frameworks in question were related to FBL coding theory at the physical layer, and effective bandwidth/capacity, SNC, Lyapunov optimization, and Markov decision process at the medium access control layer.

In 2021, She *et al.* [33] illustrated how to integrate domain knowledge (models, analytical tools, and optimization frameworks) of communications and networking into deep learning (DL) algorithms for URLLCs. For this, they first overviewed URLLCs together with promising architectures and DL frameworks for the sixth-generation (6G) wireless networks. Then, they revisited model-based analytical tools and cross-layer optimization frameworks, including FBL coding theory, queuing theory, and stochastic geometry for delay analysis, and hinted at how to improve learning algorithms with such knowledge. Finally, they validated the effectiveness of several learning algorithms via simulation

³Note that for a thorough understanding of a specific tool or methodology, the best approach might be to consult a book or a comprehensive tutorial paper on the matter.

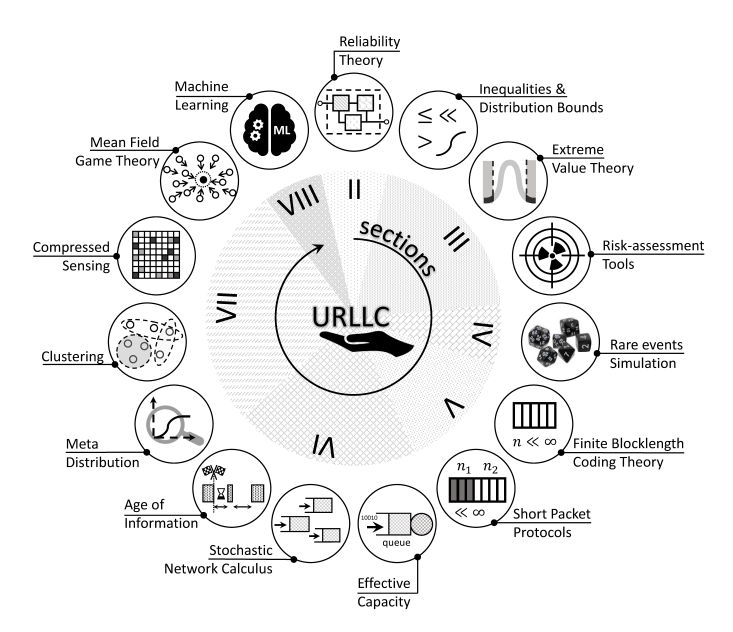


Fig. 1. Tools and methodologies are overviewed in this work for the design and analysis of URLLC systems. Here, they appear in the same order as addressed in the paper, and the corresponding section number is also indicated

and experimental results.

B. Our Approach and Contributions

It is worth noting that the state-of-the-art tutorials covering tools and methodologies for the analysis and design of URLLC systems have mostly focused on a few approaches only. In some cases, the main contributions are not even around them, e.g., [31], [32]. Therefore, our approach here is more exhaustive and fully focused on tools and methodologies that seem appealing for the analysis and design of URLLC systems.

Last row of Table I collects the 15 specific tools and methodologies that we cover in this tutorial. Observe that some of them have been already discussed in prior tutorials, e.g., FBL coding theory in [14], [32], [33], short packet protocols in [14], EVT in [12], risk-assessment tools in [12], meta distribution in [12], [33], compressed sensing in [31], effective capacity/bandwidth and SNC in [12], [32], machine learning (ML) in [33], and MF game theory in [12]. For these, we provide fresh and intuitive discussions, in many cases accompanied by novel examples to propitiate a better understanding of the approaches and their, not always evident, link to URLLC design/analysis. Meanwhile, some other tools and methodologies that we discuss here have not been covered in the state-of-the-art tutorials. That is the case of reliability theory, inequalities and distribution bounds, rare events simulation tools, clustering, age of information (AoI), and time series prediction tools. Therefore, our contributions in this regard are even stronger and more evident, and comprise an overview of the tool/methodology, its potential for URLLC design/analysis, and novel examples. In some cases, we also identify convenient links among the different approaches, i.e., by highlighting how a certain

TABLE II
ACRONYMS AND CORRESPONDING DEFINITIONS

#G 3GPP AMP AoI AWGN BLER bpcu CDF	#-th generation of cellular networks third generation partnership project approximate message-passing age of information additive white Gaussian noise block error rate bits per channel use cumulative density function channel state information
AMP AoI AWGN BLER bpcu	approximate message-passing age of information additive white Gaussian noise block error rate bits per channel use cumulative density function
AoI AWGN BLER bpcu	age of information additive white Gaussian noise block error rate bits per channel use cumulative density function
AWGN BLER bpcu	additive white Gaussian noise block error rate bits per channel use cumulative density function
BLER bpcu	block error rate bits per channel use cumulative density function
bpcu	bits per channel use cumulative density function
	cumulative density function
CDE	,
CDF	channel state information
CSI	Chamici state illiorillation
CVaR	conditional VaR
DL	deep learning
EVT	extreme value theory
FBL	finite blocklength
FL	federated learning
GPD	generalized Pareto distribution
LOS	line of sight
LSTM	long short-term memory
MBB	mobile broadband
MC	Monte Carlo
MDO	minimum duration outage
MDT	mean downtime
MF	mean-field
MGF	moment generating function
MIMO	multiple-input multiple-output
ML	machine learning
MTC	machine-type communication
MTTFF	mean time to first failure
MUT	mean uptime
NOMA	non-orthogonal multiple access
PDF	probability density function
QoS	quality-of-service
QPSK	quadrature phase shift keying
RBD	reliability block diagram
RL	reinforcement learning
RV	random variable
SINR	signal-to-interference-plus-noise ratio
SNC	stochastic network calculus
SNR	signal-to-noise ratio
SS	subset simulation
UAV	unmanned aerial vehicle
URLLC	ultra-reliable low-latency communication
VaR	value-at-risk

tool/methodology can be leveraged by another one to (often more efficiently) meet the desired goals. Additionally, throughout the paper, we briefly review the state-of-the-art works using the addressed tools/methodologies, especially when they link them to URLLC systems, and identify key challenges. Finally, key research directions are highlighted, which might hint at how URLLC analysis/design research may evolve in the coming years.

C. Organization

In the following, Sections II-VIII overview the specific tools and methodologies for the design and/or analysis of URLLC systems as illustrated in Fig. 1, while providing examples and fresh views. Section IX concludes the paper and discusses interesting challenges and research directions. The acronyms and main notations used throughout this article are listed in Table II and Table III, respectively.

TABLE III
NOTATIONS AND CORRESPONDING DESCRIPTIONS

Notatio	n Description
$f_X(x)$ f(x; y)	probability density function (PDF) of random variable (RV) X joint PDF of RVs X and Y
$F_X(x)$	cumulative density function (CDF) of RV X
$\bar{F}_X(x)$	complementary CDF of RV X
Pr[A]	probability of event A occurrence
A B	RV A conditioned on the realization of RV B
$\mathbb{E}_X[\;\cdot\;]$	expected value of the argument w.r.t RV X
$\mathbb{V}_X[\cdot]$	variance of the argument w.r.t RV X
(:)	binomial coefficient
$\Gamma(\cdot)$	complete gamma function
$\Gamma(\cdot,\cdot)$	upper incomplete gamma function
$li(\cdot)$	logarithmic integral function
Υ	Euler–Mascheroni constant (0.577215664901532···)
$Q(\cdot)$	Gaussian Q function
$I_{v}(\cdot)$	modified Bessel function of the first kind and order ν
$K_{v}(\cdot)$	modified Bessel function of the second kind and order v
$\mathscr{O}(\cdot)$	big-O notation
$\operatorname{sgn}(\cdot)$	sign/signum function
⊕	exclusive OR operator
~	distributed as
$\text{Exp}(\lambda)$	
$\mathbb{G}(\alpha,\beta)$	
≪, ≫	much less/greater than
T, H	transpose, Hermitian transpose operation
$\mathbb{C}^{N \times M}$	domain of $N \times M$ complex matrices
•	absolute value
$ \cdot _{\#}$	$\ell_{\#}$ -norm
$\inf \cdot$	infimum operation
$a \rightarrow b$	a approaches (converges to) b , or domain-image mapping
\mathbb{R}, \mathbb{R}^+	real, and non-negative real domain
[{·}	indicator function: 1 (0) if the input is true (false)

II. RELIABILITY THEORY

Reliability theory comprises a set of mathematical methods for analyzing the life cycles and failures of technical systems [11]. Systems, subsystems, and components, hereinafter referred to as "items", can be classified as repairable or non-repairable. In case of the latter, it does not matter what happens after the first failure occurs, i.e., the item might be discarded or even repaired, while all the operational and failed cycles matter in the case of repairable systems. Notice that a wireless communication system can be composed of several items, e.g., transmitters, receivers, and links/channels, all of which might constitute sources of failure. Next, we overview key aspects of the reliability theory framework and exemplify their potential application to URLLC analysis/design.

A. Key Dependability Quantities

Here, we overview key dependability quantities within the reliability theory framework⁴. Such quantities are expressed by probabilities and time durations. A common condition is that the considered item is operational at time t = 0. By convention, "up" and "down" respectively refer to operational and failure (i.e., in repair if repairable) states.

1) Availability: The instantaneous availability, or point availability, of an item is defined as [35]

$$A(t) = \Pr[\text{"item is up at time } t^{"}].$$
 (1)

Meanwhile, the steady-state availability is defined as

$$A = \lim_{t \to \infty} A(t),\tag{2}$$

and allows characterizing the long-term probability that an item is available. Observe that (2) converges to the fraction of the mission time in which the item remains in the "up" state.

2) Reliability: Reliability refers to the probability of a failure-free operation of the item during the interval [0, t], i.e.,

$$R(t) = \Pr[\text{"item is up throughout the interval } [0, t]\text{"}].$$
 (3)

Here, R(t) is also referred as survival function. Meanwhile, the amount of time elapsed before a failure occurs can be measured/characterized by the time to failure RV T, and notice that

$$R(t) = 1 - F_T(t), t \ge 0.$$
 (4)

Notice that *reliability* is usually the measure of interest for non-repairable systems because failures for such systems are permanent for the remainder of the mission, while *availability* is preferred for repairable systems. In general, $A(t) \geq R(t)$, while $\lim_{t \to \infty} R(t) = 0$ and $\lim_{t \to \infty} A(t) = A \geq 0$. In both cases, the equality holds only in the special case of no repairs.

- 3) Mean downtime/uptime: The mean downtime (MDT) and mean uptime (MUT) constitute the mean duration of a system failure and mean system operational time, respectively. Notice that A = MUT/(MUT + MDT).
- 4) Mean time to first failure (MTTFF): MTTFF characterizes the average duration of an item in "up" state before the failure occurs, thus, it can be written as [36], [37]

$$MTTFF = \int_0^\infty R(t) dt.$$
 (5)

Notice that this metric is equivalent to the mean time to failure and MUT, and also to the mean time between failures in memoryless settings. Nevertheless, the mean time to failure and mean time between failures are only conceptually applicable to non-repairable and repairable systems, respectively.

5) Failure Rate: The failure rate, also known as Hazard function, refers to the conditional probability that an item that operates failure-free until time t, i.e., R(t) = 1, also survives a sufficiently small additional period Δt . Mathematically, the failure rate is given by

$$\lambda(t) = \frac{R(t + \Delta t)}{R(t)} = \frac{f_T(t)}{R(t)}.$$
 (6)

Moreover, as shown in [38], the probability that the item fails within the (short) time interval Δt after being operational until time t is approximately $\lambda(t)\Delta t$.

Failure rates of the form Kt^m with m > -1 are more common in practical systems [36], [37] and correspond

⁴Notice that the term *dependability* is a broader concept that fits better here as it encompasses availability, reliability, maintainability, and in some cases, other characteristics such as durability, safety, and security [34].

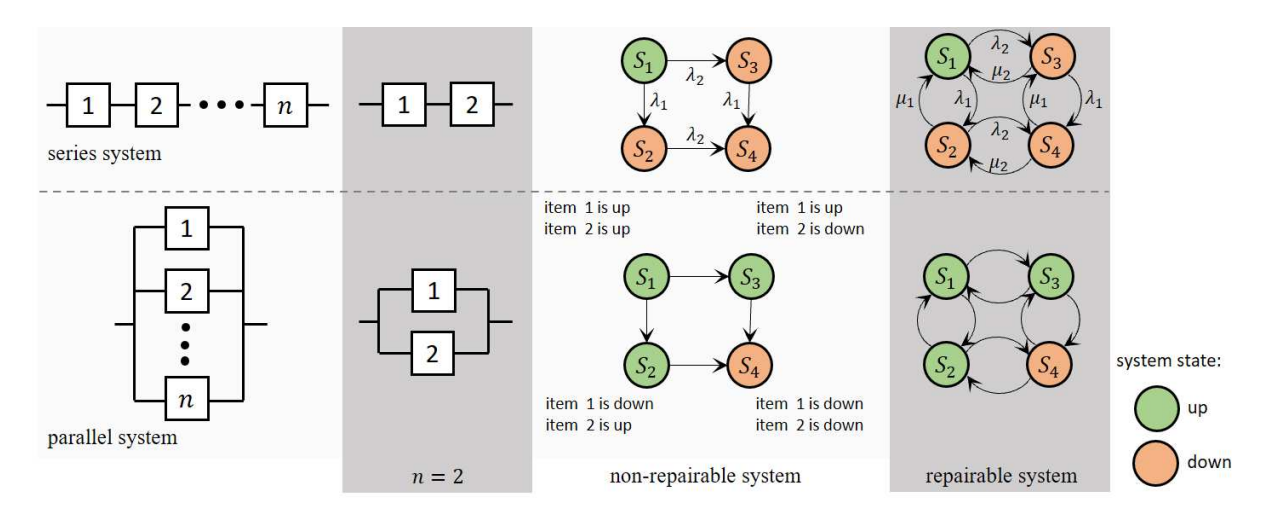


Fig. 2. RBD for the two special systems, and Markov modeling for non-repairable and repairable systems with two items. Here, λ_i and μ_i respectively denote the failure and repair rate of item $i \in \{1,2\}$.

to a Weibull-distributed time to failure. Interestingly, the exponential distribution (a Weibull distribution with m = 0) is the only continuous distribution with constant failure rate, i.e., $\lambda(t) = \lambda$, thus, memoryless. This implies that the distribution of the additional system lifetime does not depend on its age.

- 6) Maintainability: Maintainability refers to the ability of repairing a system within a given period of time. Notice that if the repair time follows an exponential distribution, it is possible to define the repair PDF and CDF based on a single parameter, the repair rate, μ .
- 7) Importance measures: Importance measures are not dependability quantities per se, but rather they evaluate absolutely or relatively the contribution of the elements (e.g., failures modes, items, or events) to a dependability quantity of interest. Some examples are the Birnbaum importance, criticality importance measure, risk achievement worth, risk reduction worth, Fussell-Vesely, and differential importance measure. Since their potential benefits for URLLC design/optimization/analysis are unclear (have not vet been explored) and they seem more relevant in systems design and industrial engineering applications, we do not delve into them here. The interested reader can refer to [34] for more details.

B. Structure Functions

Assume a system is composed of n items, and let the vector $\mathbf{x} = [x_1, x_2, \dots, x_n]^T$ indicate which of the items are functioning and which have failed. Mathematically,

$$x_i = \begin{cases} 1, & \text{if the } i - \text{th item is "up"} \\ 0, & \text{if the } i - \text{th item is "down"} \end{cases}$$
 (7)

The structure function of the system, denoted as $\phi(\mathbf{x})$, captures the operability of the whole system given a state vector x as

$$\phi(\mathbf{x}) = \begin{cases} 1, & \text{if the system is "up" given } \mathbf{x} \\ 0, & \text{if the system is "down" given } \mathbf{x} \end{cases}$$
 (8)

Meanwhile, the probability of the system being "up" or available can be written as $A = \Pr[\phi(\mathbf{x}) = 1] = \mathbb{E}_{\mathbf{x}}[\phi(\mathbf{x})].$ Notice that A is solely a function of $\mathbf{p} = [p_1, p_2, ..., p_n]^T$, where $p_i \triangleq \Pr[x_i = 1]$, when all the items' states are independent. In such case, $A(\mathbf{p})$ is an increasing function of \mathbf{p} , and $A(\mathbf{p}^{\alpha}) \ge A(\mathbf{p})^{\alpha}$ with $\alpha \in [0,1]$ [39, Ch. 9].

A system, as a composition of several items, can be assessed via a fault tree analysis or a reliability block diagram (RBD). The former is a graphical tool used mainly for system-level risk assessment and mitigation purposes, while the latter illustrates, in a simple manner, how component reliability contributes to the success or failure of a system. Both can be used to model and analyze similar types of logical configurations required for system reliability and related analyzes, although RBDs are usually more mathematically abstracted and can be handled more straightforwardly. Here, we focus only on RBDs, while the interested reader can refer to [40], [41] for further details on fault tree analysis.

The way in which the items are interconnected determines the redundancy level of the whole system. Mathematically, a k-out-of-n structure models a system that is functioning if and only if at least k of the n items are "up" [42], i.e.,

$$\phi_{k,n}(\mathbf{x}) = \begin{cases} 1, & \text{if } \mathbf{1}^T \mathbf{x} \ge k \\ 0, & \text{otherwise} \end{cases}$$
 (9)

There are two special systems: i) a parallel or full redundancy system, which corresponds to a 1-out-of-n structure, and ii) a series or non-redundancy system, which corresponds to an n-out-of-n structure. Their RBDs are illustrated in Fig. 2, while their structure functions are given by

$$\phi_{1,n}(\mathbf{x}) = \max\{x_1, x_2, \dots, x_n\} = 1 - \prod_{i=1}^{n} (1 - x_i),$$
 (10)

$$\phi_{1,n}(\mathbf{x}) = \max\{x_1, x_2, \dots, x_n\} = 1 - \prod_{i=1}^{n} (1 - x_i), \qquad (10)$$

$$\phi_{n,n}(\mathbf{x}) = \min\{x_1, x_2, \dots, x_n\} = \prod_{i=1}^{n} x_i. \qquad (11)$$

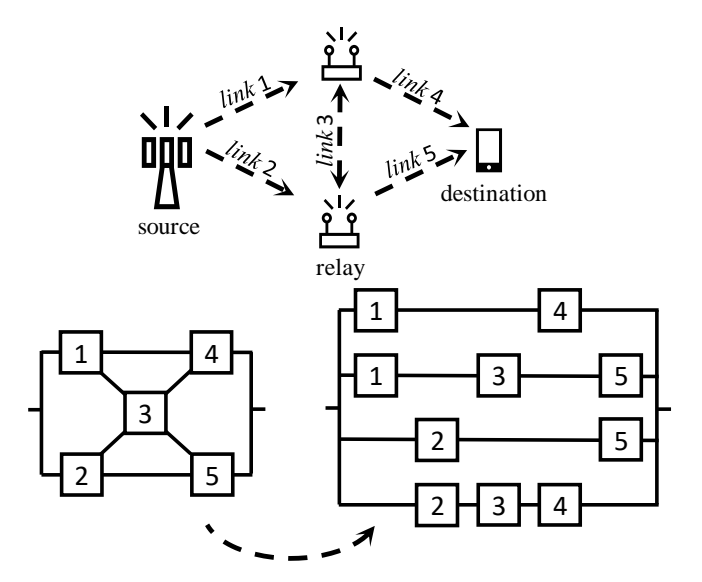


Fig. 3. a) Example of a wireless relaying scenario (top), and its b) structure representation (bottom-left) and c) series-parallel equivalent representation (bottom-right).

Moreover, $A_{1,n}(\mathbf{p}) = 1 - \prod_{i=1}^{n} (1-p_i)$ and $A_{n,n}(\mathbf{p}) = \prod_{i=1}^{n} p_i$ in case of independent items' states. Notice that any general structure (and corresponding structure function) can be scrutinized as a combination of series and parallel structures, thus, they may be seen as canonical structures.

EXAMPLE 1 (RBD ANALYSIS OF A RELAYING SYSTEM).

Consider that the wireless link between a source and a destination node is obstructed, thus, a potential direct communication between these nodes is discarded. Instead, the source sends a data packet to the destination via a wireless network composed of two relays as illustrated in Fig. 3a. There are five active wireless links in total, and each link $i \in \{1,2,3,4,5\}$ is in state x_i at a given time instant. Notice that the operation of a wireless link, thus the realizations of $\{x_i\}$ are commonly affected in practice by, e.g., the fading, shadowing, path-loss, and interference phenomena.

Based on Fig. 3a, one can straightforwardly draw the structure representation of the system, followed by its seriesparallel equivalent representation, as shown respectively in Fig. 3b and Fig. 3c. Based on the latter, one can write the structure function of such a hybrid system as shown in (12) (at the top of the next page), where the last step follows from simple algebraic transformations, including $x_i^2 = x_i$. Meanwhile, assuming independent items, the availability of the system can be expressed as

$$A_{hyb}(\mathbf{p}) = \mathbb{E}_{\mathbf{x}}[\phi_{hyb}(\mathbf{x})]$$

$$= p_1 p_2 + p_4 p_5 + p_1 p_3 p_5 + p_2 p_3 p_4 + p_2 p_4 p_5$$

$$- p_1 p_4 p_5 - p_1 p_2 p_3 p_5 - p_1 p_3 p_4 p_5 - p_1 p_2 p_4 p_5$$

$$- p_2 p_3 p_4 p_5 - p_1 p_2 p_3 p_4 + 2 p_1 p_2 p_3 p_4 p_5.$$
(13)

Notice that by exploiting the methodological approach discussed earlier in this section, one has rigorously and straightforwardly derived the structure and availability/reliability functions of the example scenario.

TABLE IV
ADVANTAGES AND DISADVANTAGES OF MARKOV MODELING

Advantages

- Repairs (individually or in groups) can be modeled in a natural way, including sequential and partial repairs
- Inherent ability to probabilistically model system failures
- Feasibility to model imperfect fault coverage, which arises when a dynamic reconfiguration process triggered by an item failure may lead to the system failure
- Feasibility to model standby spares (namely, items that replace those in "down" state) and dependencies on sequences of events

Disadvantages

- System modeling may require many states, making the whole modeling complex and often intractable
- Some models might be difficult to construct and validate
- The Markov assumptions/properties and the specific item failure distributions that are required may not be suitable for proper system modeling

C. Markov Models

RBDs and fault tree analysis are essentially static and Boolean (there are only two possible states: "up" and "down") tools. For more complex systems, one may resort to Markovian analysis, which is essentially dynamic and can include several component states, thus allowing to capture a variety of important aspects of the temporal and sequential dependence among events [43]. The interested reader can refer to [44] for a detailed analysis and mathematical characterization of Markov models.

To formulate a Markov model, the system behavior is abstracted into a set of mutually exclusive system states, and a set of equations, describing the probabilistic transitions among states and initial state probability distributions, is set. Moreover, the transition from one state to another depends only on the current state, thus, the way in which the entire past history affects the future of the process is completely summarized in the current state of the process. A Markov model can be defined over discrete (either finite or countable infinite) or continuous state spaces. The former case is commonly known as Markov chain, whereas the latter is defined as a continuous-space Markov model. Regarding the time granularity of the state transitions, Markov models are classified as continuous-time or discrete-time if they allow transitions at any time or at fix intervals, respectively. Next, we discuss and exemplify key principles and methodological aspects of Markov modeling within the reliability theory framework.

In Markov models for repairable systems, the repairs are represented by cycles depicting the loss and the restoration of the functionality of an item. Meanwhile, the Markov models for non-repairable systems are acyclic. As an example, the last two blocks in Fig. 2 illustrates the Markov models for the series and parallel repairable and non-repairable systems with two items.

Table IV summarizes the main advantages and disadvantages of Markov modeling within the reliability theory framework [45]. Notice that Markov modeling should not be used when: *i*) the system can be well-modeled with simpler combinatorial methods, e.g., RBDs and fault tree analysis,

$$\phi_{\text{hyb}}(\mathbf{x})$$

$$= \phi_{4,4} \Big(\Big[\phi_{1,2} \Big([x_1, x_4]^T \Big), \phi_{1,3} \Big([x_1, x_3, x_5]^T \Big), \phi_{1,2} \Big([x_2, x_5]^T \Big), \phi_{1,3} \Big([x_2, x_3, x_4]^T \Big) \Big]^T \Big)$$

$$= \min \Big\{ \max\{x_1, x_4\}, \max\{x_1, x_3, x_5\}, \max\{x_2, x_5\}, \max\{x_2, x_3, x_4\} \Big\}$$

$$= \min \Big\{ 1 - (1 - x_1)(1 - x_4), 1 - (1 - x_1)(1 - x_3)(1 - x_5), 1 - (1 - x_2)(1 - x_5), 1 - (1 - x_2)(1 - x_3)(1 - x_4) \Big\}$$

$$= \min \Big\{ x_1 + x_4 - x_1 x_4, x_1 + x_3 + x_5 - x_1 x_5 - x_3 x_5 - x_1 x_3 + x_1 x_3 x_5, x_2 + x_5 - x_2 x_5, x_2 + x_3 + x_4 - x_2 x_4 - x_3 x_4 - x_2 x_3 + x_2 x_3 x_4 \Big\}$$

$$= (x_1 + x_4 - x_1 x_4)(x_1 + x_3 + x_5 - x_1 x_5 - x_3 x_5 - x_1 x_3 + x_1 x_3 x_5)(x_2 + x_5 - x_2 x_5)(x_2 + x_3 + x_4 - x_2 x_4 - x_3 x_4 - x_2 x_3 + x_2 x_3 x_4 \Big)$$

$$= x_1 x_2 + x_4 x_5 + x_1 x_3 x_5 + x_2 x_3 x_4 + x_2 x_4 x_5 - x_1 x_4 x_5 - x_1 x_2 x_3 x_5 - x_1 x_3 x_4 x_5 - x_1 x_2 x_4 x_5 - x_1 x_2 x_3 x_4 + 2x_1 x_2 x_3 x_4 + 2x_1 x_2 x_3 x_4 \Big)$$

$$= x_1 x_2 + x_4 x_5 + x_1 x_3 x_5 + x_2 x_3 x_4 + x_2 x_4 x_5 - x_1 x_4 x_5 - x_1 x_2 x_3 x_5 - x_1 x_3 x_4 x_5 - x_1 x_2 x_4 x_5 - x_1 x_2 x_3 x_4 + 2x_1 x_2 x_3 x_4 + 2x_1 x_2 x_3 x_4 \Big\}$$

$$= (12)$$

ii) modeling the system requires a very large number of states⁵, *iii)* system behavior is too detailed or complex to be expressed in a Markov/semi-Markov model, or *iv)* a detailed performance estimate is required. In the case of the latter three, simulation tools are usually preferred.

EXAMPLE 2 (MARKOV-ENABLED RELIABILITY ANALYSIS).

Consider that a Rayleigh-faded receive signal can be successfully decoded if the instantaneous signal-to-noise ratio (SNR) at time t, $\gamma(t)$, is above a certain threshold, γ_{th} . Thus, there are two states, i.e.,

$$x(t) = \begin{cases} 0, & \text{if } \gamma(t) < \gamma_{th} \rightarrow \text{"down"} \\ 1, & \text{if } \gamma(t) \ge \gamma_{th} \rightarrow \text{"up"} \end{cases}$$
 (14)

According to the Gilbert-Elliot model [46], [47], one can interpret the wireless channel as a repairable item and model it as a continuous-time Markov chain of two states. The corresponding failure rate and repair rate are respectively given by [48]

$$\lambda = \sqrt{\frac{2\pi\gamma_{th}}{\bar{\gamma}}} f_D, \qquad \mu = \frac{\lambda}{\exp(\gamma_{th}/\bar{\gamma}) - 1},$$
 (15)

and are obtained based on a level crossing analysis [49]. In (15), $\bar{\gamma}$ is the average SNR over time, and f_D is the maximum Doppler frequency. Notice that the rates λ and μ are constants, which is consistent with the exponential distribution of $\gamma(t)$ since the channel is subject to Rayleigh fading.

Meanwhile, the steady state probabilities are given by

$$P_0 = \Pr[x(t) = 0] = \frac{\lambda}{\lambda + \mu}, \qquad P_1 = \Pr[x(t) = 1] = \frac{\mu}{\lambda + \mu}.$$
 (16)

They are obtained by solving $\{[P_0, P_1]\mathbf{M} = \mathbf{0}, P_1 + P_2 = 1\}$, where

$$\mathbf{M} = \begin{bmatrix} -\mu & \mu \\ \lambda & -\lambda \end{bmatrix} \tag{17}$$

⁵Observe that the state space grows exponentially with the number of items. Specifically, given n items and s states per item, the state space would be composed of s^n states. Considering a system with 10 items and 2 states per item, there are $2^{10} = 1024$ system states, while that number increases to $3^{10} = 59049$ if an additional state is considered for each item.

is the system transition matrix. With all this at hand, one obtains

$$A(t) = A = P_1 = \frac{\mu}{\lambda + \mu},$$
 (18a)

$$R(t) = \exp(-\lambda t), \tag{18b}$$

$$MTTFF = MUT = \frac{1}{\lambda}, \tag{18c}$$

$$MDT = \frac{1}{\mu}.$$
 (18d)

Notice that $1-A=\frac{\lambda}{\lambda+\mu}=1-\exp(-\gamma_{th}/\bar{\gamma})$, which, as expected, matches the so-called outage probability or packet loss rate in wireless communications.

Some comments are in order regarding the previous example:

- In URLLC systems with short packet transmissions, there is no such a threshold γ_{th} that fully guarantees a failure-free system operation. The reasons are discussed in Section V. Instead, an appealing approach that is leveraged in [23] relies on defining the system "up" state as the state in which the failure-free operation is guaranteed with a certain (potentially high) confidence level. By setting a target confidence level, the value of γ_{th} can be computed using (55) in Section V.
- There is no system redundancy. The interested reader can refer to [50], [51], where the authors assume there are *n* ≥ 1 links and the system is operational if at least one of the links is "up", i.e., redundancy via selection combining. In the case of [50], this leads to a birth-death continuous-time Markov chain, while the Markov chain is more evolved in [51] since the authors assume Rician fading and incorporate another cause of failure, interference. The analysis in [51] is facilitated by a hybrid series-parallel structure representation of the system (see Section II-B).
- One may wonder how the dependability metrics in (18d) are really relevant in a URLLC context. In the case of the steady-state availability, A, there is not much more to say as this quantity (or its complement, the outage probability 1 – A) has been the most commonly adopted for assessing the performance of URLLC systems in the literature. In the case of the instantaneous availability and the reliability quanti-

ties, the main attraction lies in their time-dependency feature, specially in systems with non-constant failure rate. Finally, although MTTFF, MUT and MDT are quantities comprising averaging over time, which is not per se appealing in a URLLC context [12], they provide an overarching view of the system in terms of average times in "up", "down" and transition states. Maybe more importantly, they can facilitate more rigorous reliability analysis as we illustrate in the following example.

EXAMPLE 3 (MINIMUM DURATION OUTAGE).

Consider the same system setup as in Example 2. Moreover, assume that such wireless system can tolerate error bursts of u symbols by implementing an appropriate channel coding mechanism. The symbol duration is denoted by T_s . Herein, we are interested in determining the SNR margin, defined as $F = \bar{\gamma}/\gamma_{th}$, such that the packet loss rate does not exceed the value of $\xi \ll 1$.

Obviously, uT_s must be greater than MDT, but by how much? The notion of minimum duration outage (MDO) introduced in [52] addresses this kind of problems. Specifically, a MDO occurs only when the signal level remains below a pre-specified threshold for a certain minimum duration. Mathematically, the probability of MDOs is given by

$$P_{\text{MDO}} = \Pr[\tau > uT_s | x(t) = 0] \Pr[x(t) = 0],$$
 (19)

where τ is a RV defined as the duration of a fade. Observe that this formulation neglects the possibility that a given packet experiences more than one deep fade event. Nevertheless, this would extremely rarely occur for $\xi \ll 1$, thus, we can safely adopt it. Then, one must configure F such that $P_{\text{MDO}} \leq \xi$.

Since $\Pr[x(t) = 0]$ can be easily computed as $1 - A = \lambda/(\lambda + \mu)$, the only inconvenience for evaluating (19) lies in finding the distribution of τ [53]. Herein, we adopt a much simpler approach that exploits the already available MDT quantity. Specifically, based on the simplest form of Markov's inequality (see first row of Table VI in Section III), one obtains

$$\Pr[\tau > uT_s | x(t) = 0] \le \frac{\mathbb{E}[\tau]}{uT_s} = \frac{\text{MDT}}{uT_s}.$$
 (20)

By substituting (20) into (19), while exploiting (18d), we have that

$$P_{\text{MDO}} \le \frac{\text{MDT}}{uT_s} (1 - A)$$

$$= \frac{\lambda}{uT_s \mu(\lambda + \mu)} = \sqrt{\frac{2F}{\pi}} \frac{\cosh(1/F) - 1}{uT_s f_D}.$$
 (21)

As expected, the upper bound of P_{MDO} is a decreasing function of F, and $\lim_{F\to\infty}P_{\text{MDO}}(F)=0$. This means that there is a unique solution F^* for the equation

$$\sqrt{\frac{2F}{\pi}} \frac{\cosh(1/F) - 1}{uT_s f_D} = \xi,\tag{22}$$

which, in fact, constitutes our solution for the original problem. Finally, we can obtain a closed-form solution

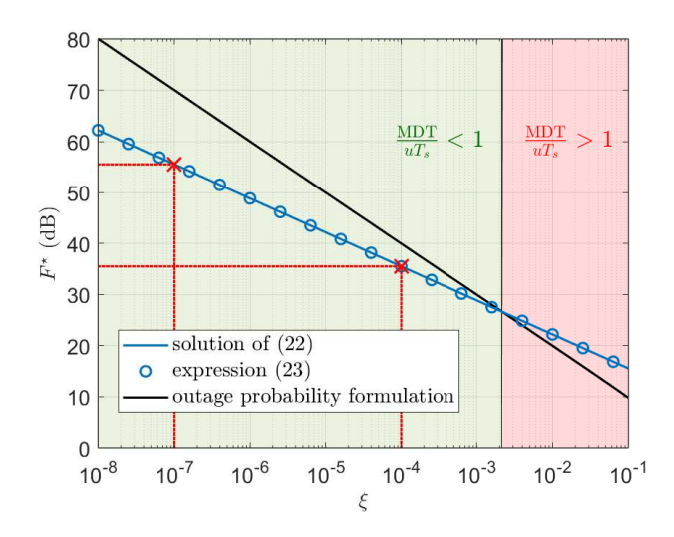


Fig. 4. The SNR margin, F^* , as a function of a target MDO probability constraint, ξ . We set $uT_s=0.2$ ms and $f_D=93.33$ Hz (corresponding to an operation frequency of 28 GHz and a relative velocity of 1 m/s between transmitter and receiver). A curve corresponding to the SNR margin required to only satisfy an outage probability constraint, ξ , is also illustrated as a benchmark.

for (22) for the high-SNR regime. Specifically, by using $\cosh(1/F) \approx 1 + 1/(2F^2)$, which comes from the Taylor series expansion, one obtains

$$F^* \approx \frac{1}{\sqrt[3]{2\pi\xi^2 u^2 T_s^2 f_D^2}}.$$
 (23)

Fig. 4 shows F^* as a function of ξ for a certain system configuration, while confirming the high accuracy of (23) driven by the relatively large values of F^* . Notice that the adopted upper-bound in (21) is only relevant when MDT/ (uT_s) < 1 since P_{MDO} < 1 – A must hold. Therefore, as shown in the figure, it can be only used when ξ < 2×10^{-3} . According to the figure, F = 35.5 dB and F = 55.5 dB can respectively guarantee a MDO probability below 10^{-4} and 10^{-7} . Meanwhile, in terms of outage probability, which is agnostic of the channel coding correcting errors potentialities, the required SNR margin values would be F = 40 dB and F = 70 dB, respectively.

III. TAMING DISTRIBUTION TAILS

URLLC is about limiting the occurrence of extreme and rare events. Thus, a proper URLLC design relies ultimately on taming the tail distribution of latency and/or reliability system performance. Next, we overview key bounds, approximations, and risk-assessment tools for taming distributions' tails .

A. Bounds & Limiting Forms

Assume X is a RV and $X \leq Y$, where Y = g(X) and $g(\cdot)$ is a real increasing function, hence, $F_X(x) \geq F_Y(g(x))$. Therefore, one may tractably bound the distribution of X by properly designing $g(\cdot)$. Alternatively, bounds to the

TABLE V Limiting forms of some popular functions

Function	$x \rightarrow 0$	$x \to \infty$
$\exp(x)$	1 + x	_
$\sin x$, $\sinh x$, $\tan x$,	X	_
ln(1+x), $tanh x$		
cos x	$1 - x^2/2$	_
$\cosh x$	_	$1 + x^2/2$
$\binom{2x}{x}$	_	$4^{x}/\sqrt{\pi x}$
$ \prod_{i=1}^{\binom{2x}{x}} (1+x_i) $	$(1 + \sum_{i=1}^{N} x_i / N)^N$	=
$\Gamma(x)$	1/x	$\sqrt{2\pi/x}(x/e)^x$
$\Gamma(a,x)$	$-x^a/a \ \forall a \in \mathbb{R}^+$	$x^{a-1}\exp(-x)$
li(1+x)	$\Upsilon + \ln x$	$\frac{1+x}{\ln(1+x)}$
Q(x)	$\frac{\frac{1}{2} - \frac{x}{\sqrt{2\pi}}}{\frac{x^{\nu} \Gamma(\nu+1)}{2^{\nu} \Gamma(\nu+1)}} \forall \nu \neq -1, -2, \cdots$	$\frac{1}{2\sqrt{2\pi}x}\exp(-x^2/2)$
$I_{v}(x)$	$\frac{x^{\nu}}{2^{\nu}\Gamma(\nu+1)} \forall \nu \neq -1, -2, \cdots$	$\exp(x)/\sqrt{2\pi x}, x \in \mathbb{R}^+$
$K_{\nu}(x)$	$-\ln x \text{ for } v = 0, \text{ and}$ $2^{\nu-1}x^{-\nu}\Gamma(-\nu) \ \forall \nu \in \mathbb{R}^+$	$\sqrt{\pi/(2x)} \exp(-x),$ $\forall x \in \mathbb{R}^+$

distribution of X, if known, can be directly established, e.g., by applying fundamental algebra.

In practice, bounding the entire distribution of X is not often necessary, but only one of its tails according to the specific URLLC problem at hand. Therefore, one may resort to limiting forms, which are often obtained by taking only the asymptotically-dominant terms of a series (e.g., Taylor, Laurent, and Puiseux) expansion or similar (e.g., Poincaré expansion and Padé approximant). Table V lists simple limiting forms of popular functions, which can be used to construct the limiting forms of more evolved functions.

Notice that

- if the distribution of *X* is known, the limiting forms may help to simplify it in the tail region (see Example 4 below); otherwise,
- if RV X is, or can be represented, as a transformation of other RV(s), one may leverage their limiting forms to bound/approximate the tail distribution of X. For instance, assume $X = \exp(Y - 1) + \cosh(1/Z) - 2$, where $Y, Z \ge 1$ are some arbitrary RVs, and one is interested in the left tail of the distribution of X, i.e., $F_X(x)$ as $x \to 0$. In this case, finding the whole distribution of X may be cumbersome even in the case that the distributions of Y and Z are simple. Instead one may realize that the small realizations of X are obtained when Y and Z approach 1 and ∞ , respectively, and consequently may leverage the limiting forms in the rows one and four of Table V. As a result, one obtains that the distribution of $Y + 1/(2Z^2) - 1$ converges to the distribution of X in the left tail. Notice obtaining the distribution of such expression seems much more analytically friendly than directly obtaining the distribution of X.

EXAMPLE 4 (RELIABLE INTERFERENCE NETWORKS [54], [55]). Consider a point-to-point wireless communication link subject to the interference of K neighboring nodes. Assume single-antenna nodes and that all channels are subject to Rayleigh fading. Then, the receive SINR can be written as

SINR =
$$\frac{\bar{\gamma}_0 h_0}{\sum_{k=1}^K \bar{\gamma}_k h_k + 1}$$
, (24)

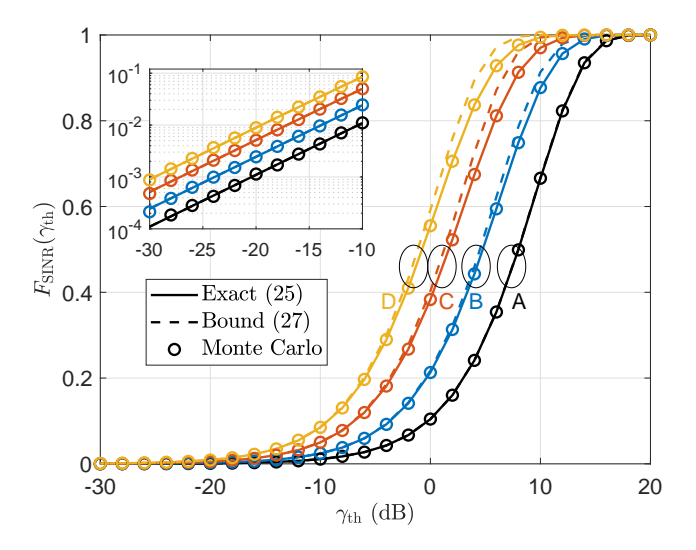


Fig. 5. CDF of the SINR for the system model of Example 4. We set $\bar{\gamma}_0 = 10$ dB, and consider four scenarios: A) $\bar{\gamma}_k = -10$ (dB) with K = 1; B) $\bar{\gamma}_k = -20 + 5k$ (dB) with K = 4; C) $\bar{\gamma}_k = -20 + 4k$ (dB) with K = 6; and D) $\bar{\gamma}_k = -21 + 3k$ (dB) with K = 9. Y-axis is illustrated in linear scale to be able of visualizing the divergence of the bound (27) with respect to the exact (25) and Monte Carlo's curves as the value of γ_{th} increases.

where $\tilde{\gamma}_0$ and $h_0 \sim \text{Exp}(1)$ denote the average SNR of the received signal from the intended transmitter and the experienced normalized channel power gain, respectively. Similarly, $\tilde{\gamma}_k$ and $h_k \sim \text{Exp}(1)$ denote the average SNR of the receive interfering signal from node k and the corresponding normalized channel power gain, respectively.

The CDF of the SINR, i.e., outage probability for a certain SINR threshold γ_{th} , can be computed as follows

$$F_{\text{SINR}}(\gamma_{\text{th}}) = 1 - \Pr[\text{SINR} > \gamma_{\text{th}}]$$

$$\stackrel{(a)}{=} 1 - \Pr\left[h_0 > \gamma_{\text{th}}\left(\sum_{k=1}^K \bar{\gamma}_k h_k + 1\right) / \bar{\gamma}_0\right]$$

$$\stackrel{(b)}{=} 1 - \mathbb{E}\left[\exp\left(-\gamma_{\text{th}}\left(\sum_{k=1}^K \bar{\gamma}_k h_k + 1\right) / \bar{\gamma}_0\right)\right]$$

$$\stackrel{(c)}{=} 1 - \exp(-\gamma_{\text{th}} / \bar{\gamma}_0) \prod_{k=1}^K \mathbb{E}\left[\exp(-\gamma_{\text{th}} h_k \bar{\gamma}_k / \bar{\gamma}_0)\right]$$

$$\stackrel{(d)}{=} 1 - \exp(-\gamma_{\text{th}} / \bar{\gamma}_0) \prod_{k=1}^K \frac{1}{1 + \frac{\bar{\gamma}_k}{\bar{\gamma}_0} \gamma_{\text{th}}},$$
(25)

where (a) comes from using (24), (b) from using the complementary CDF of h_0 , (c) from exploiting the property $\exp(\sum_i a_i) = \prod_i \exp(a_i)$, and (d) after taking the expectation over every h_k . Observe that although (25) is in closedform, it is of little, if any, relevance for designing practical resource allocation mechanisms. For instance, let us focus on a power control mechanism and try to shed some light to the following problem: what is the average SNR $\bar{\gamma}_0$ required for satisfying $F_{\text{SINR}}(\gamma_{\text{th}}) \leq \xi$, where $\xi \ll 1$? It is important to note that neither the specific values of the average SNR of the interfering signals $\{\bar{\gamma}_k\}$ nor the number of interferers are generally known in practice. Nevertheless, observe that $\gamma_{\text{th}}/\bar{\gamma}_0$ must be small to guarantee $\xi \ll 1$, thus, one may

TABLE VI COROLLARIES OF THEOREM 1

Corollary	Transformation of (28)	Resulting Bound
Simple form of Markov's inequality	g(t) = t	$\bar{F}_X(x) \le \frac{\mathbb{E}[X]}{x}$
Chebychev's bound	$g(t) = t \& X \leftarrow X - \mathbb{E}[X]$	$\bar{F}_{ X-\mathbb{E}[X] }(x) \le \frac{\sqrt{\mathbb{V}[X]}}{r^2}$
Chernoff's bound	$g(t) = e^{\theta t}, \ \theta \ge 0$	$\bar{F}_X(x) \le C_1(x)$
		$= \inf_{\theta \ge 0} e^{-\theta x} \mathbb{E}[e^{\theta X}]$
moment bound	$g(t) = t^{\theta}, \ \theta \ge 0$	$\bar{F}_X(x) \le C_2(x)$
		$= \inf_{\theta \ge 0} \frac{1}{x^{\theta}} \int_{0}^{\infty} t^{\theta} f_{X}(t) dt$

leverage the limiting forms in the sixth and first rows⁶ of Table V to state

$$\prod_{k=1}^{K} \left(1 + \frac{\bar{\gamma}_{k}}{\bar{\gamma}_{0}} \gamma_{\text{th}} \right) \underset{\gamma_{\text{th}}/\bar{\gamma}_{0} \to 0}{=} \left[1 + \frac{\gamma_{\text{th}}}{K\bar{\gamma}_{0}} \sum_{k=1}^{K} \bar{\gamma}_{k} \right]^{K}$$

$$= \left[1 + \frac{\gamma_{\text{th}}}{K\bar{\gamma}_{0}} \bar{\gamma} \right]^{K}$$

$$\stackrel{=}{=} \exp(\gamma_{\text{th}} \bar{\gamma}/\bar{\gamma}_{0}), \tag{26}$$

where $\bar{\gamma} = \sum_{k=1}^K \bar{\gamma}_k$. Substituting this into (26) and combining with (25) yields

$$F_{\text{SINR}}(\gamma_{\text{th}}) \underset{\gamma_{\text{th}}/\bar{\gamma}_{0} \to 0}{=} 1 - \exp\left(-\gamma_{\text{th}}/\bar{S}\,\overline{IN}\,R\right),\tag{27}$$

where $\overline{S} \, \overline{IN} \, R = \bar{\gamma}_0/(1+\bar{\gamma})$ is the average-signal-to-average-interference-plus-noise ratio. Note that the complexity can be further reduced, e.g., for diversity order analysis, by exploiting again the limiting form in the first row of Table V such that (27) converges to $\gamma_{\rm th}/\overline{S} \, \overline{IN} \, R$ as $\gamma_{\rm th}/\overline{S} \, \overline{IN} \, R \to 0$. Fig. 5 illustrates the incredible tightness of (27) with respect to left tail of (25). This evinces that the outage probability in the URC regime for the considered scenario depends merely on the $\overline{S} \, \overline{IN} \, R$, whose value may be acquired in practice. Back to the original power control problem, $F_{\rm SINR}(\gamma_{\rm th}) \leq \xi$ with $\xi \ll 1$ is satisfied for $\bar{\gamma}_0 \geq -(1+\bar{\gamma})\gamma_{\rm th}/\ln(1-\xi)$ or simply $\bar{\gamma}_0 \geq (1+\bar{\gamma})\gamma_{\rm th}/\xi$.

When some information on the statistics of X is known beforehand, one may exploit the following result.

THEOREM 1 (MARKOV'S INEQUALITY [56]). Let $X \in \mathbb{R}^+$ be a RV and $g : \mathbb{R}^+ \mapsto \mathbb{R}^+$ a non-decreasing function such that $\mathbb{E}[g(X)] < \infty$ exists, then

$$\bar{F}_X(x) \le \frac{\mathbb{E}[g(X)]}{g(x)}.$$
 (28)

Observe that (28) includes an infinite variety of bounds since there are infinite choices for g. The most popular bounds derived from (28) are illustrated in Table VI.

EXAMPLE 5 (CHANNEL HISTORY -BASED PRECODING [57]). Assume that a critical data message arriving to the data

⁶The limiting form in the sixth row comes from the inequality relation between the geometric and arithmetic mean. Indeed, both means are equivalent when the terms are equal, which is what asymptotically happens when the terms are $\{1+x_i\}$ and each x_i tends to zero. Finally, the limiting form in the first row is applied in the reverse direction for convenience.

queue of a multi-antenna node A demands an urgent URLLC transmission to a single-antenna node B. Because of the stringent latency constraints, the transmission needs to be carried out immediately in one shot, thus instantaneous channel state information (CSI) cannot be acquired at A. However, in the past, A had kept a record of L CSI entries of the communication channel with B, which it may now exploit for the current URLLC transmission. The set of CSI entries is given by $\mathcal{L} = \{\mathbf{h}_1, \mathbf{h}_2, ..., \mathbf{h}_L\}$, where $\mathbf{h}_l \in \mathbb{C}^{M \times 1}$ is the channel vector coefficient corresponding to the l-th CSI entry, and M is the number of transmit antennas.

Assume an interference-free scenario, and denote by $\mathbf{h} \in \mathbb{C}^{M \times 1}$ the unknown channel coefficient for the URLLC transmission. Then, the corresponding SNR is given by

$$SNR = \frac{|\mathbf{w}^H \mathbf{h}|^2}{N},$$
 (29)

where N is the receive noise power, and $\mathbf{w} \in \mathbb{C}^{M \times 1}$ is the transmit precoder. Here, we aim to attain the lowest-power precoder to guarantee a data reception's SNR of at least γ_{th} with probability $1-\xi$, where $\xi \ll 1$, thus $\min_{\mathbf{w}}\{||\mathbf{w}||^2: \Pr[\text{SNR} < \gamma_{th}) \leq \xi]\}$. Observe that for a sufficiently large record of CSI entries, i.e., $L \to \infty$, the distribution of \mathbf{h} (thus, the distribution of the SNR for a fixed \mathbf{w}) can be acquired, making the design of \mathbf{w} relatively easy to optimize. However, in a practical setup, the number of channel samples L may be rather limited due to limited training, memory and/or channel coherence time. Herein, we employ the simple form of Markov's inequality to state

$$\Pr[\text{SNR} < \gamma_{\text{th}}] = \Pr[\text{SNR}^{-1} > \gamma_{\text{th}}^{-1}] \le \frac{\mathbb{E}[|\mathbf{w}^H \mathbf{h}|^{-2}]}{(N\gamma_{\text{th}})^{-1}} \le \xi. \quad (30)$$

Now, the best estimator for $\mathbb{E}[|\mathbf{w}^H\mathbf{h}|^{-2}]$ is the sample mean $\frac{1}{L}\sum_{l=1}^L |\mathbf{w}^H\mathbf{h}_l|^{-2}$. Then, the problem translates to $\min_{\mathbf{w}} \left\{ ||\mathbf{w}||^2 : \frac{N\gamma_{\text{th}}}{L}\sum_{l=1}^L |\mathbf{w}^H\mathbf{h}_l|^{-2} \le \xi \right\}$, which is herein solved numerically to illustrate some performance results in the following.

Fig. 6 shows the truly attainable information outage as a function of the number of channel history samples for $\xi = 10^{-3}$ and quasi-static Rician fading channels with lineof-sight (LOS) factor of -10 dB. Observe that for a relatively small number of samples, i.e., L < 16, the outage constraint may not be met. This is because the sample mean converges to the population mean only as $L \to \infty$. Thus, substituting the sample mean into (30) does not fully guarantee that the bound still holds, but only for large L. The situation may worsen if tighter bounds such as Chernoff's or moment bounds are used. In such cases, one might need to limit the possible range of values for parameter θ (see Table VI) to prevent excessive skewness of the distribution of g(SNR) that may significantly slow down the convergence of the sample mean to the population mean. Alternatively, and/or in addition, one might leverage a probabilistic upper bound of the sample mean to ensure (30) is met with a certain confidence level. Such bound can be designed exploiting the central limit theorem, as in [57]. Meanwhile, Fig. 7 leverages 10⁴ Monte Carlo runs to illustrate the empirical distribution of the outage probability (Fig. 7a) and transmit

TABLE VII					
OTHER USEFUL DISTRIBUTION BOUNDS	S				

	Assumptions	Bound
Paley-Zygmund [58]	X is non-negative, $0 \le \theta \le 1$	$\bar{F}_X(x) \ge \frac{(1-\theta)^2 x^2}{\theta^2 \mathbb{E}[X^2]}$
Hoeffding [59]	$X_i \in [a_i, b_i], \ \forall i \ \text{are i.i.d. RVs}$	$\bar{F}_{\sum_{i=1}^{n} X_{i}}(x) \leq \exp\left(-\frac{2(x + \sum_{i=1}^{n} \mathbb{E}[X_{i}])^{2}}{\sum_{i=1}^{n} (b_{i} - a_{i})^{2}}\right)$
Vysochanskij–Petunin [60]	X is unimodal	$\bar{F}_{ X-\mathbb{E}[X] }(x) \le \frac{4\mathbb{V}[X]}{9x^2}, \ \forall x \ge \sqrt{8\mathbb{V}[X]/3}$
Cantelli [61]	X is real-valued	$\begin{split} \bar{F}_{ X - \mathbb{E}[X] }(x) &\leq \frac{4\mathbb{V}[X]}{9x^2}, \ \forall x \geq \sqrt{8\mathbb{V}[X]/3} \\ \bar{F}_X(x) &\leq \frac{\mathbb{V}[X]}{\mathbb{V}[X] + (x - \mathbb{E}[X])^2}, \ \forall x > \mathbb{E}[X] \end{split}$
(tightened) Gauss (Dharmad- hikari & Joag-Dev [62])	X is unimodal, $r > 0$, $s > r + 1and s(s - r - 1) = r^r$	$\bar{F}_{ X }(x) \le \max\left\{ \left(\frac{r}{(r+1)x}\right)^r \mathbb{E}[X ^r], \frac{s\mathbb{E}[X ^r]}{(s-1)x^r} - \frac{1}{s-1} \right\}$
Dvoretzky–Kiefer–Wolfowitz [63]	X is non-negative	$\bar{F}_{\sup_{y \in \mathbb{R}} F_X^{(n)}(y) - F_X(y) }(x) \leq 2e^{-2nx^2}, \ \bar{F}_{\sup_{y \in \mathbb{R}} \left(F_X^{(n)}(y) - F_X(y)\right)}(x) \leq e^{-2nx^2} \ \ \forall x \geq \sqrt{\frac{\ln 2}{2n}}$

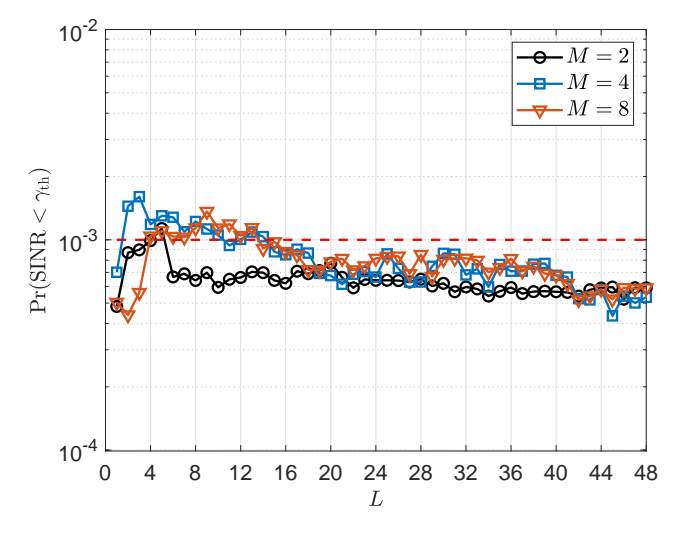


Fig. 6. Outage probability as a function of the number of history channel samples. Channel is subject to quasi-static Rician fading with LOS factor of -10 dB. We set $\gamma_{th}=1$, $\xi=10^{-3}$, and average channel path-loss over noise equal to 10 dB.

power (Fig. 7b) for L=32 and quasi-static Rician fading with different LOS factors. Results evince that the target outage probability $\xi=10^{-3}$ is met regardless of the channel features, although less tightly as LOS increases since channel becomes more deterministic. Moreover, the transmit power requirements tend to decrease as LOS increases.

Theorem 1 has been extensively utilized in the literature for the analysis and design of wireless communication systems, e.g., [15], [17], [30], [64]–[66], including URLLC. However, a fixed transformation function g is always assumed, thus intrinsically discarding an optimization over g for potentially tightening the bounds. For instance, let's say we have a function space of positive non-decreasing real functions \mathcal{G} , then (28) can be tightened as

$$\bar{F}_X(x) \le \inf_{g \in \mathcal{G}} \frac{\mathbb{E}[g(X)]}{g(x)}.$$
 (31)

In practice, the main challenge lies in having accurate estimates of $\mathbb{E}[g(X)]$ since these statistics converge at a different pace for different functions g given limited data samples.

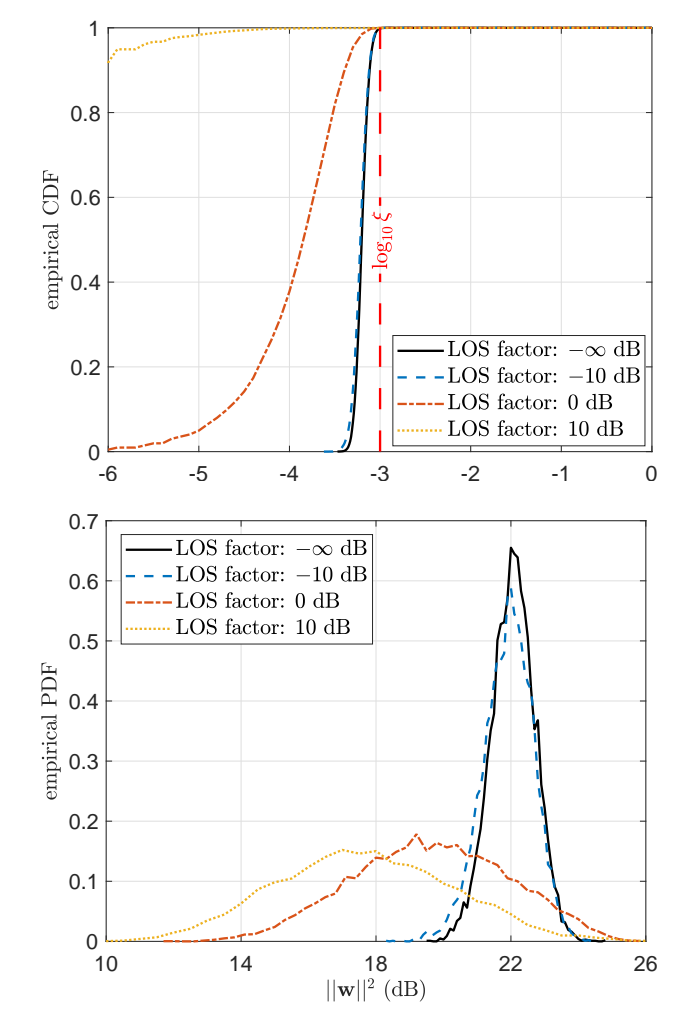


Fig. 7. Empirical distribution of the a) outage probability (left) and b) transmit power (right). Channel is subject to quasi-static Rician fading. We set M=4, L=32, $\gamma_{\rm th}=1$, $\xi=10^{-3}$, and average channel path-loss over noise to 10 dB. We consider 10^4 Monte Carlo realizations.

Finally, a selection of other less popular, but valuable, distribution bounds is compiled in Table VII.

B. Extreme Value Theory

Estimating the extreme values of an underlying process, which are scarce by definition, inevitably requires extrapolation from available observations. The EVT provides a class of models to enable such extrapolation [67]. The cornerstone of EVT revolves around the statistical characterization of the following RV

$$M_n = \max\{X_1, X_2, \cdots, X_n\} \text{ as } n \to \infty, \tag{32}$$

where X_1, X_2, \dots, X_n are independent RVs sharing a common, but unknown, CDF $F_X(x)$.

THEOREM 2 (Extreme Value Distribution [67, Th.3.1.1]). If there exists a sequence of constants $\{a_n > 0\}$ and $\{b_n\}$ such that

$$\Pr\left[(M_n - b_n) / a_n \le z \right] \to F_Z(z) \text{ as } n \to \infty$$
 (33)

for a non-degenerative distribution function $F_Z(z)$, then

$$F_Z(z) = \exp\left(-\left[1 + \kappa \left(\frac{z - \mu}{\sigma}\right)\right]^{-1/\kappa}\right),\tag{34}$$

defined on $\{z: 1+\kappa(z-\mu)/\sigma>0\}$, where $-\infty<\mu<\infty$ is the location parameter, $\sigma>0$ is the scale parameter, and $-\infty<\kappa<\infty$ is the shape parameter.

Theorem 2 states that if suitably normalized maxima of RVs converge in distribution, then the limit distribution must be an extreme value distribution as in (34) for some μ, σ and κ . The apparent difficulty that $\{a_n\}$ and $\{b_n\}$ are unknown in practice is easily resolved as follows. Assume that $\Pr\left[(M_n-b_n)/a_n \leq z\right] \approx F_Z(z)$ for large enough n. Then, $\Pr\left[M_n \leq z\right] \approx F_Z((z-b_n)/a_n) = F_Z^*(z)$, and note that $F_Z^*(z)$ also has the form (34) but with potentially different parameters μ and σ . Since the parameters of the distribution must be estimated anyway, it is irrelevant in practice that the parameters of the distribution $F_Z(z)$ are different from those of $F_Z^*(z)$. Theorem 2 can be easily transformed to characterize the asymptotic distribution of the minima of RVs [67, Th.3.3], and the asymptotic distribution of the k-th ordered statistics [67, Th.3.5].

A key EVT result describing the behaviour of large observations exceeding high thresholds is presented next.

Theorem 3 (Limiting distribution of excesses [67, Th.4.1]). For large enough u, the distribution function of X-u, conditioned on X>u, and where $X\in\{X_1,X_2,\cdots,X_n\}$ with $\Pr[\max_{i=1,\dots,n}X_i< z]\approx F_z(z)$ given in (34), follows approximately a generalized Pareto distribution (GPD) such as

$$F_{X-u|X>u}(y) \approx 1 - \left(1 + \frac{\kappa y}{\bar{\sigma}}\right)^{-1/\kappa},$$
 (35)

where $\bar{\sigma} = \sigma + \kappa(u - \mu)$. Such distribution is defined on $\{y : y > 0, (1 + \kappa y/\bar{\sigma}) > 0\}$.

Although Theorem 2 and Theorem 3 assume an underlying process consisting of a sequence of independent RVs, their claims are still usually valid when such an assumption does not hold, as in case of time-correlated data [67].

EXAMPLE 6 (CHANNEL HISTORY - BASED PRECODING (II)). Let's exploit the EVT framework to solve the problem described in Example 5, i.e.,

$$\min_{\mathbf{w}}\{||\mathbf{w}||_2^2, \Pr[SNR < \gamma_{th}] \le \xi\},\tag{36}$$

where $\xi \ll 1$. Here, the difficulty lies in addressing the URLLC constraint, thus, we proceed as follows

$$\begin{aligned} \Pr[\text{SNR} < \gamma_{\text{th}}] &= \Pr\left[N|\mathbf{w}^{H}\mathbf{h}|^{-2} > 1/\gamma_{\text{th}}\right] \overset{(a)}{=} \Pr\left[\Theta > f(1/\gamma_{\text{th}})\right] \\ &\overset{(b)}{=} \Pr\left[\Theta - u > f(1/\gamma_{\text{th}}) - u \mid \Theta > u\right] \Pr[\Theta > u] \\ &\overset{(c)}{\approx} \frac{1}{L} \left(1 - F_{\Theta - u|\Theta > u} \left(f(1/\gamma_{\text{th}}) - u\right)\right) \sum_{l=1}^{L} \mathbb{I}\{\Theta_{l} > u\} \\ &\overset{(d)}{\approx} \frac{1}{L} \left(1 + \frac{\kappa(\mathbf{w}, \mathcal{L})}{\bar{\sigma}(\mathbf{w}, \mathcal{L})} \left(f\left(\frac{1}{\gamma_{\text{th}}}\right) - u(\mathbf{w}, \mathcal{L})\right)\right)^{-\frac{1}{\kappa(\mathbf{w}, \mathcal{L})}} \\ &\times \sum_{l=1}^{L} \mathbb{I}\{\Theta_{l} > u(\mathbf{w}, \mathcal{L})\}, \quad (37) \end{aligned}$$

where (a) comes from introducing an increasing function f and defining $\Theta \triangleq f(N|\mathbf{w}^H\mathbf{h}|^{-2})$. Note that by adopting a concave f one can mitigate the impact of potentially disperse samples $\Theta_l \triangleq f(N|\mathbf{w}^H\mathbf{h}_l|^{-2})$ as a more compact sample set $\{f(\Theta_I)\}\$ is obtained, thus, facilitating a better GPD fitting in the next steps. Thereafter, (b) comes from exploiting the conditional probability framework, specifically, the probability conditioned on exceeding a threshold u, which is introduced here and designed to be relatively large but smaller than $1/\gamma_{th}$. Meanwhile, the empirical distribution of Θ (obtained from Θ_l) is used in (c) to estimate $Pr[\Theta > u]$. Note that for this estimation to be somewhat accurate it is required that $u < \max_{l} \Theta_{l}$. Finally, Theorem 3 result is leveraged to obtain (d), and therein we have highlighted the dependency of κ , $\bar{\sigma}$ and μ on the adopted beamformer **w** and channel sample set \mathcal{L} .

Then, the following procedure can be followed to determine if a certain beamformer **w** satisfies the URLLC constraint:

- 1) Set $u(\mathbf{w}, \mathcal{L})$ as the quantile of $\{\Theta_l\}$ for the cumulative probability $\rho \in (0.5, 1)$. This leads to $\frac{1}{L} \sum_{l=1}^{L} \mathbb{I} \{\Theta_l > u(\mathbf{w}, \mathcal{L})\} = \rho$
- 2) Fit the GPD (35) to the samples $\{\Theta \mid \Theta > u\}$ and obtain $a \ 100 \times \alpha\%$ confidence intervals $[\kappa_{lb}, \kappa_{ub}], \ [\bar{\sigma}_{lb}, \bar{\sigma}_{ub}]$ respectively for $\kappa(\mathbf{w}, \mathcal{L}), \ \bar{\sigma}(\mathbf{w}, \mathcal{L})$
- 3) by exploiting (37), \mathbf{w} surely satisfies the URLLC constraint if $\left(1 + \frac{\kappa(\mathbf{w},\mathcal{L})}{\bar{\sigma}(\mathbf{w},\mathcal{L})} \left(\frac{1}{N\gamma_{\text{th}}} u(\mathbf{w},\mathcal{L})\right)\right)^{-1/\kappa(\mathbf{w},\mathcal{L})} \leq \xi/\rho, \forall \kappa(\mathbf{w},\mathcal{L}) \in [\kappa_{lb},\kappa_{ub}], \bar{\sigma}(\mathbf{w},\mathcal{L}) \in [\bar{\sigma}_{lb},\bar{\sigma}_{ub}].$

Observe that ρ and α are heuristic parameters that must be pre-defined. The closer ρ is to 1, the more extreme, right-tailed, data samples $\{\Theta|\Theta>u(\mathbf{w},\mathcal{L})\}$ become, thus, the better the suitability of a GPD fitting. However, fewer samples are employed for the fitting, which ultimately reduces the accuracy. Meanwhile, the closer α is to one, the more flexible the GPD fitting becomes, but the chances of misdetecting an appropriate beamformer increase.

We resort to a brute force numerical optimization where the beamformer, out of 10^5 randomly generated beamformers, with the lowest power but satisfying the URLLC

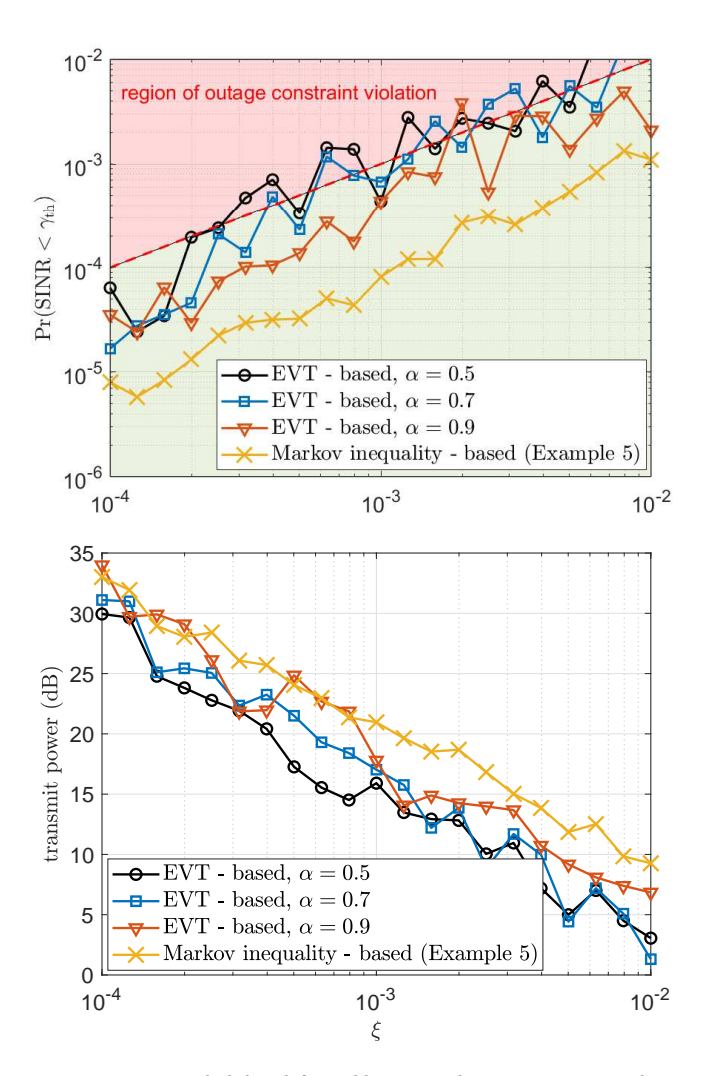


Fig. 8. a) Outage probability (left) and b) required transmit power (right) as a function of outage constraint ξ for f(x)=x. Since satisfying increasingly stringent reliability requirements require more extreme data samples in the EVT framework, here L and ρ are varied according to ξ as $L=\lceil 1/\xi \rceil$ and $\rho=1-\sqrt{\xi}$. Channel is subject to quasi-static Rician fading with LOS factor of 0 dB, and we set M=8, $\gamma_{\rm th}=1$, and average channel path-loss over noise to 10 dB.

constraint as described above, is selected. The performance resulting from employing the EVT framework is illustrated in Fig. 8 and compared to the that of the Markov inequality -based solving framework used in Example 5. Observe that EVT-based solutions may be more energy efficient, specially by reducing GPD estimator confidence intervals (smaller α), although this leads to greater chances of violating the reliability constraints. Moreover, EVT-based solutions exploit some tail data, thus, they usually require more data than Markov-inequality -based solutions, which are based on averages. Therefore, Markov-inequality -based solutions are preferable when a limited data set is available, while EVT -based solutions become more appealing as more data can be exploited.

Several works have exploited the EVT framework for designing and assessing the performance of URLLC systems, e.g., [3], [68], [69]. For example, the authors in [68] leverage

EVT to approximate the extreme probability of exceeding a queue length threshold, and develop a federated learning (FL) approach for resource allocation mechanisms upon it. Meanwhile, an EVT-based methodology, which includes determining the optimum threshold u and ascertaining the required number of channel samples, is introduced in [69] to statistically model the behavior of extreme events in a URLLC wireless channel. Moreover, the Pickands-Balkemade Haan theorem [70, Th. 2.1.1] in EVT, which states that

$$F_X(x) \to \alpha x^{\beta}$$
 as $x \to 0$, for some $\alpha, \beta > 0$ (38)

(or alternatively, $F_X(x) \to 1 - \alpha x^{-\beta}$ as $x \to \infty$ in case the interest is in the right tail) holds for a large class of distributions, has been exploited in [3] for estimating channel tails followed by transmit rate adaptation with ultra-reliability guarantees. Note that estimators of the tail index, i.e., $1/\beta$, include Pickands estimator [71], the moment estimator [72], and Hill's estimator [73]. Note that the asymptotic convergence of (38) tends to be slower compared to the previously discussed Pareto approximation, thus although simpler, its accuracy is more limited, specially when exploiting limited data sets.

C. Risk-assessment tools

Risk management theory [74], widely used in the field of finance, represents a fundamental tool for the design and analysis of URLLC systems [75]. Two widely used metrics to characterize risks are:

- value-at-risk (VaR), which is defined as the worst loss over a target horizon within a given level of confidence, thus, it is a quantile of the loss distribution;
- conditional VaR (CVaR) or expected shortfall, which characterizes the expected loss in the right tail of the distribution given a particular threshold has been crossed, thus, measuring the risky realizations.

In terms of a RV X, and given a confidence of $100 \times (1-\alpha)\%$, these metrics are given by

$$\operatorname{VaR}_{1-\alpha}(X) = F_X^{-1}(1-\alpha), \tag{39}$$

$$\operatorname{CVaR}_{1-\alpha}(X) = \mathbb{E}[X | X > \operatorname{VaR}_{1-\alpha}(X)]$$

$$= \frac{1}{\alpha} \int_0^{\alpha} \operatorname{VaR}_{1-t}(X) dt, \tag{40}$$

and are illustrated in Fig. 9.

Relying on distribution bounds such as those discussed in Section III-A, one can obtain bounds for VaR and CVaR as well. For instance, by exploiting (28), one attains

$$VaR_{1-\alpha}(X) \le g^{-1} \left(\mathbb{E}[g(X)] / \alpha \right), \tag{41}$$

which holds for every non-negative non-decreasing function *g*. Similarly, Theorem 3 can be leveraged to attain VaR and CVaR estimates, which are less conservative than those based on bounds, thus, generally more efficient for URLLC-related resource allocation.

Recently, there has been an increasing interest in applying the risk-management framework to design and analyze URLLC systems. Specifically, the authors in [15] use a risk-sensitive approach exploiting CVaR to schedule URLLC

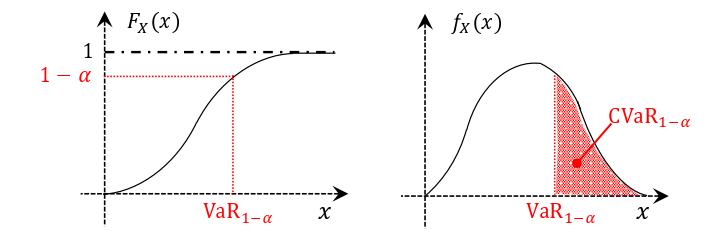


Fig. 9. Illustration of VaR and CVaR measures.

traffic in coexistence with punctured mobile broadband (MBB) services. Meanwhile, CVaR rate is a metric introduced and thoroughly investigated in [76] to characterize the expected rate of a worst-case fraction of clients in broadcast/multicast URLLC systems. Finally, in [77], the authors realize that the FBL error probability (see (54) and related discussions) is in fact a RV in fading scenarios, for which they provide accurate PDF analytical approximations. Based on this, they leveraged VaR and CVaR measures to illustrate that statistically different risks may be experienced even on services with similar performance in terms of average reliability.

Note that VaR can be directly exploited for modeling URLLC given its design constraints. Meanwhile, CVaR quantifies the performance impact of violating the URLLC operation, thus can be indirectly used for URLLC system design as well. In addition, CVaR can be leveraged to design resource-efficient resilience mechanisms. For instance, the number of wireless re-transmissions of a data message after failure can be designed based on the CVaR level. The higher the CVaR, the more re-transmissions should be scheduled after a data message fails.

IV. RARE EVENT SIMULATION

In wireless communications, we are often confronted with noisy observations from which we would like to estimate some unknown distribution and/or its parameters, or the unknown parameters. Among the many solutions, constructing posterior distributions is normally adopted as it facilitates incorporation of the prior information into the observed data. However, closed-form solutions for such problems are often infeasible, leading to the development of approximate inference techniques, such as Monte Carlo (MC) methods [78], [79]. MC methods comprise a large class of simulation-based algorithms optimized to perform random drawing from a target probability distribution. These methods can be used *i*) to generate independent random samples from a probabilistic model, or *ii*) to perform numerical integration, or *iii*) in optimization.

Therefore, MC methods became an essential tool in URLLC systems because reliability can be posed as rareevent estimation/simulation⁷. In the reminder of this section, we overview classical MC methods and assess their limitations in terms of computation time and accuracy. We then overview alternative solutions dedicated to rare-event sampling and provide examples of their efficiency in terms of computation time, complexity and accuracy.

A. Conventional MC

To introduce the MC method, let us define the following high-dimensional integral, that estimates the probability, p, of a rare-event

$$p = \Pr[S(x_i) \ge x_{\text{th}}] = \int_{\mathbf{X}} f_{\mathbf{X}}(x) \mathbb{I}\{S(x_i) \ge x_{\text{th}}\} dx$$
$$= \mathbb{E}_{\mathbf{X}} \left[\mathbb{I}\{S(x_i) \ge x_{\text{th}}\} \right], \tag{42}$$

where **X** is a $d \times N$ random matrix, where d denotes the dimensions and N the number of samples, its PDF is $f_{\mathbf{X}}$, $S(\mathbf{x}): \mathbb{R}^d \to \mathbb{R}$ is a real-valued function, and x_{th} is a threshold parameter. The x_{th} parameter determines the rarity of the event, i.e., $p = \Pr[S(x_i) \ge x_{\text{th}}] \to 0$ as $x_{\text{th}} \to \infty$. In other words, this parameter indicates how far into the tail of the distribution we are attempting to estimate the probability p.

Conventional (also known as naive or crude) MC method is a convenient way to estimate p, i.e., $\hat{p} = \mathbb{E}_X [\mathbb{I}\{S(x_i) \geq x_{\text{th}}\}]$. The idea behind conventional MC to estimate the probability \hat{p} using many independently generated samples of $X = [X_1, \cdots, X_N]^T$ per dimension. In this case, the unbiased estimator of choice is the sample mean, i.e., $\hat{p} = \frac{1}{N} \sum_{i=1}^{N} \mathbb{I}\{S(x_i) \geq x_{\text{th}}\}$; in other words, the ratio between the samples that belong to the event $\{S(x_i) \geq x_{\text{th}}\}$ and the total number of samples. Therefore, conventional MC relies on the law of large numbers and the central limit theorem to increase the accuracy of the estimation, as the number of samples grows to infinity, the sample mean converges to the expectation, i.e.,

$$\mathbb{E}[\hat{p}] = \lim_{N \to \infty} \frac{1}{N} \sum_{i=1}^{N} \mathbb{I}\{S(x_i) \ge x_{\text{th}}\}$$

$$= \frac{1}{N} \sum_{i=1}^{N} \mathbb{E}_X \left[\mathbb{I}\{S(x_i) \ge x_{\text{th}}\} \right] = p. \tag{43}$$

We resort to the coefficient of variation, $\delta(\hat{p})$ as a measure of the accuracy of the conventional MC, and therefore as $\delta(\hat{p}) \to 0$ the more accurate is the estimation. We define this measure as $\delta(\hat{p}) = \frac{\sqrt{\mathbb{V}[\hat{p}]}}{\mathbb{E}[\hat{p}]}$, which is the ratio of the standard deviation and expected value of the estimate \hat{p} . Following the same steps as in (43) we calculate the estimate's variance

$$V[\hat{p}] = V_X \left[\frac{1}{N} \sum_{i=1}^{N} \mathbb{I} \{ S(x_i) \ge x_{\text{th}} \} \right]$$

$$\stackrel{(a)}{=} \frac{1}{N^2} \sum_{i=1}^{N} \left(\mathbb{E}_X \left[\mathbb{I} \{ S(x_i) \ge x_{\text{th}} \}^2 \right] - p^2 \right)$$

$$\stackrel{(b)}{=} \frac{1}{N^2} \sum_{i=1}^{N} \left(p - p^2 \right) = \frac{p(1-p)}{N}, \tag{44}$$

⁷Notice that there are alternative sampling solutions to MC methods. For instance, the class of variational inference, particularly variational Bayesian, methods emerges as a computationally efficient alternative to sampling methods. We refer the reader to [80], [81] for a tutorial introduction to variational inference.

where (a) expands the definition of the variance, and (b) uses the identity $\mathbb{I}\{\cdot\}^2 = \mathbb{I}\{\cdot\}$ and (43). Now, we can calculate the coefficient of variance as

$$\delta(\hat{p}) = \sqrt{\frac{1-p}{Np}} \approx \frac{1}{\sqrt{Np}},\tag{45}$$

where last step holds accurate for $p \ll 1$. The latter corresponds to the probability of a rare event, which is of particular interest in URLLC setups.

One advantage of conventional MC is the independence on the dimension of the input state for the accuracy measure. Note that the accuracy varies with the number of samples and the target probability; therefore, the lower the desired estimate, the higher the number of samples required. Let us exemplify this point with the 3GPP target probability for URLLC of $p = 10^{-5}$. We expect a low variability, therefore, a coefficient of variation of 1% is appropriate. Then, replacing these values into (45), the required number of samples for such estimate is $N = 10^9$, which is costly with conventional simulation tools. In addition, for every sample there are additional computations required, e.g, $\mathbb{I}\{\cdot\}$ and $S(\cdot)$, which may increase the computational cost and render the URLLC analysis infeasible with conventional MC.

Notably, conventional MC is particularly useful when the target probability is around the mean of the distribution. However, conventional MC becomes inefficient when the target probability is at the distribution's tail. This is the case in URLLC scenarios as discussed in Section III. Therefore, robust MC methods are needed to evaluate URLLC with limited costs (e.g., computation and time). Indeed, we are interested in computationally affordable methods that allow evaluating reliability levels in the order of five or more nines, as in (extreme) URLLC use-cases [75], [82], by effectively sampling the region of the distribution's domain where such rare events occur. Fortunately, several methods can help in this task.

B. Importance sampling

Importance sampling (IS) is perhaps one of the most common MC methods for rare-event simulation, which is a variance reduction technique in the estimation of (42). In general, for a fixed degree of relative error, IS achieves sufficient variance reduction to decrease total computational effort by several orders of magnitude compared to that of conventional MC. This is achieved because IS draws samples from another distribution where the original rare events happen more often. Precisely, assume a PDF g_Y such that if $g_Y(x) = 0$ then $\mathbb{I}\{S(x_i) \ge x_{th}\} f(x) = 0 \ \forall x$; thus, we can re-write the expectation in (42) as

$$\mathbb{E}_{X} \left[\mathbb{I} \{ S(x_i) \ge x_{\text{th}} \} \right] = \int \mathbb{I} \{ S(x_i) \ge x_{\text{th}} \} \frac{f_X(x)}{g_Y(x)} g_Y(x) dx$$
$$= \mathbb{E}_{Y} \left[\mathbb{I} \{ S(x_i) \ge x_{\text{th}} \} \frac{f_X(X)}{g_Y(X)} \right]. \tag{46}$$

Notice that one must carefully select the PDF such that the variance of X is reduced. For this, the PDF must have i) finite variance, i.e.,

$$\mathbb{E}_X\left[\mathbb{I}\{S(x_i)\geq x_{\rm th}\}^2\frac{f_X^2(X)}{g_Y^2(X)}\right]=\mathbb{E}_Y\left[\mathbb{I}\{S(x_i)\geq x_{\rm th}\}^2\frac{f_X^2(X)}{g_Y^2(X)}\right]<\infty,$$

and ii) heavier tails than f_X and the bounded likelihood ratio $\frac{f_X}{g_Y}$. Notably, a poor selection of the PDF compromises the quality of the estimate [83].

Observe that the optimum PDF is the one that minimizes the variance of the estimate, i.e.,

$$\arg\min_{g_Y} \mathbb{V}_{g_Y} \left[\mathbb{I}\{S(x_i) \ge x_{\text{th}}\} \frac{f(X)}{g(X)} \right], \tag{47}$$

whose solution is the zero-variance IS density [83]

$$\pi(x) = \frac{\mathbb{I}\{S(x_i) \ge x_{\text{th}}\} f(x)}{l}.$$
 (48)

However, (48) depends on the unknown estimate l, therefore it cannot be directly used. Instead, we approximate the π and the IS density g_Y , e.g., by resorting to differential entropy and by allowing g_Y to be in product form $g_Y(x) = \prod_{i=1}^d \pi_i(x_i)$, which usually simplifies the analysis.

Thought relevant, IS method is particularly useful for light-tailed distributions, e.g., where the rare-event probability decays exponentially. Moreover, the selection of the desired density can be optimized for instance with the cross-entropy method [83], which minimizes a density g_Y for a parametric family of probability densities instead of a single function. By doing so, the cross-entropy method allows to iteratively update the target density, helping with effective sampling.⁸

C. Markov-chain MC Algorithms

Current MC methods are based on the initial works of Stanislaw Ulam, John von Neumann, among others, during the Manhattan Project in the 1940s. One of the key contribution was the Metropolis algorithm, which relies on a Markov chain for the generation of a desired distribution based on symmetric proposal densities. After improvements to accept asymmetric proposal densities by Hastings, the algorithm is now known as Metropolis-Hastings algorithm [78]. The Markov-chain MC algorithms rely on a basic idea: run a sufficiently long Markov chain such that its stationary distribution approximates an arbitrary distribution, known as target distribution, from which we can generate samples. In other words, suppose our target distribution is $f_X(x)$, as in (42), then construct a Markov chain with states $\{X_t, t = 0, 1, 2, \dots\}$, where X_t is a given state at time t and stationary probability distribution is $f_X(x)$. The Metropolis-Hastings algorithm core idea relies on calculating the transition from a state to the next. To do so, we first draw a proposal state, e.g., Y from a transition density $q_Y(\cdot|X_t)$. Then, the proposal state is accepted based on the acceptance probability

$$\alpha(x, y) = \min \left\{ \frac{f_X(y) \, q_Y(x|y)}{f_X(x) \, q_Y(y|x)}, 1 \right\}. \tag{49}$$

⁸Please, see [83] for detailed discussion on alternative algorithms.

Algorithm 1: Metropolis-Hastings Algorithm [83]

```
Input: X_0, N, f_X(x), q_Y(y|x)

1 Initialization: t = 0

2 repeat

3 | Draw Y \sim q_Y(y|X_t)

4 | Calculate \alpha(X_t, Y) in (49) Draw U \sim \mathcal{U}(0, 1)
(uniform distribution)

5 | X_{t+1} = \begin{cases} Y, & \text{if } U \leq \alpha(X_t, Y) \\ X_t, & \text{otherwise} \end{cases}

6 | Increase t

7 until N samples were generated, i.e. t = N;
Output: X_1, \dots, X_N
```

Otherwise, the proposed state is rejected and the the chain remains in current state. This can be observed in Algorithm 1 lines 4-5 when the proposal is accepted or rejected compared to a draw form a uniform distribution. Notice that the transition density satisfies the balanced detailed equations, i.e., $f_X(x)q_Y(y|x) = f_X(y)q_Y(y|y)$. Therefore, $f_X(x)$ is the stationary distribution of the chain. Notably, if the event $\{X_{t+1} = X_t\}$ has positive probability, i.e., $\Pr[\alpha(X_t, Y) < 1|X_t] > 0$ and $q_Y(x|y) > 0 \,\forall x, y$ in the domain, then the Markov chain is ergodic and its limiting distribution is $f_X(x)$ [83].

Note that computing the acceptance probability $\alpha(x, y)$ requires knowing the distribution $f_X(x)$ only up to a normalizing constant, i.e., $f_X(x) = cf(x)$ where f(x) is a known function while c > 0 is an unknown constant. Moreover, the efficiency of the Metropolis-Hastings algorithm heavily depends on the choice of the transition density, which ideally should be close to the target function $f_X(y)$ regardless of x. In such circumstances, the proposal function can be independent of x, thus $q_Y(y|x) = g_Y(y)$ for some distribution $g_Y(y)$. Consequently, (49) reduces to $\alpha(x, y) = \min \left\{ \frac{f_X(y)g_Y(x)}{f_X(x)g_Y(y)}, 1 \right\}$, and this method is known as an independence sampler. However, notice that the generated samples are dependent and the proposal function should be close to the target function. Moreover, if $f_X(x) \le c g_Y(x) \forall x$, where c > 0 is a normalizing constant, then, the acceptance rate in Algorithm 1 Step 5 is at least 1/c. A simple alternative is to consider a symmetric proposal function, i.e., $q_Y(y|x) = q_Y(x|y)$, hence $\alpha(x, y) = \min\left\{\frac{fX(y)}{f_X(x)}, 1\right\}$.

A particular case of the Metropolis-Hastings algorithm is the Gibbs sampler, commonly used for n-dimensional random vectors. In this case, the conditional distribution governs the construction of the Markov chain. Notably, Gibbs sampler is helpful when sampling the conditional distribution is less computationally expensive than the joint distribution. In addition, the Gibbs sampler distribution, f_X , is the stationary distribution of the Markov chain and has a geometrically fast convergence [83].

D. Subset simulation

With origins in structural reliability theory, subset simulation (SS) is a powerful and efficient method for simulation

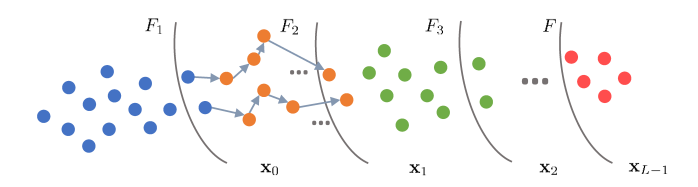


Fig. 10. Schematic illustration of the SS Algorithm. First, a small number of samples are generated from a target distribution (blue circles). These samples are sorted and after selecting the samples closer to the desired domain (boundaries between subsets in gray) Markov-chain MC is applied using those samples as seeds. For example, see region F_2 , notice that the blue circles are seeds, and the arrows indicate the Markov-chain MC sampling; orange circles are new samples from the conditional distribution. Then, the process repeats until the last domain L.

of rare events and estimation of tail probabilities. Moreover, SS decomposes the rare event into a sequence of nested events such that the most frequent events are supersets of the less frequent ones. [84]. In other words, let the rare event F be decomposed into a sequence of F progressively rarer events from F to F i.e., F = F composed into a sequence of F to F is a frequent event. Therefore, the probability of the rare event F follows the chain rule as

$$\Pr[F] = \Pr[F_L] = \Pr[F_1] \Pr[F_2|F_1] \cdots \Pr[F_L|F_{L-1}].$$
 (50)

However, in many applications, it is cumbersome to decompose the events and obtain closed-form or tractable expressions for the conditional probabilities. Thus, to overcome this issue, it relies on Markov-chain MC methods to adaptively obtain the conditional probabilities, and consequently the intermediate events.

In a nutshell, the SS algorithm generates a small number of samples to explore the input space, thus, generating a rough approximation of the failure domain F. This process is repeated iteractively such that the domain approximations converge to the domain F, and sufficient samples are generated in F to estimate the rare event, as illustrated in Fig. 10. Notice that some samples serve as seeds for the Markov-chain MC algorithm at the upper level L, thus, drawing from $\pi(\cdot|F_L)$. These steps are summarized in Algorithm 2. Notice that any Markov-chain MC algorithm can be used to sample from the conditional distribution. The particular choice depends on the scenario, e.g., difficulty on sampling from the conditional distribution.

Based on [84], we describe the key points of the SS algorithm. For the first domain, SS generates the initial sample set comprising the realizations $x_0 = \begin{bmatrix} x_0^1, \cdots, x_0^n \end{bmatrix}^T \sim \pi(x)$, n < N, $N = n^d$, as shown in line 2 of Algorithm 2. Then, the SS algorithm computes the response $y_0 = S(x_0)$ in line 4. As the sample size is small and we want to estimate a rare event, it is likely that the samples x_0 do not belong to F. However, x_0 contains relevant information about F since by ordering y_0 we can identify which are the samples that are closest to the target set. As in (42), we can define the first intermediate failure domain, i.e., $F_1 = x : S(x_i) > y_1^*$, which is the set of samples that lead toward the rare event and are ordered in line 5. By construction, x_0^1, \cdots, x_0^{nq} belong to F_1 and $x_0^{np+1}, \cdots, x_0^n$ do not, which is obtained by the

Algorithm 2: SS Algorithm [84]

```
Input: N, d, S(\cdot), q

1 Initialization: l = 0

2 Draw the first subset:
x_0 = x_0^1, \cdots, x_0^n \approx \pi(\cdot), n < N, N = n^d
3 repeat

4 | Calculate the response y_l = S(x_l)

5 | Order x_l based on the response y_l = S(x_l)

6 | Define the intermediate failure domain
F_l = \{x : S(x_i) > y_l^*\}

7 | Draw a sample from \pi(\cdot|F_l) using Markov-chain
MC and nq samples from x_l as seeds
Increment l

8 until \frac{n(l+1)}{n} < p;
Output: \Pr[F] \approx q^L \frac{n(L)}{n}
```

intermediate failure domain $y_1^* = (y_0^{nq} + y_0^{nq+1})/2$ (line 6), where $q \in (0,1)$ is an arbitrary input parameter such that nqis a natural number. Consequently, the probability estimate of F_1 is $Pr[F_1] = q$, which can be estimated via conventional MC since F_1 is by design not rare and the number of samples, n, is small. Moreover, we can calculate the rare event probability as in (50), which for first domain reduces to $q \Pr[F|F_1]$. Therefore, $\Pr[F|F_1]$ using a Markov-chain MC method (line 7), e.g., a modified Metropolis-Hastings or Gibbs sampling [83], [84]. Once we generate the samples based on $\pi(x|F_1)$, we apply the same steps and determine the next domain. This process is repeated iteratively until the stopping criteria is met (see [84] for details on the stopping criteria and an alternative implementation of the algorithm). By design, the SS algorithm controls the probability of the intermediate steps, therefore, (50) approximates to $q^L \Pr[F|F_l]$ where $l \le L$ indicates the number of domains, $\Pr[F|F_l] = n(L)/n$, and n(L) is the number of samples in the last domain. Thus, the output of Algorithm 2 line 8 is the rare event probability, which is given as

$$\Pr[F] \approx q^L \frac{n(L)}{n}.$$
 (51)

A key advantages of the SS algorithm is that by design one can control input variable q, which influences the number of chains, number of samples in each chain, and the stopping criteria. Therefore, with proper selection of q, the SS algorithm efficiently samples the conditional distributions to (approximately) match this probability ensuring that each factor in (50) is larger than q. Such an iterative process yields an accurate estimate of the the rare event even for a small sample size.

EXAMPLE 7. Multi-connectivity emerged as a promising solution for URLLC as it allows the devices to connect to two or more base stations. See for instance [85] for a comprehensive overview and [4], [22], [23] for related works and applications. Herein, we assume a simple system model where a device connects to $d \in \{2,4,8,16\}$ base stations. The channel coefficients follow a Rayleigh distribution and we are interested in coherently combining these signals via

maximal ratio combining. Therefore, the SNR of each link X follows an exponential distribution 10 , i.e., $X \sim \text{Exp}(1)$. Under this setting, the SNR of the combined received signal can be described as $Y = \sum_{i=1}^d X_i$. For this particular case the distribution of the sum is known in closed-form, i.e., $Y \sim \mathbb{G}(d,1)$, which helps the comparison between conventional MC and SS algorithms here. However, in many cases, we are unable to express the target distribution in closed-form due to the complexity of the model, or intractability of the functions that lead to intricate integrals that require numerical analysis. This is one more example of the usefulness of MC methods in practice.

We are interested in the outage probability, i.e.,

$$P_{\text{out}} = \Pr \left[\log_2 (1 + \bar{\gamma} Y) < r \right] = \Pr \left[Y < (2^r - 1)/\bar{\gamma} \right],$$

where r represents a target rate and $\bar{\gamma}$ the average SNR. In Fig. 11, we compare the analytical expressions to the conventional MC and SS algorithms as a function of $\bar{\gamma}$ for different number of base stations (dimensions) and r=1 bits per channel use (bpcu). For the conventional MC, we draw $N=10^7$ samples for each dimension d, while for the SS algorithm we draw $n=10^4$ samples and we assume q=0.1. We implement Algorithm 2 using the modified Metropolis-Hastings algorithm, as in Algorithm 1.

As discussed above, conventional MC is inefficient as the $\bar{\gamma}$ grows, thus, as the events become more rare, and therefore, it can only reliably estimate the probabilities as $P_{\text{out}} > 10^{-6}$. Increasing the sample size, $N \gg 10^7$ becomes computationally expensive. On the other hand, SS algorithm, uses a small sample size for each domain yielding a faster simulation compared to conventional MC. The number of samples grows with the increase in $\bar{\gamma}$. For instance, for d=4, $\bar{\gamma}=20$ dB, SS requires approximately 91000 samples to estimate an event with probability around 410^{-10} . Moreover, it is able to estimate the probabilities for region below 10^{-10} . This is particularly relevant for the analysis of performance metrics in the extreme URLLC cases. Notice that the SS algorithm can be optimized to reduce the variance for extreme events, e.g. by selecting a different target distribution or different input parameters such as the number of samples or q.

V. FINITE BLOCKLENGTH CODING

In any communication systems, the received message is not always the same as the transmitted message. An error is said to occur when this happens. This can happen due to a number of reasons in a wireless system, for example, deep fades due to random channel fluctuations or outages due to strong interference. One way to recover such errors is to use use error correction codes, where redundant information are added to the transmitted message to facilitate error detection and/or correction. However, this requires additional decoding algorithms at the receiver end to recover the original message from the transmitted

⁹The feasibility of such solution is discussed in, e.g., [4], [22].

¹⁰For simplicity of presentation, we assume all links have the same mean, which in practice presumes that the nodes are equidistant from the base station, or the devices employ some path-loss compensation.

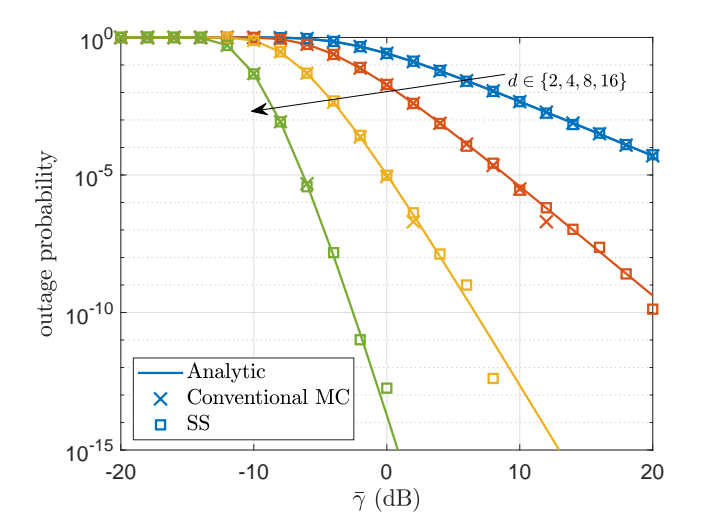


Fig. 11. Comparison between conventional MC and SS algorithms in terms of outage probability against the average SNR $\tilde{\gamma}$. The closed-form result is shown as the baseline. We set r=1 bpcu and consider different numbers of connected base stations, i.e, $d \in \{2,4,8,16\}$.

encoded information [86]. The first error correcting code was the Hamming (7,4) code invented in 1950 [87].

Error-correcting codes are usually classified into convolutional codes and block codes. Convolutional codes work on a bit-by-bit basis as a sliding window of the bits. A (k_c, k_d) block code acts on a block of k_d information bits of input data to produce $k_c(k_c > k_d)$ bits of coded output data, also known as a codeword symbol. The ratio $r_c \triangleq k_d/k_c$ is known as the coding rate. The price to pay for this error resilience is that the introduction of redundant bits decreases the data rate in proportion to the coding rate r_c .

A. Finite Blocklength Theory

The capacity of a wireless channel dictates the maximum data rate that can be transmitted with asymptotically small error rates in the absence of any complexity or delay constraints in the coding and encoding process. For example, the well known Shannon capacity of additive white Gaussian noise (AWGN) channels for SNR γ given by $C_{\rm AWGN} = \log_2(1+\gamma)$ in bpcu assumes that the channel's mutual information is maximized over all possible input distributions, i.e., an infinite blocklength. Encoding over a large number of bits increases the diversity order of the code and hence provides better error resilience. Notice that such increased reliability adds complexity and delay to the encoding and decoding processes.

The payload in the novel URLLC and massive MTC service classes introduced in 5G are usually small in size. Moreover, the low-latency constraint in URLLC implies that messages have to be transmitted as soon as they arrive and cannot afford to be buffered in a queue. Thus, the amount of data available for encoding is usually small. Alongside, the massive contention to access the channel and/or strict energy limitations that are common in massive MTC imposes further constraints. Altogether, many URLLC and massive MTC use cases do not allow coding over a

large block length and hence there is a need to evaluate the performance of a wireless system transmitting FBL data. We next present Polyanskiy, Poor and Verdú's *FBL theory*, which is a unified approach to obtain tight bounds on the maximum transmission rate $r(N,\epsilon)$ as a function of the blocklength N and the error probability ϵ .

Theorem 4 (Maximum FBL Transmission Rate [88]). For a given channel with capacity C, the difference between the channel capacity and the maximum transmission rate in the FBL regime is a function of the blocklength N, the error probability ϵ , and the channel dispersion V. The latter is a measure of the stochastic variability of the channel relative to a deterministic channel with the same capacity. In concrete terms,

$$r(N,\epsilon) = C - \sqrt{\frac{V}{N}} Q^{-1}(\epsilon) + \mathcal{O}\left(\frac{\log N}{N}\right), \tag{52}$$

where $Q^{-1}(\cdot)$ is the inverse of the Gaussian Q function.

Notice that for an AWGN channel with SNR γ , the capacity matches the well known Shannon rate C_{AWGN} , and the dispersion is given by [88]

$$V(\gamma) = \gamma \frac{2+\gamma}{(1+\gamma)^2} \log_2^2 e.$$
 (53)

Fig. 12 leverages (52) and (53) to illustrate the maximum transmission rate achievable in AWGN channels as a function of the error probability ϵ for SNR values $\gamma \in \{10,20\}$ dB, and blocklengths $N \in \{100,1000\}$. The transmission rate is normalized by the corresponding AWGN capacity in the infinite blocklength regime, $C_{\rm AWGN}$. We can observe that the penalty incurred with FBL transmissions is higher for shorter blocklengths, lower SNRs, and tighter error probability targets, as typical in the case of URLLC transmissions. The interested reader is referred to [14] and [89] for expositions on the derivation of the maximum FBL transmission rate under fading channels and in a random wireless network, respectively.

Meanwhile, one can obtain the achievable error probability given a fixed transmission rate r = k/N from (52) as

$$\epsilon(\gamma) \approx Q\left(\frac{C(\gamma) - k/N}{\sqrt{V(\gamma)/N}}\right),$$
 (54)

for which we have ignored the residual terms of order $\log N/N$ in (52) for simplicity. Consequently, the average error probability for block fading channels is given by $\bar{\epsilon} = \mathbb{E}_{\gamma}[\epsilon(\gamma)]$. Interestingly, it has been shown in [14], [90], [91] that the effect of the fading on (54) vanishes the FBL impact in two cases, when i) k is not extremely small, and ii) there is not a strong LOS component (e.g., as in Rayleigh fading). In such cases, the asymptotic outage probability is a good approximation for $\bar{\epsilon}$, i.e., $\bar{\epsilon} = \Pr[\gamma < 2^{k/N} - 1] = F_{\gamma}(2^{k/N} - 1)$. Unfortunately, this is not yet completely understood by the scientific community, which often adopts $\mathbb{E}_{\gamma}[\epsilon(\gamma)]$ in situations where $F_{\gamma}(2^{k/N} - 1)$ is very accurate and much easier to evaluate.

Next, we present an application example of the above complete framework and some follow-up discussions.

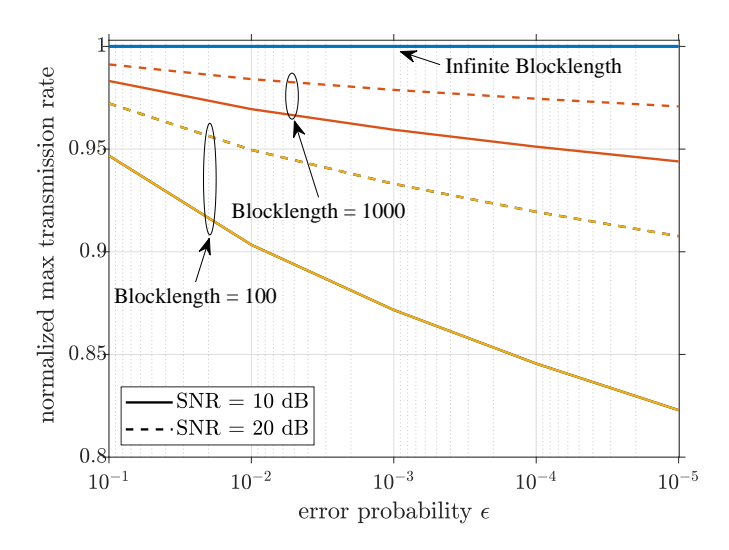


Fig. 12. The normalized maximum transmission rate with FBL transmission for different values of SNR γ , blocklength N, and target error probability ϵ .

EXAMPLE 8 (ERROR-CONSTRAINED FBL POWER CONTROL). Assume a node A wants to transmit a data message of k bits through N channel uses to a node B. For this, A has already acquired the CSI of the communication link. Specifically, A perfectly knows the value of γ' , which is defined as the receive SNR at B given a normalized transmit power. What is the minimum transmission power that A must set to ensure a decoding error probability ϵ at B?

In this case, both the transmission rate r = k/N and the error probability ε are fixed. Also, given a transmit power p, the receive SNR at B becomes $\gamma = p\gamma'$. Therefore, the problem reduces to finding the required SNR γ such that (54) (or alternatively (52)) holds. It has been shown in [92] that the required γ is a fixed point solution of

$$\gamma^{(t+1)} = 2^{k/N + \sqrt{V(\gamma^{(t)})}Q^{-1}(\varepsilon)/\sqrt{N}} - 1, \tag{55}$$

where t is the iteration index. Here, one can initially set $\gamma^{(0)} \to \infty$ for which $V = \log_2^2 e$ according to (53). The corresponding iterative procedure was shown in [92] to converge fast, i.e., in no more than five iterations for $N \le 1000$ with an accuracy superior to 99.9%. Finally, after solving (55), the required transmit power is given by $p = \gamma/\gamma'$.

In the previous example, the solution of (55) becomes $\gamma = 2^{k/N} - 1$ when $N \to \infty$ (and also $k \to \infty$ such that k/N = r is fixed). This agrees with Shannon's framework in which the error probability becomes arbitrarily small when the received SNR exceeds $2^{k/N} - 1$. Here, an interesting question is: how much greater must the SNR at a FBL N be in comparison with the asymptotic result? The answer comes by defining and simplifying the quotient between the required SNR at FBL and infinite blocklength as [92]

$$\delta \triangleq \frac{2^{r+\sqrt{V(\gamma^{(\infty)})}Q^{-1}(\varepsilon)/\sqrt{N}} - 1}{2^r - 1}$$

$$= 2^{\sqrt{V(\gamma^{(\infty)})}Q^{-1}(\varepsilon)/\sqrt{N}} + \frac{2^{\sqrt{V(\gamma^{(\infty)})}Q^{-1}(\varepsilon)/\sqrt{N}} - 1}{2^r - 1}.$$
 (56)

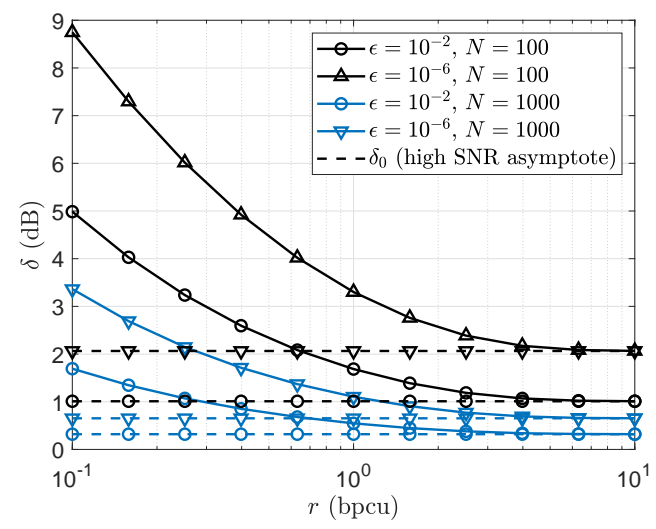


Fig. 13. δ and δ_0 as a function of r for $N \in \{100, 1000$ channel uses and $\epsilon \in \{10^{-2}, 10^{-6}\}$.

Interestingly δ is a decreasing function of r [92], thus

$$\delta \ge \delta_0 = \lim_{r \to \infty} \delta = e^{Q^{-1}(\varepsilon)/\sqrt{N}},\tag{57}$$

which exploits the fact that $r \to \infty$ implies $\gamma \to \infty$, for which $V(\gamma) \to \log_2^2 e$. Fig. 13 corroborates this behavior, and already evinces the convergence of δ to δ_0 for $r \approx 4$ bpcu. Notably, the main remark from (57) and Fig. 13 is that the SNR has to be at least $e^{Q^{-1}(\varepsilon)/\sqrt{N}}$ times greater than the asymptotic threshold of 2^r-1 to reach an error probability no lower than ϵ while transmitting the information through N channel uses. Obviously, this criterion is also applied to the transmit power.

B. Encoding of data and metadata in URLLC transmissions

Most wireless systems group the information bits to be transmitted into transmission blocks whose duration is sufficiently short compared to the channel coherence time. Thus, all bits in the block experience the same channel condition. The bits in a transmission block are of two types, metadata, i.e., the control information needed to decode the packet, and the intended data message.

In conventional MBB transmissions, the modulation and coding scheme of the data message within each transmitted block is selected to meet a target block error rate (BLER). It has been shown that for a large range of system parameters, a 10% BLER leads to near-optimal performance [26]. In contrast, the metadata is transmitted with a much lower BLER target, which means that the contribution of the metadata in the final error probability calculations is negligible.

This is no longer the case for URLLC, where both metadata and the data have to be transmitted with ultra-low BLER targets. Instead, the final success probability is the product of the probabilities of successfully decoding both metadata and the data, i.e.,

$$P_{s} = (1 - P_{e,m})(1 - P_{e,d}), \tag{58}$$

TABLE VIII
SUCCESS PROBABILITY FOR THE FIRST TRANSMISSION AND A SINGLE RETRANSMISSION OF TYPICAL MBB AND URLLC SERVICES

Transmission type	metada n	ta considered $n=1$	metadat $n = 0$	a neglected $n=1$
MBB	0.9	0.99	0.899	0.989
URLLC	0.999	0.999999	0.998	0.999

where $P_{e,m}$ and $P_{e,d}$ are the error probabilities for the metadata and the data, respectively. The success probability can be further improved via retransmissions in the event of a failure [26]. In this case too, the error probability of the feedback link should not be ignored. The success probability $P_{s,n}$ after the n-th (n > 1) retransmission is given by

$$P_{s,n} = P_{s,n-1} + \underbrace{\left(1 - P_{e,m}\right) P_{e,d}}_{\text{metadata decoded, feedback success}} \underbrace{\left(1 - P_{e,f}\right)}_{\text{feedback success}} \times \underbrace{\left(1 - P_{e,m}\right) \left(1 - P_{e,d}\right)}_{\text{success after retransmission}}, \quad (59)$$

where $P_{e,f}$ is the error probability of the feedback link. Eq. (59) indicates that a feedback is only possible if the metadata is successfully decoded, allowing the receiver to establish the transmitter and the packet identity. It is worth mentioning here that this only holds under the assumption of independence between subsequent transmission slots. Such assumptions may not hold under very stringent latency constraints where the retransmission occurs within the channel coherence time [93].

Let us illustrate the importance of considering the metadata error probability in the success probability calculation through an example.

Example 9 (Impact of the Metadata Error Probability). Consider two services: i) MBB transmissions characterized by $\{P_{e,m} = P_{e,f} = 10^{-3}, P_{e,d} = 0.1\}$, and ii) URLLC transmissions characterized by $\{P_{e,m} = P_{e,f} = P_{e,d} = 10^{-3}\}$. The success probabilities up to the first retransmission (n = 1) is shown in Table VIII for the case when the error probability of the metadata is considered (the middle column) and compared against the case when the metadata is ignored (the right column). We can observe that the difference between the two cases (considering vs. neglecting the metadata error probability) is almost neglible for conventional MBB transmissions, whereas it is several orders of magnitude for URLLC transmissions. This highlights the importance of considering the metadata error probability when analyzing URLLC transmissions.

C. Polar codes for FBL transmissions

We have seen in Section V-A that using FBL in URLLC transmissions reduces the maximum achievable rate. One of the reason for this is the reduced coding gain due to the reduced blocklength. Hence there is a need to study channel codes that perform well in the FBL regime. The

channel code selected by 3GPP for MBB data transmissions, namely low-density parity check codes, are not particularly suitable for FBL scenarios [13]. Recently, 3GPP has adopted Polar codes for short blocks of metadata in MBB transmissions. Current investigations also demonstrated that Polar codes outperform low-density parity check codes in short block lengths and low code rates, therefore they might be appealing for URLLC use cases [13].

Polar codes, invented by Professor Erdal Arikan in 2009 [94], are the first codes with an explicit construction to achieve the channel capacity using low-complexity encoding and decoding. Specifically, low complexity successive cancellation and belief propagation decoding are used at the receiver side. A polar code $\mathcal{P}(k_c, k_d)$ is a code sequence containing a codeword symbol of k_c bits carrying k_d information bits. Channel polarization is proposed in [94] as a way to construct code sequences in order to achieve the symmetric channel capacity of the binary-input discrete memoryless channel.

Channel polarization refers to the fact that it is possible to synthesize the channel into a set of k_c binary-input channels such that, as k_c becomes large, a fraction of the channels becomes reliable (i.e., the symmetric capacity approaches 1) while the remaining fraction becomes unreliable (i.e., the symmetric capacity approaches 0). Thus, the information bits can be transmitted at rate 1 through the k_d most reliable channels, while "dummy" frozen bits (usually zero) are transmitted through the unreliable channels. Reliable transmission can be achieved if k_d is less than equal to the number of reliable polarized channels.

1) Encoding of Polar codes: The transformation matrix for a polar code of length k_c is constructed through a $\log_2 k_c$ –Kronecker product of the polarization kernel

$$\mathscr{G} = \begin{bmatrix} 1 & 0 \\ 1 & 1 \end{bmatrix}.$$

As $k_c \to \infty$, this construction creates channels that are either perfectly noiseless or completely noisy. For smaller values of k_c , the synthetic channels polarization may be incomplete, generating intermediary channels that are only partially noisy.

2) Decoding of Polar codes: The successive cancellation algorithm used to decode Polar codes can be represented as a depth-first binary tree search with priority to the left branch, which has a decoding complexity of $\mathcal{O}(k_c \log_2 k_c)$ [94], [95]. The leaf nodes are the k_c bits to be estimated. The soft information on the received code bits are input at the root node. Fig. 14 shows the decoding tree of a (8,4) Polar code where bits numbered 1,2,3,5 are frozen. The black leaf nodes represent information bits and the white ones are the frozen bits.

Each node at stage t_p uses the 2^{t_p} -length soft input vector α_{t_p} , received from its parent node, to calculate the soft output $\alpha_{t_p-1}^l$ and forward it to its left child. The i-th element of $\alpha_{t_p-1}^l$ is given by $\alpha_{t_p-1,i}^l = f(\alpha_{t_p,i},\alpha_{t_p,i+2^{t_p-1}})$, with $f(a,b) = \operatorname{sgn}(a)\operatorname{sgn}(b)\operatorname{min}(|a|,|b|)$. The soft output $\alpha_{t_p-1}^r$ to the right child is calculated by combining α_{t_p} with the

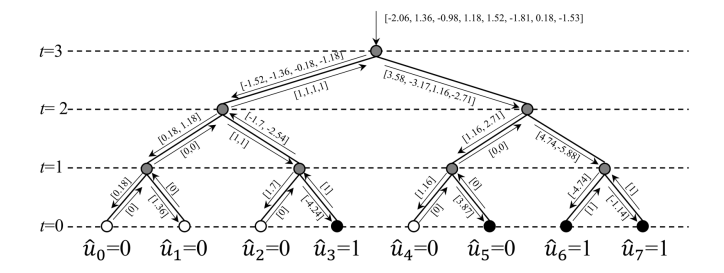


Fig. 14. Successive cancellation decoding of an (8,4) Polar code over a binary phase shift keying (BPSK) modulated transmission; white and black circles represent frozen and information bits, respectively.

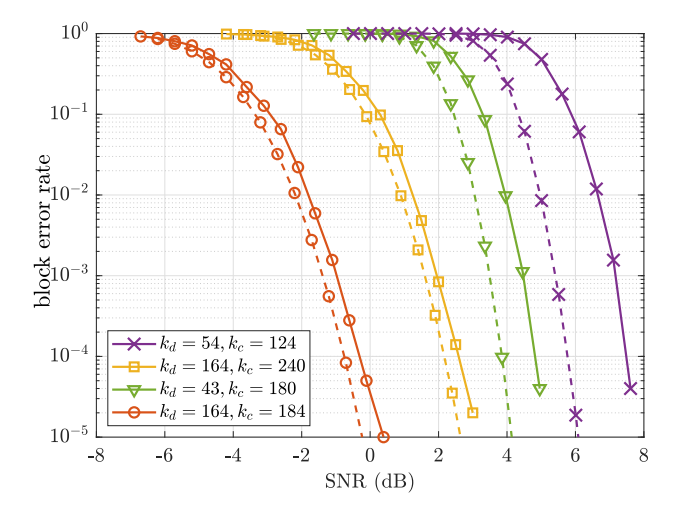


Fig. 15. BLER performance for different code rates and message lengths in the downlink with QPSK modulation. The dashed lines show the error rate with FBL theory, as given by Eq. (54).

 2^{t_p-1} —length hard decision $\beta_{t_p-1}^l$ received from its left child, where $\alpha_{t_p-1,i}^r = g(\alpha_{t_p,i},\alpha_{t_p,i+2}{}^{t_p-1},\beta_{t_p-1,i}^l)$ with g(a,b,c) = b+(1-2c)a. The final hard decision vector is then obtained as $\beta_{t_p} = [\beta_{t_p-1}^l \oplus \beta_{t_p-1}^r,\beta_{t_p-1}^r]$. Lastly, the hard decision at the i-th leaf node is given by $\hat{u}_i = \beta_{0,i} = (1-\mathrm{sgn}(\alpha_{0,i}))/2$; while frozen bits are always decoded as zero.

The BLER of Polar codes for different codeword sizes (k_c) , data size (k_d) , and different coding rates (k_d/k_c) are illustrated in Fig. 15. The codeword and the data sizes are chosen to cover a range of coding rates, from ~ 0.24 to a value close to one. The downlink transmission and quadrature phase shift keying (QPSK) modulation are considered. The BLER performance results indicate that polar codes can deliver very low BLERs in the FBL regime with a blocklengths in the order of 100-200 bits. The performance is compared against the ideal FBL error rates obtained by Eq. (54). We observe that the performance gap is small with robust coding whereas a larger gap is seen for coding rates close to one. It is worth highlighting that even lower BLERs can be achieved through retransmissions (cf. Section V-B), albeit at the cost of higher latency.

The recursive nature of the successive cancellation decoding algorithm may impose a large latency and low errorcorrection performance in the FBL regime [95]. Different approaches have therefore been proposed to enhance the coding efficiency and reduce the latency for URLLC applications. For example, the binary-tree can be pruned to decrease the number of calculations, thereby reducing the decoding latency and complexity [96]. Altering the polar code construction is another way to further reduce the latency of polar codes, though this induces a trade-off with the error-correction performance [97]. This can be addressed by taking advantage of the high degree of parallelism to provide a favorable tradeoff between throughput and energy efficiency at short to medium block length [98], or through a more efficient memory utilization [99].

D. GRAND: a generic maximum likelihood decoder

In this last subsection, we briefly introduce a novel lowlatency decoding algorithm called guessing random additive noise decoding, GRAND for short. Traditional channel codes are co-designed with specific decoders that use the codebook structure to decode the received encoded signal, which may limit their applicability. Recently, GRAND has been proposed as a new algorithm for realizing maximum likelihood decoding in discrete channels with random codebooks [100]. The algorithm operates by subtracting ordered noise sequence from the received signal and estimating the first instance that results in a member of the codebook to be the transmitted message.

The basic principle of the GRAND algorithm is as follows. Let X^N, Y^N and Z^N be RVs representing the coded transmitted message, received message and random noise of blocklength N over a discrete channel. The arbitrary codebook \mathscr{C}_N used to generate the encoded message X^N is commonly known to the transmitter and the receiver. Assume that the input output relation of the channel is reversible such that noise can be subtracted from the received message to recover the transmitted message, i.e.,

$$Y^N = X^N + Z^N \qquad \to \qquad X^N = Y^N - Z^N. \tag{60}$$

For a given received message y^N , the receiver orders the possible noise sequences from the most likely to the least likely, and then queries one by one whether the sequence $y^N - z_p^N$ is an element of the codebook \mathcal{C}_N . Here z_p^N is the p-th ordered noise sequence. For the channel structure described above, irrespective of how the codebook is constructed, the first instance such that $x^N = y^N - z_p^N \in \mathcal{C}_N$ corresponds to the maximum likelihood decoding. GRAND operates by attempting to identify the random noise that has corrupted the transmitted message, and hence is independent of the code structure. It is inherently highly parallelizable, resulting in the low latency desired in URLLC and other similar applications [101].

GRAND's accuracy depends on the ability to query the noise sequences, whose probability distribution depend on the channel statistics. For instance, in a binary symmetric channel, the relationship among the binary output symbol y^N , the binary input codeword x^N , and the independent binary additive channel noise z^N is given in (60). Considering the likelihood ordering determined by such a channel, the most likely noise sequence is the all zeros, followed by

each of those with one bit flip in any order, followed by those with two bit flips in any order, and so on [102].

VI. QUEUING THEORY & INFORMATION FRESHNESS

URLLC is about taming the tail distributions of reliability and latency (see Section III), while considering the inherent trade-offs associated to energy consumption, throughput, and data freshness. All this makes the design/analysis of URLLC systems extremely challenging in practice, and motivates the exploitation of queuing theory metrics/tools such as effective capacity, AoI, and SNC, which can natively capture several of these trade-offs and constitute the scope of our discussions in this section.

A. Effective capacity

Metrics such as effective capacity and effective bandwidth capture tail statistical delay requirements in parallel with transmission throughput. Specifically, the effective capacity is defined as the highest arrival rate that can be served by the network under a particular latency constraint. Conversely, its dual twin, the effective bandwidth, characterizes the minimum service rate required to support the arrival of data in a certain network subject to a QoS constraint. Here, we focus on the foundations of effective capacity, which can be easily extended to effective bandwidth as well.

To begin with, the effective capacity, denoted as C_e , is a metric that captures the physical and link layers characteristics in terms of specific latency QoS guarantees, thus, allowing a further investigation of the latency-reliability tradeoff. For low latency communication, C_e is a powerful metric that characterizes the relation between the communication rate and the tail distribution of the packet delay violation probability [12]. A statistical delay violation model implies that for relatively large delay, an outage occurs when a packet delay exceeds a maximum delay bound $D_{\rm max}$, and its probability is defined as [103]

$$P_{\text{out}} = \Pr[\text{delay} \ge D_{\text{max}}] \approx e^{-\theta C_e D_{\text{max}}}.$$
 (61)

Meanwhile, system's availability (or reliability in case of no repairs) is given by $A=1-P_{\rm out}$. Conventionally, a system's tolerance to long delay is measured by the delay exponent θ . The system tolerates large delays for small values of θ (i.e., $\theta \to 0$) while for large values of θ , it becomes more delay-sensitive.

The following examples aim to facilitate a practical understanding of the effective capacity and the corresponding trade-off between latency and availability in a real communication scenario.

EXAMPLE 10. Consider 5G New Radio numerology 1 transmission with $C_e = 1$ bpcu, for which the symbol period is 35.7 μ s. For a delay outage probability of $P_{\text{out}} = 10^{-5}$ (i.e., 99.999% availability), the network can tolerate, on average, a maximum delay of $\delta = 1151$ symbol periods (≈ 41 ms) for $\theta = 0.01$, and $\delta = 115$ symbol periods (≈ 4.1 ms) when $\theta = 0.1$.

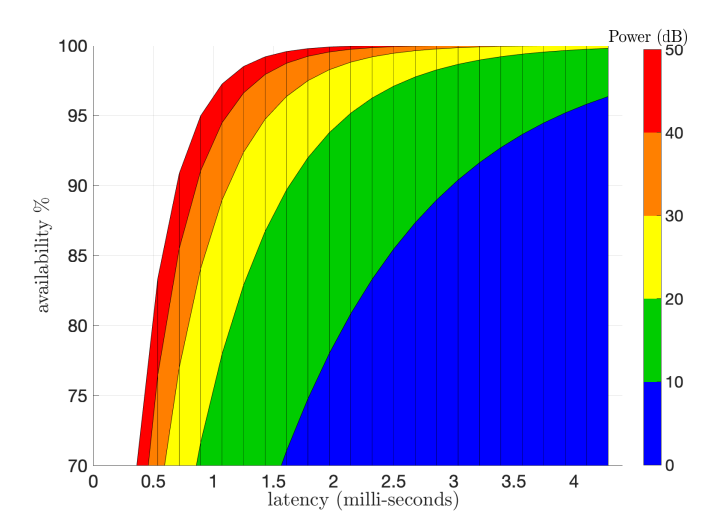


Fig. 16. Trade-off between availability, latency, and power consumption for 5G New Radio in Rayleigh fading.

EXAMPLE 11. Consider a Rayleigh block fading channel with blocklength T_f . For a transmission rate r and channel fading coefficient $|h|^2$, then

$$C_e(r,\theta) = -\frac{1}{\theta T_f} \ln \left(E_{|h|^2} \left[e^{-\theta T_f r} \right] \right)$$
 (62)

in bpcu. In case of fixed rate transmission with no CSI availability at the transmitter, a transmission outage may occur if the transmission rate is higher than the channel capacity. For Rayleigh fading channel, the mean outage probability for a transmission SNR of ρ is given by

$$\epsilon = \Pr[\log_2(1 + \rho z) < r] = 1 - e^{-\frac{2^r - 1}{\rho}}.$$
 (63)

Due to the fast channel variation, the transmission might be successful with probability of $1-\epsilon$. In case of transmission failure, the transmission rate is effectively zero; then, the average effective capacity is given by

$$C_e(r,\theta) = -\frac{1}{\theta T_f} \ln \left(\epsilon + (1 - \epsilon) e^{-\theta T_f r} \right). \tag{64}$$

Fig. 16 depicts the trade-off between availability, latency, and power consumption from the effective capacity perspective for 5G New Radio numerology 1 with symbol period of 35.7 μ s, and transmission rate of 0.5 bpcu. The maximum arrival rate is set to $C_e = 0.2$ bpcu. The figure shows a contour plot for the achievable availability-latency regions for different transmit power ranges. This reveals the contradicting achievability of URLLC transmission where achieving both high availability and low latency together requires high power consumption. We also observe that there is a dead zone of extremely low latency (below 1.5 ms) and high availability (>99%) that can not be achieved at the same time for this setup except at extremely high transmit power. For more details about how Fig. 16 was generated, one can refer to Algorithm 3.

Algorithm 3: Solving the statistical interplay between availability, latency, and power consumption

Input: Ce, T_f , and r.

1 for every ρ and D_{max} do

2 | Compute ϵ using (63)

3 | Solve (64) for θ^* 4 | Compute $A = 1 - P_{\text{out}}$ using (61)

5 end

Output: $\{A, D_{max}, \rho\}$ triplets

B. Stochastic Network Calculus

SNC is a framework that enables the end-to-end analysis of networks by means of non-asymptotic performance bounds. SNC builds upon the theory of network calculus, which analyzes performance guarantees of queuing systems via convolutional forms based on (min,+) dioid algebra. Network calculus enables the derivation of workcase performance bounds such as backlog and delay. In the deterministic case, network calculus models the arrival and service process as envelope functions, and thus, it does not capture the stochasticity of the arrival and service processes. SNC addresses this issue by relaxing the deterministic assumptions introduceing envelope violation probability [104]-[106]. Compared to conventional queuing theory, SNC is broader and includes several stochastic processes such as long-range dependent, self-similar, and heavy-tailed traffic. In addition, it can incorporate the variability of wireless fading channels.

Fidler and Rizk provide a comprehensive guide to SNC in [104]. Commonly, SNC resorts to envelope functions of the MGF of the arrival and service processes. Nonetheless, the framework is robust and supports general envelope models and models that provide strong guarantees. For instance, statistical delay analysis in fading channels is introduced [105] using a new representation based on the Mellin transform, and a (min, ×) calculus, leading to tractable closedform results that incorporate the channel variability to the model, yielding non-asymptotic performance bounds of the fading and arrival processes [105]. Due to its properties, SNC, and its simplified variants, effective bandwidth and effective capacity, are suitable for modeling end-to-end performance in URLLC (e.g., see [106]–[111]).

Next, we focus on the fundamental components of SNC, namely the arrival process (cumulative number of bits arriving) between times τ and t, $t \ge \tau \ge 0$, $A^{\circ}(\tau, t)$, the service process (e.g., dynamic server), $S^{\circ}(\tau, t)$, and the departure process, $D^{\circ}(\tau, t)$. We can relate these quantities as

$$D^{\circ}(t) \ge \min_{\tau \in [0,t]} \left\{ A^{\circ}(\tau) + S^{\circ}(\tau,t) \right\}, \tag{65}$$

where $A^{\circ}(0) = A^{\circ}(t,t) = 0$ and $S^{\circ}(0) = S^{\circ}(t,t) = 0$, $\forall t \geq 0$, and both arrival and service functions are non-negative. In addition, assuming a first-come first-served approach, the delay bound at time $t \geq 0$ is

$$W(t) \le \min \left\{ w \ge 0 : \max_{\tau \in [0,t]} \left\{ A^{\circ}(\tau, t) - S^{\circ}(\tau, t + w) \right\} \le 0 \right\}.$$
 (66)

For other arrival-service approaches see [104].

To calculate the actual delay bounds, we resort to i) affine traffic envelope functions, introduced in deterministic network calculus, and denoted as $\varrho(t-\tau)+b$, where ϱ is a rate parameter related to the traffic and b is the burst parameter; and ii) MGFs, from effective bandwidth theory, since it determines the distribution of a random process, and the sum of two or more random processes can be calculated by the product of their MGFs. We write the MGF of the arrival process as

$$M_A(\theta, t - \tau) = \mathbb{E}\left[\exp\left(\theta A^{\circ}(t, \tau)\right)\right] \le \exp\left(\theta(\varrho(t - \theta) + b)\right), \quad (67)$$

where $\theta \ge 0$ is a free parameter. Similarly, we can write the MGF of the service process as

$$M_S(\theta, t - \tau) = \mathbb{E}\left[\exp\left(-\theta S^{\circ}(t, \tau)\right)\right] \le \exp\left(-\theta(\varrho(t - \theta) + b\right).$$
 (68)

Then, we calculate the delay bound as in (66) and upper bound the delay violation probability, i.e., $P_{out} = \Pr[W(t) > w]$ as in (76). Note that when we introduce fading to the model, the rate expressions include logarithmic terms, which makes it cumbersome to find closed-form expressions for MGFs and the metrics. To alleviate this issue, [105] introduces a transformation facilities analysis under fading conditions.

EXAMPLE 12. The log normalized MGFs of the arrival and service process are known as effective bandwidth [104], and effective capacity [103], respective as

$$B_e(\theta) = \frac{1}{\theta t} \ln M_A(\theta, t), \tag{69}$$

$$C_e(\theta) = -\frac{1}{\theta t} \ln M_S(-\theta, t). \tag{70}$$

Then, we can derive C_e as in (62) in Example 11.

Let us consider a simple arrival model known as two-state (ON-OFF) Markovian model. In this model, the data arrival process is described as a two-state discrete-time Markov chain, r bits arrive during ON state with an arrival rate of r bits/block, while no arrivals occur during the OFF state. Such system has a transition probability matrix $\mathbf{J} = \begin{pmatrix} p_{11} & p_{12} \\ p_{21} & p_{22} \end{pmatrix}$, where $p_{11} \in [0,1]$ denotes the probability of staying in the off state, while $p_{22} \in [0,1]$ denotes the probabilities are $p_{21} = 1 - p_{22}$ and $p_{12} = 1 - p_{11}$. At the steady state, the probability of ON state is $p_{ON} = \frac{1-p_{11}}{2-p_{11}-p_{22}}$ [112], [113]. Then, working out the MGF expressions for the arrival process, we obtain a closed-form expression for the effective bandwidth as

$$B_{e}(\theta) = \frac{1}{\theta} \log \left(\frac{1}{2} \left(p_{11} + p_{22} e^{r\theta} \right) + \frac{1}{2} \sqrt{\left(p_{11} + p_{22} e^{r\theta} \right)^{2} - 4(p_{11} + p_{22} - 1)e^{r\theta}} \right)$$

$$\stackrel{(a)}{=} \frac{1}{\theta} \log \left(1 - s + se^{r\theta} \right), \tag{71}$$

where (a) comes from a simplified version of the source with $p_{11} = 1 - s$ and $p_{22} = s$, hence $p_{ON} = s$. Thus, the parameter s can be interpreted as a measure of the burstiness, which is relevant to model different traffic generated by a device. Then, the maximum average arrival rate is $\overline{r}_{max} = r p_{ON}$.

For the particular case when $B_e(\theta) = C_e(\theta)$, we can calculate the maximum average arrival rate of the discrete-time Markov source supported by the wireless channel as

$$\overline{r}_{\max} = \frac{s}{\theta} \log \left(\frac{e^{\theta E_c(\theta)} - (1 - s)}{s} \right). \tag{72}$$

Note that the SNC is general and accommodates the cases when $B_e(\theta) \neq C_e(\theta)$ given queuing stability constraints [104], [105]. Moreover, this framework can be extend to other types of sources for the effective bandwidth, or in general for the SNC. The maximum average arrival rate enables us to characterize the impact of the variability of the arrival process as function of the service process. Therefore, when the effective capacity is optimized, as in Example 11, we assess the impact of the arrivals so that fluctuations are accommodated, reducing delay violation and latency. All in all, SNC constitutes a valuable framework for the statistical QoS delay and end-to-end performance analysis of URLLC networks, whose traffic diverges from conventional light tailed models as discussed in [4], [12].

C. Age of Information

AoI was introduced in [114] as a tool to measure the degree of freshness of the received data corresponding to a certain process. It is defined as the time elapsed since the latest received packet about a process under observation was generated. Hence, the AoI at time t can be written as

$$\Delta(t) = t - t_g,\tag{73}$$

where $t_g < t$ is the generation time (i.e, timing anchor) of the most recently received packet [115]. Herein, in order to maintain fresh information, AoI should be minimized.

Note that, the minimization of AoI is a non-trivial problem of great interest. In fact, system utilization can be maximized by making the source send more and faster updates which would lead to packets congestion and higher delay. In this case, delay can be reduced by decreasing the rate of updates. Alternatively, decreasing the update rate can lead to the destination having outdated information due to lack of updates. Hence, timely updating a destination about a remote process is neither the same as maximizing the system utilization nor reducing the delay.

The design of URLLC focuses more on peak and tail age metrics rather than the average AoI. In what follows, we discuss two important metrics of information freshness in time-sensitive applications, e.g., remote factory automation, where decisions should be based on fresh information.

1) Peak AoI: measure of the maximum AoI that could occur within a network. Therefore, the peak AoI measures the worst case scenario with respect to reliability. Many works have studied the peak AoI for different network models. According to [116], the average peak AoI for the M/M/1 model is given by

$$\hat{\Delta}_{M/M/1} = \frac{1}{\mu} \left(1 + \frac{1}{\rho_o} + \frac{\rho_o}{1 - \rho_o} \right),\tag{74}$$

where λ is the arrival rate, μ is the service rate, $\rho_o = \frac{\lambda}{\mu}$ is the server utilization. Moreover, for the just-in-time

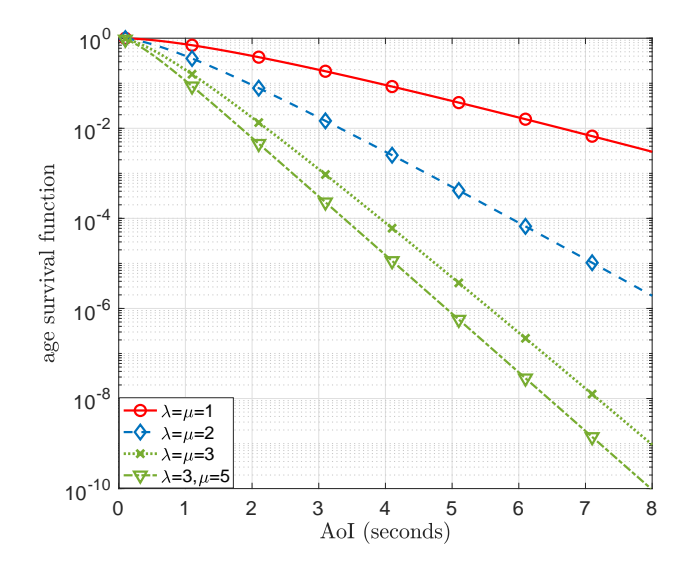


Fig. 17. Age survival function.

transmission model, a packet is generated at time t_i and received at $t_{i+1} = t_i + d_{i+1}$, where d_{i+1} is the service time of packet i. Notice that a new packet is instantaneously generated by the source node and starts its service time right after the current update packet in service is received at the destination node. The average peak AoI of this model is given by [117]

$$\hat{\Delta}_{JiT} = \frac{1}{N-1} \sum_{i=1}^{N-1} d_i + d_{i+1},\tag{75}$$

which is dependent only on the average service time.

2) Age survival function: complimentary CDF of the AoI, i.e., $\bar{F}_{AoI}(t)$. It allows computing the probability that the AoI exceeds a certain threshold Δ_{th} , i.e., $\bar{F}_{AoI}(\Delta_{th})$, which is referred to as age violation probability. This is relevant for time-sensitive networking, where the age violation probability should not exceed a small value ϵ , i.e.,

$$\bar{F}_{AoI}(\Delta_{th}) = \Pr[\Delta(t) \ge \Delta_{th}] \le \epsilon.$$
 (76)

EXAMPLE 13. Consider an M/M/1 last-come first-serve transmission with preemption. According to [118], the age survival function for this case is given by

$$\bar{F}_{AoI}(t) = \begin{cases} \frac{\lambda}{\lambda - \mu} e^{-\mu t} - \frac{\mu}{\lambda - \mu} e^{-\lambda t}, & \lambda \neq \mu \\ (\lambda t + 1) e^{-\lambda t}, & \lambda = \mu \end{cases}$$
(77)

which is depicted in Fig. 17 for different values of μ and λ . Obviously, the age survival function decays with the age, and more rapidly for higher values of λ and/or μ . For example, $\lambda=3$ and $\mu=3$, the age survival function is about 10^{-2} for $\Delta(t)>2$ s. This means that the AoI exceeds 2 seconds for only 1% of the time. This is because the queue updates arrive and are served more rapidly resulting in fresher information at the receiver side. For the same setup, the age survival percentage becomes even lower ($\approx 0.5\%$) when increasing the service rate μ to 5. This is because the queue is able to deliver data faster which improves information freshness. Meanwhile, for $\lambda=1$ and $\mu=1$, the AoI exceeds 2 s for

more than 50% of the time, since the amount of updates and service time are low, which results in less fresh data at the receiver.

VII. ANALYSIS & DESIGN OF LARGE-SCALE URLLC

Here, we overview some key mathematical and algorithmic tools for designing and/or assessing the performance of large-scale URLLC systems.

A. Meta Distribution

In general, the performance of wireless networks is highly influenced by their spatial configuration because phenomena like large and small scale fading, shadowing, and cochannel interference, are location dependent. Hence, it is not surprising that the stochastic geometry, which allows modeling the network as a point process, constitutes a fundamental theoretical tool for the analysis and characterization of large-scale wireless systems such as cellular, *ad-hoc*, vehicular, RF wireless power transfer, and satellite networks [19], [66], [119]–[131].

Within the stochastic geometry framework, the most popular performance metric is the success probability of the transmission over the typical link of a point process Φ , which is defined as the probability that the corresponding SINR is greater than a given threshold $\gamma_{\rm th}$, i.e., $p_s(x_{\rm th}) \triangleq \Pr[{\rm SINR} \geq \gamma_{\rm th}] = 1 - F_{\rm SINR}(\gamma_{\rm th})$. However, large-scale URLLC systems cannot directly benefit from $p_s(\gamma_{\rm th})$, neither for system design nor analysis, since the computation of such metric involves averaging over space (and/or time). Instead, a more refined metric has been proposed and leveraged in the last years: the *meta distribution* of the SINR, which is defined as

$$p_m(\gamma_{\rm th}, \xi) \triangleq \mathbb{P}^! \left(\Pr[\text{SINR} \ge \gamma_{\rm th} \mid \Phi] \ge 1 - \xi \right). \tag{78}$$

Here, $\mathbb{P}^!$ denotes the reduced Palm measure of Φ , 12 while $1-\xi$, with $\xi\in[0,1]$, denotes a target per-node success probability, where $\xi\ll 1$ in the context of URLLC. Note that $p_m(\gamma_{\rm th},\xi)$ denotes the fraction of users that attain an SINR of at least $\gamma_{\rm th}$ in $(1-\xi)$ fraction of the time, whereas $p_s(\gamma_{\rm th})$ just characterizes the fraction of users that can communicate successfully. Observe that $p_s(\gamma_{\rm th})$ can be obtained from $p_m(\gamma_{\rm th},\xi)$ as $p_s(\gamma_{\rm th})=\int_0^1 (1-\xi)p_m(\gamma_{\rm th},\xi) {\rm d}\xi$, thus, $p_m(\gamma_{\rm th},\xi)$ is indeed a broader performance metric.

Example 14 (Meta-Analysis of a Large-Scale Network). Assume the setup described in Example 4, but where the communicating (typical) nodes are at a distance r_0 between each other while the interfering nodes are distributed according to a bi-dimensional homogeneous Poisson point process Φ with density λ . Thus, the total number of interfering nodes is infinite, i.e., $K \to \infty$, but the number of interfering nodes in a given area $A \subset \mathbb{R}^2$ is finite and follows a Poisson distribution with mean λA . Ignore the

noise power for simplicity, and assume no power control mechanism such that the average SNR (with respect to the Rayleigh small-scale fading) of the receive and interfering signal is given by $\bar{\gamma}_k = r_k^{-\alpha} \ \forall k \in \Phi \cup 0$, where $\alpha > 2$, thus $\overline{SIN} R = r_0^{-\alpha} / \sum_{k \in \Phi} r_k^{-\alpha}$. Then, by substituting (27) into (78), one obtains

$$p_{m}(\gamma_{\text{th}}, \xi) \leq \mathbb{P}^{!}\left(\exp(-\gamma_{\text{th}}r_{0}^{\alpha}\nu) \geq 1 - \xi\right)$$

$$= F_{V}\left(-\frac{\ln(1 - \xi)}{\gamma_{\text{th}}r_{0}^{\alpha}}\right), \tag{79}$$

where $v \triangleq \sum_{k \in \Phi} r_k^{-\alpha}$ is the average interference with respect to small-scale fading realizations (or alternatively, interference without fading [119]). Now, since V is obtained via transformations to RVs $\{r_k\}$, one may exploit latters' distributions, which were provided in [120] for Poisson networks, and/or a procedure exploiting the probability generating functional of a Poisson point process, to compute (79). Unfortunately, this has been proved to be a cumbersome task for general path-loss exponents, i.e., $\alpha > 2$. Fortunately, for some special cases, e.g., $\alpha \in \{3,4,5,6,8,10,12\}$, $f_V(v)$ has been derived in closed- or semi-closed form [119], [121]. For instance, for $\alpha = 4$, the PDF of V is given by [119]

$$f_V(\nu) \stackrel{\alpha=4}{=} \frac{\pi \lambda}{2\nu^{3/2}} \exp\left(-\frac{\pi^3 \lambda^2}{4\nu}\right). \tag{80}$$

By leveraging (80), one can get back to (79) to bound $p_m(\gamma_{th}, \xi)$ as

$$p_{m}(\gamma_{\text{th}}, \xi) \leq \int_{0}^{-\frac{\ln(1-\xi)}{\gamma_{\text{th}}r_{0}^{\alpha}}} f_{\nu}(\nu) d\nu$$

$$\stackrel{\alpha=4}{=} \int_{0}^{-\frac{\ln(1-\xi)}{\gamma_{\text{th}}r_{0}^{\alpha}}} \frac{\pi \lambda}{2\nu^{3/2}} \exp\left(-\frac{\pi^{3}\lambda^{2}}{4\nu}\right) d\nu$$

$$\stackrel{(a)}{=} \frac{1}{\sqrt{\pi}} \Gamma\left(\frac{1}{2}, \frac{\pi^{3}\lambda^{2}}{4\nu}\right) \Big|_{\nu=0}^{\nu=-\frac{\ln(1-\xi)}{\gamma_{\text{th}}r_{0}^{\alpha}}}$$

$$\stackrel{(b)}{=} \frac{1}{\sqrt{\pi}} \Gamma\left(\frac{1}{2}, -\frac{\pi^{3}\lambda^{2}\gamma_{\text{th}}r_{0}^{\alpha}}{4\ln(1-\xi)}\right), \tag{81}$$

where (a) follows from solving the indefinite integral by exploiting [132, eq. (2.325.6)], while (b) comes from evaluating the extremes.

The above bound is expected to be tight because of the same reasons given in Example 4. This is corroborated in Fig. 18, where $p_m(\gamma_{th}, \xi)$ is plotted against $1-\xi$. In Fig. 18, we do not only plot $p_m(\gamma_{th}, \xi)$ but also the success probability $p_s(\gamma_{th})$. The latter metric reveals that the average success probability in the network is 90% and 99.85% for a density of 10^{-5} and 10^{-7} nodes/ m^2 , respectively, but says nothing about the reliability performance per node. Instead, $p_m(\gamma_{th}, \xi)$ reveals directly the percentage of nodes achieving a reliability of $1-\xi$. Based on the results in Fig. 18, we can observe that only 44% of the nodes are operating with a success probability not inferior to 99% when $\lambda = 10^{-5}$ nodes/ m^2 , while that percentage of nodes increases up to 99.4% when $\lambda = 10^{-7}$ nodes/ m^2 .

Note that $p_m(\gamma_{th}, \xi)$ can be leveraged to properly adjust the per-link reliability via rate control, which does not affect the SINR realizations, thus potentially guaranteeing

¹¹Recall that URLLC mandates a radical departure from expected utility-based approaches relying on average quantities [12].

¹²Also, given that there is an active transmitter (as in case of bipolar networks) or receiver (as in cellular networks) at a prescribed location and the SIR is measured at the receiver.

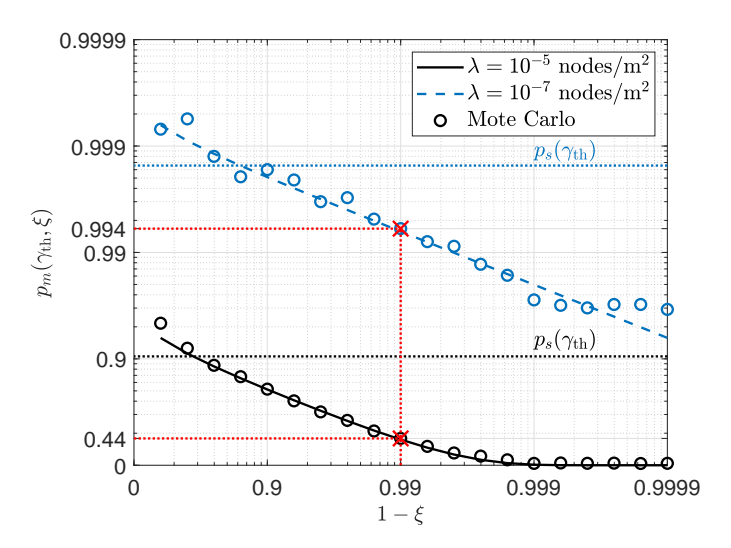


Fig. 18. Meta distribution of the SIR as a function of $1-\xi$ for $\lambda \in \{10^{-5},10^{-7}\}$ nodes/m². We set $\gamma_{th}=-10$ dB, $r_0=80$ m, and $\alpha=4$.

network-wide reliability guarantees [129]. Moreover, similar to the SINR or SIR meta distribution, one can formulate the meta distribution of other relevant figures, e.g., the energy in wireless-powered networks [127], the secrecy rate in the presence of eavesdroppers [122], and the number of transmission attempts to accomplish a success or reliability guarantee. In fact, outside the stochastic geometry framework, the so-called *meta-probability* is leveraged in [3], [4], [77], at least implicitly, to impose stricter and more firm guarantees on URLLC design/performance.

Unfortunately, MC methods for estimating $p_m(\gamma_{\rm th},\xi)$ are in general computationally-expensive as they require separate averaging over fading and point realizations. Meanwhile, analytical closed-form characterizations are not often attainable, as in case of Example 14 for any $\alpha>2$. Therefore, efficient numerical and approximate analytical methods for obtaining $p_m(\gamma_{\rm th},\xi)$ take significant relevance here. The most prominent methods include moment-matching, the Gil-Pelaez theorem, and bounding approaches such as Markov inequalities and Paley-Zygmund bound (refer to Section III) [66], [123]. Interestingly, the beta distribution (by default defined in [0,1]) and the Fourier-Jacobi expansion framework fit typical meta distributions with high accuracy in most cases [123].

B. Clustering

Clustering relies on building groups or hierarchies among *points/observations* based on their (dis-)similarities. The main clustering methods and example algorithms are summarized in Table. IX and described briefly in the following.

1) Partitioning methods: The most popular partitioning method, K-Means (K-Modes for categorical data), iteratively relocates the cluster centers by computing the points' mean (mode). K-Means scales well on huge data sets, even though, it is very sensitive to outliers and fails to perform well on arbitrary shapes of data. These issues are mitigated by K-Medoids, which chooses actual data points as centers

TABLE IX
MAIN CLUSTERING METHODS AND EXAMPLE
ALGORITHMS/IMPLEMENTATIONS

Method	Description	Implementations
Partitioning	Partitioning the data by grouping similar items. The results vary according to a pre-defined number of clusters.	 K-Means K-Medoids K-Modes
Hierarchical	Decomposing the data hierarchically. The number of clusters is not specified in advance.	AgglomerativeDivisive
Others	Special methods that group the the items according to their density or another abstract model.	Density-basedModel-based

(medoids or exemplars), and can be used with arbitrary dissimilarity measures.

- 2) Hierarchical methods: There are two main types of hierarchical methods [133]: i) agglomerative, where each point starts in its own cluster, and pairs of clusters are merged as one moves up the hierarchy; and ii) divisive, where all points start in one cluster, and splits are performed recursively as one moves down the hierarchy. For clusters' merging/splitting, not only a distance metric, but also a linkage criterion specifying the dissimilarity of clusters as a function of the pairwise distances of points in the clusters, must be specified. Merges/splits are often determined in a greedy manner, and the results are presented in a dendrogram.
- 3) Other methods: In density-based clustering, the points that are highly dense are grouped together, which allows identifying low-density/extreme points. Meanwhile, model-based approaches involve applying a model to find the best cluster structures.

In the context of large-scale URLLC, clustering algorithms can be mainly leveraged for:

- · Configuration of NOMA groups.
- NOMA promotes spectral and energy efficiency, which are both relevant performance figures in large-scale systems. A key challenge here lies in the optimal grouping of users exploiting the same orthogonal spectrum resource. It has been shown in [19], [134] that users with the most heterogeneous characteristics/requirements should be clustered together for optimum performance.
- Pilot allocation.
- Assigning orthogonal pilots to all users becomes inefficient, or even unaffordable, as the network grows. This issue can be addressed by resorting to clustering based on *i*) channel covariance matrices such that the pilots are reused among the users having sufficiently orthogonal channel subspaces [135], [136], and/or *ii*) traffic profiles such that devices with smaller activation probabilities (more stringent reliability requirements) can be grouped in clusters with smaller (greater) pilot pools [16].
- Data aggregation.
 In large-scale systems, devices may be clustered in

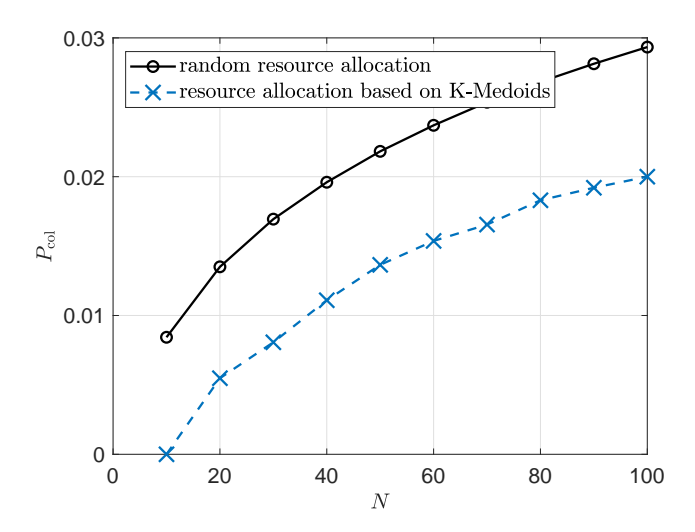


Fig. 19. Average collision probability as a function of the number of devices. We set $A_{i,j} = (i+j+|i-j|)^{-1}, \forall i,j \in \{1,2,\cdots,N\}$ and L=10.

local area networks, which then connect to the core networks through a gateway or data aggregator [126], [129], [137]–[141]. Instead of a traditional spatial clustering relying on geometric distances and/or energy-related measures [126], [129], [137]–[140], a more advisable approach in the context of large-scale URLLC lies in jointly considering traffic profiles (both in terms of traffic intensity and performance requirements), and network dynamics. Interestingly, the authors in [141] have initially proposed a priority-based spatial aggregation algorithm that gives priority to URLLC devices through power ramping in the physical random access channel.

· Coordinated multi-point.

In coordinated multi-point scenarios, a group of network nodes (e.g., base stations) transmits/receives the same data to/from a device, thus inducing spatial diversity, which is key for supporting large-scale URLLC. Here, clustering plays a key role in selecting the set of network nodes for jointly serving each device. This can be implemented based on the instantaneous reference signal received power [142], SNR [143], distance [144] or even links LOS/non-LOS classification [21] from multiple network nodes.

Next, we illustrate how clustering can also be leveraged for access resource scheduling in large-scale systems.

EXAMPLE 15 (CLUSTERING-BASED ACCESS SCHEDULING).

Consider a set $\mathcal{N} = \{1, 2, \cdots, N\}$ of devices with a given activation matrix $\mathbf{A} \in [0, 1]^{N \times N}$, where $A_{i,j}$ denotes the probability that devices $i, j \in \mathcal{N}$ become simultaneously active, thus, \mathbf{A} is symmetric, while $A_{i,j} \leq A_{i,i}$ and $A_{i,j} \leq A_{j,j}$. Such activation matrix can be learned over time [145], [146]. Moreover, assume that there is a set \mathcal{L} of L < N orthogonal spectrum resources either in time/frequency/code domain that can be used by the devices to access the wireless medium. Consider that a given spectrum resource $l \in \mathcal{L}$ is allocated to a sub-set of devices $\mathcal{N}_l \subset \mathcal{N}$, and assume

 $\bigcup_{l \in \mathscr{L}} \mathscr{N}_l = \mathscr{N}$ and $\mathscr{N}_{l_1} \cap \mathscr{N}_{l_2} = \emptyset$, $\forall l_1, l_2 \in \mathscr{L}$ and $l_1 \neq l_2$. A collision occurs if at least two devices attempt to access the medium by exploiting the same orthogonal resource, thus, the collision probability within the l-th spectrum resource is given by

$$P_{col}^{(l)} = \sum_{i \in \mathcal{N}_l} A_{i,i} \left[1 - \prod_{j \in \mathcal{N}_l, j > i} (1 - A_{i,j}) \right], \tag{82}$$

while

$$P_{col} = \frac{1}{L} \sum_{l \in \mathcal{L}} P_{col}^{(l)} \tag{83}$$

denotes the average collision probability in the network.

The optimum resource allocation comes from solving $\underset{\mathcal{N}_{l},\forall l \in \mathcal{L}}{\mathbb{Z}P_{col}}$, which is an NP-hard problem due to its combinatorial structure. Interestingly, a sub-optimal but also scalable and simple approach relying on K-Medoids clustering can be designed by adopting $d_{i,j} = \mathbb{I}\{i \neq j\}A_{i,j}$ as dissimilarity measure between points (devices) $i, j \in \mathcal{N}$. In this way, two devices with small joint activation probability are likely to be clustered together. Fig. 19 illustrates the attainable performance gains of such an approach with respect to a traditional pure random allocation. Here, we would like to emphasize that the adopted K-Medoids approach is by no means optimized, and better results may be attainable by, e.g., more tightly coupling the dissimilarity measure with the problem's objective.

C. Compressed Sensing

Compressed sensing comprises a set of mathematical tools for either fully or partially recovering sparse signals from a small set of measurements. The sparsity $f(\mathbf{s})$ of a given signal \mathbf{s} is defined as the number of non-zero entries, i.e., $f(\mathbf{s}) = ||\mathbf{s}||_0$. Moreover, \mathbf{s} is considered to be sparse if $f(\mathbf{s})$ is sufficiently small compared with the dimension of

Assume $\mathbf{s} \in \mathbb{C}^n$ is sparse, i.e., $f(\mathbf{s}) \ll n$, and needs to be estimated from m < n samples that are collected via a sensing matrix $\mathbf{H} \in \mathbb{C}^{m \times n}$ as

$$\mathbf{y} = \mathbf{H}\mathbf{s} + \mathbf{w},\tag{84}$$

where $\mathbf{y} \in \mathbb{C}^m$ and $\mathbf{w} \in \mathbb{C}^m$ denote respectively the receive and noise signals. Then, compressed sensing problems are commonly formulated to find the sparsest signal such that the estimated measurement noise power is upper bounded by a pre-configured noise level η as

$$\mathbf{s}^* = \operatorname{argmin}_{\mathbf{s}} f(\mathbf{s}), \text{ s.t. } ||\mathbf{y} - \mathbf{H}\mathbf{s}||_2^2 \le \eta.$$
 (85)

Observe that the number of possible vectors \mathbf{s} that satisfy $||\mathbf{y} - \mathbf{H}\mathbf{s}||_2^2 \leq \eta$ is potentially infinite since $\mathbf{y} = \mathbf{H}\mathbf{s}$ is an underdetermined system of equations. However, the sparsity-reduction objective function forces the solution to be unique, the sparsest one. Unfortunately, since $f: \mathbb{C}^n \to \{0,1,\cdots,n\}$, there is no way but to rely on a combinatorial search to get the optimum solution of (85). The complexity of this approach increases exponentially in n, thus, the ℓ_0 -norm minimization approach is infeasible for most realworld applications [147].

Several techniques and heuristics have been suggested in the last few years to solve (85), including regularization, greedy, and message-passing approaches. Specifically,

- regulation techniques, e.g., the ℓ_1 -norm approximation of the ℓ_0 -norm [148], [149] and the alternative direction method of multipliers [150], rely on transforming (85) into a convex problem via regularized, often iterative, procedures;
- greedy algorithms, e.g., orthogonal matching pursuit [151], make a local optimal selection at each time with either the hope of ultimately finding the global optimum solution, or just a sufficiently good local solution with low complexity and/or in a reasonable amount of time; and
- message-passing algorithms exploit factor graphs [152], thus, the *a posteriori* distribution of the signal to be reconstructed.

In wireless communications, compressed sensing has been exploited for solving problems related to sparse estimation/detection and support identification [147], [153]–[155]. The latter relates to a partial recovering of **s**, specifically, of the indexes of the non-zero elements of **s**, and it is particularly relevant here as it can mimic the multi-user detection problem in massive MTC systems with grant-free and sporadic random access. We next discuss an example linking both the multi-user detection and support identification problems. A simple approximate message-passing (AMP) solving algorithm relying on iterative thresholding is also provided. Readers are encouraged to refer to [147] for additional examples on how the compressed sensing framework can be applied to wireless communications-related problems.

EXAMPLE 16 (SPARSE MTC ACTIVITY DETECTION [153]).

Consider the uplink communication between a coordinator with M antennas and N single antenna devices, out of which only a few are simultaneously active. Quasi-static fading is assumed, and the small-scale channel between the n-th device and the coordinator is denoted as \mathbf{h}_n . The coherence interval comprises τ samples, out of which τ_p are used for user identification (and potentially channel estimation). The coordinator is aware of the pilot sequence associated to each device, whereas \mathbf{h}_n coefficients, which change independently between consecutive coherence intervals, are unknown.

The signal $\mathbf{Y} \in \mathbb{C}^{\tau_p \times M}$ received at the coordinator in a given user identification phase can be written as

$$\mathbf{Y} = \sum_{n=1}^{N} \sqrt{\tau_p \tilde{\gamma}} \alpha_n \varphi_n \mathbf{h}_n^T + \mathbf{W}$$
$$= \sqrt{\tau_p \tilde{\gamma}} \mathbf{\Phi} \mathbf{S}^T + \mathbf{W}$$
 (86)

where α_n denotes the device activity indicator for device n, $\bar{\gamma}$ is the average SNR of the signal received at the coordinator from each active device, $\sqrt{\tau_p}\varphi_n\in\mathbb{C}^{\tau_p}$ with $||\varphi||_2^2=1$ is the pilot sequence of the n-th device, and \mathbf{W} is the powernormalized AWGN samples. Observe that the signals arrive at the coordinator with the same average SNR, which can

Algorithm 4: AMP for MTC activity detection

```
Input: Y, \psi
1 Initialization: \hat{\mathbf{S}}^0 = \mathbf{0}, \mathbf{R}^0 = \mathbf{Y}, t = 0
2 repeat
3 \begin{vmatrix} \hat{\mathbf{s}}_n^{t+1} = \vartheta((\mathbf{R}^t)^H \varphi_n + \hat{\mathbf{s}}_n^t), \ \forall n \end{vmatrix}
4 \mathbf{R}^{t+1} = \mathbf{Y} - \mathbf{\Phi}(\hat{\mathbf{S}}^{t+1})^T + \frac{1}{\tau_p} \mathbf{R}^t \sum_{\forall n} \vartheta'((\mathbf{R}^t)^H \varphi_n + \hat{\mathbf{s}}_n^t)
5 \begin{vmatrix} t = t + 1 \end{vmatrix}
6 until convergence or maximum number of iterations;
7 \forall n: set \hat{\alpha}_n = 1 if ||\hat{\mathbf{s}}_n^t||_2 \ge \psi, \hat{\alpha}_n = 0 otherwise
```

Output: $\{\hat{\alpha}_n\}$

be motivated by the use of a statistical inverse power control at the devices. Moreover, $\mathbf{\Phi} = [\varphi_1, \varphi_2, \dots, \varphi_N] \in \mathbb{C}^{\tau_p \times N}$ constitutes the pilot matrix, while $\mathbf{S} = [\mathbf{s}_1, \mathbf{s}_2, \dots, \mathbf{s}_N] \in \mathbb{C}^{M \times N}$, where $\mathbf{s}_n \triangleq \alpha_n \mathbf{h}_n$, is an effective channel matrix. Here, \mathbf{S} has a sparse structure as the rows corresponding to inactive users are zero. Therefore, the activity detection problem reduces to finding the non-zero rows of \mathbf{S} .

Algorithm 4 iteratively solves the above problem. Note that $\vartheta(\cdot)$ is a denoising function, which for the multiuser detection problem can be defined as in [153, eq. (11)]. Meanwhile, $\vartheta(\cdot)'$ is the first order derivative of $\vartheta(\cdot)$ and \mathbf{R}^t is the signal residual at iteration t. In step 1, all the devices are assumed inactive, while the estimate $\hat{\mathbf{S}}^t = [\hat{\mathbf{s}}_1^t, \hat{\hat{\mathbf{s}}}_2^t, \cdots, \hat{\hat{\mathbf{s}}}_N^t]$ and the residual signals are then iteratively updated in steps 3 and 4, respectively. In the case of the latter, a crucial term containing $\vartheta(\cdot)'$, called the Onsager term, is included as it has been shown to substantially improve the performance of the algorithm. Observe that the estimated activity indicators are returned as output of the algorithm after hard-thresholding. Specifically, the ℓ_2 -norm of each $\hat{\mathbf{s}}_n^t$ is compared with a given threshold to decide whether the n-th device is active. $\hat{\mathbf{s}}_n^t$

Unfortunately, AMP algorithms such as that illustrated in Algorithm 4 face several inconveniences. On the one hand, prior distributions of the device activity patterns and channels are usually unknown. On the other hand, the design of the denoising function $\vartheta(\cdot)$ becomes tedious, if not impossible, in most practical cases of known prior distributions. Indeed, typical prior assumptions that are difficult to handle include correlated activation patterns and/or other than zero-mean Gaussian channels. To alleviate these issues, expectation propagation algorithms [156], [157] have emerged as a more flexible (less model-dependent) approach. Moreover, it should be noted that although the basic expectation propagation algorithms are in general more computationally complex than the AMP, several stateof-the-art complexity-reduction techniques (e.g., see [158]-[161]) may be implemented to make them even more appealing in practice.

Notice that configuring the hyperparameters of the algorithm might also be quite challenging, specially for URLLC

 $^{^{13}}$ The channel estimates could be easily obtained as well as they match the entries of **S** associated to the non-zero activity indicators. Nevertheless, they could be still refined in a last step by leveraging traditional MMSE channel estimators but considering only the group of detected devices.

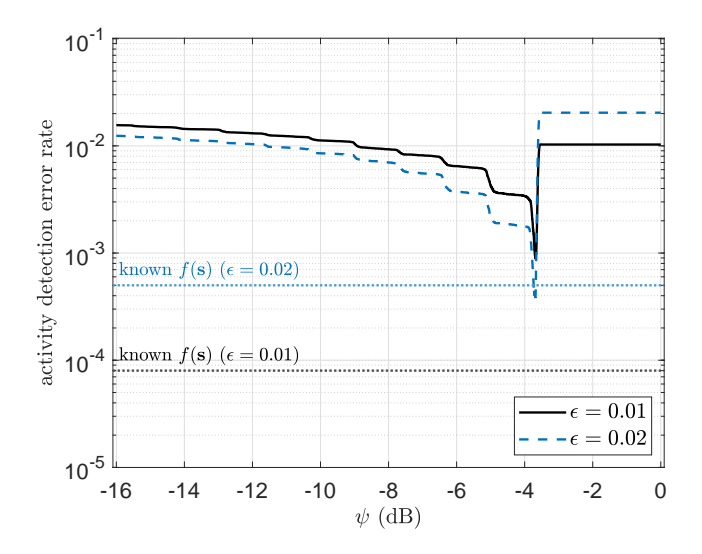


Fig. 20. Average error rate as a function of the detection threshold. We have assumed Rayleigh fading channels, i.i.d activation of the devices with $\Pr[\alpha_n=1]=\epsilon$ and $\Pr[\alpha_n=0]=1-\epsilon$, and Bernoulli pilots as in [153]. Moreover, we set $\tau_p=48$, M=64, N=200, and $\tilde{\gamma}=20$ dB.

systems with stringent performance requirements. In case of Algorithm 4, the main issue is related to properly configuring the decision threshold ψ . Notice that a relatively large (small) ψ reduces the probability of misdetection (false-alarm), but at the cost of triggering many false-alarm (misdetection) events. In fact, this is not only an issue of AMP implementations, but of most state-of-the-art procedures, as those based on regulation techniques, greedy and other message-passing algorithms.

In general, prior procedures aiming at estimating certain raw features of s can potentially mitigate the previous issue and assist the posterior estimation based on compressed sensing. For instance, the authors in [162] proposed coordinated pilot transmission mechanisms that can be run prior to the multi-user detection phase, as that described in Example 16, to detect the signal sparsity level (number of active devices), i.e, f(s), in each coherence interval. With such information, one can directly modify the step 7 in Algorithm 4 such that only the f(s) devices with the greatest associated equivalent channel powers are declared as active, thus, completely avoiding the tuning of a decision threshold. The potential performance gains of such an approach are illustrated in Fig. 20 in terms of activity detection error rate. Note that the regularized multi-user detection algorithms proposed in [163]-[167] directly exploit this information as well, although no work prior to [162] had specified how such information could be obtained. Finally, observe that a completely deterministic/accurate prior on $f(\mathbf{s})$ may not be available in practice, and one may need to consider the probability mass function of $f(\mathbf{s})$ for the multi-user detection phase design of large-scale grant-free URLLC systems.

D. Mean Field Game Theory

Mean-field (MF) game theory is an attractive tool for describing and optimizing networks with an asymptotically large number of inter-device interactions [168].

Consider a very large set \mathscr{S} of nodes, and let $s \in \mathscr{S}$ to represent a rational node/agent with associated set of states $\mathscr{X}_s \subset \mathbb{R}^n$ and set of actions \mathscr{A}_s . Then, one can formulate a strategic game $\mathscr{G} = (\mathscr{S}, \mathscr{A}, \mathscr{X}, \{u_s\})$, where $\mathscr{A} = \mathscr{A}_1 \times \cdots \times \mathscr{A}_{|\mathscr{S}|}$ and $\mathscr{X} = \mathscr{X}_1 \times \cdots \times \mathscr{X}_{|\mathscr{S}|}$ denote the overall action and state profiles, respectively, while u_s is the average utility function of s. While traditional game theory approaches consider the individual interactions among agents, MF game theory takes advantage of the massiveness of the network assuming that $|\mathscr{S}| \to \infty$ to approximate the solution.

The common underlying assumptions are:

- at any given time instance $t \in [0, T]$, individual agents' states $\mathbf{x}_s(t) \in \mathcal{X}_s$ and actions $\mathbf{a}_s(t) \in \mathcal{A}_s$ have a negligible impact on the game;
- the optimization criterion is invariant to the permutation of agents' indices;
- agents are indistinguishable, i.e., they share a common state and action space. This allows reducing the game to a generic agent with states $\bar{\mathbf{x}}(t) \in \bar{\mathscr{X}}$ and action $\bar{\mathbf{a}}(t) \in \bar{\mathscr{A}}$ playing against the MF distribution.

Let the state $\bar{\mathbf{x}}(t)$ to evolve according to $d\bar{\mathbf{x}}(t) = \mu(t)dt + \Lambda d\mathbf{w}(t)$, where $\mu:[0,T] \to \mathbb{R}^n$ is a deterministic function, $\mathbf{w}:[0,T] \to \mathbb{R}^n$ is a random process, and $\Lambda \in \mathbb{R}^{n \times n}$ is a constant matrix. Given a state transition from time $t \in [0,T]$ to $T: \bar{\mathbf{x}}(t) \to \bar{\mathbf{x}}(T)$, the utility function for the generic agent is given by

$$u(t,\bar{\mathbf{x}}(t),\bar{\mathbf{a}}(t)) = \mathbb{E}_{\bar{\mathbf{x}}} \left[\int_{t}^{T} f(\tau,\bar{\mathbf{x}}(\tau),\bar{\mathbf{a}}(\tau)) d\tau + c(T,\bar{\mathbf{x}}(T)) \right], \quad (87)$$

where $f:[0,T]\times\bar{\mathcal{X}}\times\bar{\mathcal{A}}\to\mathbb{R}$ is the instantaneous payoff, and $c:T\times\bar{\mathcal{X}}\to\mathbb{R}$ is a terminal cost associated with reaching state $\bar{\mathbf{x}}(T)$. The MF distribution, i.e.,

$$\rho(t, \bar{\mathbf{x}}(t)) = \lim_{|\mathcal{S}| \to \infty} \frac{1}{|\mathcal{S}|} \sum_{s=1}^{|\mathcal{S}|} \mathbb{I}\{\mathbf{x}_s(t) = \bar{\mathbf{x}}(t)\},\tag{88}$$

which approximates the collective behaviour of the whole population, is an implicit argument of f.

To solve the game, agents depart from a local estimate of (88) using other agents' initial states, and then run an iterative procedure. The latter consists in alternating between solving the optimal action from the Hamilton-Jacobi-Bellman equation, i.e.,

$$\frac{\partial u(t, \bar{\mathbf{x}}(t), \bar{\mathbf{a}}(t))}{\partial t} + \max_{\bar{\mathbf{a}}(t)} \left[\boldsymbol{\mu}^{T}(t) \frac{\partial u(t, \bar{\mathbf{x}}(t), \bar{\mathbf{a}}(t))}{\partial \bar{\mathbf{x}}} + f(t, \bar{\mathbf{x}}(t), \bar{\mathbf{a}}(t)) + \frac{1}{2} \mathbf{tr} \left(\Lambda^{2} \frac{\partial^{2} u(t, \bar{\mathbf{x}}(t), \bar{\mathbf{a}}(t))}{\partial \bar{\mathbf{x}}^{2}} \right) \right] = 0 \quad (89)$$

for a given MF distribution, and an improved estimate of the MF distribution from the Fokker-Planck-Kolmogorov equation, i.e.,

$$\frac{\partial \rho \left(t, \bar{\mathbf{x}}(t)\right)}{\partial t} + \frac{\partial}{\partial \bar{\mathbf{x}}} \left[\frac{\partial u \left(t, \bar{\mathbf{x}}(t)\right)}{\partial \bar{\mathbf{x}}} \rho \left(t, \bar{\mathbf{x}}(t)\right) \right] - \mathbf{tr} \left(\frac{\Lambda^2}{2} \frac{\partial^2 \rho \left(t, \bar{\mathbf{x}}(t)\right)}{\partial \bar{\mathbf{x}}^2} \right) = 0$$
(90)

given the action obtained from (89). Notice that the solution of a MF game, known as MF equilibrium, is guaranteed to converge to the Nash equilibrium in the asymptotic case $|\mathcal{S}| \to \infty$. However, since practical network deployments have a large but finite number of nodes, a MF game converges to an ϵ -approximate Nash equilibrium [169] in most of these settings. That is, some players may benefit when deviating from the equilibrium, thus violating the Nash equilibrium conditions, but the expected payoff gain will not be superior to ϵ .

In MF games, no information is exchanged among agents; thus, this approach is effective in reducing the signaling overhead of the network. This is appealing for meeting the ultra-low latency requirements in massive/dense URLLC systems. Take as an example a ultra-dense network, where the cells may experience high levels of interference due to their proximity. This demands effective interference management techniques, which may induce a severe signalling overhead if the cells treat the interfering links individually [170]. Instead, the problem can be recast as a MF game, which allows modeling the mutual interference experienced by all cells as an average interference over the state distribution (88) [171]. Therefore, each cell can locally determine a transmission policy without coordinating with its interfering cells.

With respect to the ultra-high reliability requirements in massive/scalable URLLC systems, one may need to incorporate the notion of risk or other tail statistics (refer to Section III) in the instantaneous payoff function [172]. Another interesting applications are those related to studying neural networks and multi-agent RL, and simplifying rare events simulations (refer to Section IV). Regarding the latter one, note that modeling how each agent interacts with its peers may require significant computational effort if traditional Monte Carlo methods or agent-based models are used. Fortunately, with MF game theory we can significantly reduce the complexity by abstracting the massive interactions in the evolution of one agent.

Among the main limitations related to MF games, there are the three main underlying assumptions from the framework enumerated above, and the issue that solving (89)- (90) becomes computationally expensive for highdimensional states due the curse of dimensionality. This limits the applications of classical MF game approaches for real-time applications and networks where devices have limited computational capabilities. In view of this, there is a growing interest in using DL or RL to solve MF games. Indeed, neural networks are used in [173] to approximate the optimal solutions of equations (89)- (90) at the cost of violating the conditions for convergence of the MF game framework. In another approach, a FL-based MF game approach was proposed in [174] to allow the devices periodically exchange their model parameters so that convergence is guaranteed.

VIII. MACHINE LEARNING FOR URLLC

ML constitutes a popular set of tools, which are formally classified as supervised, unsupervised, and reinforcement learning (RL), for addressing data-driven problems [175]. In the field of wireless communications, ML has been applied,

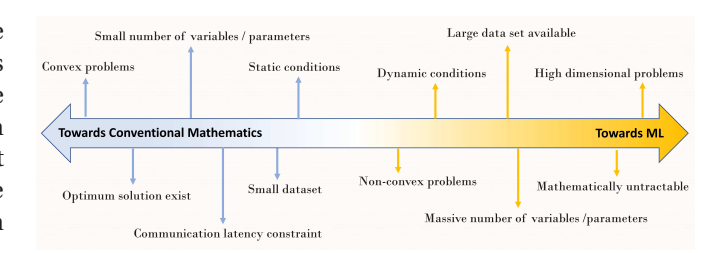


Fig. 21. ML vs conventional mathematics

for instance, in traffic and interference prediction [176]–[178], physical layer design [179], heterogeneous network traffic control [180], and multi-access edge communications [181]. More recently, URLLC systems have also been designed/optimized using ML, and some of the proposed ML approaches are collected in Table X together with popular challenges, practical use cases that could benefit from solving them, and technology enablers.

It should be noted that ML tools may fall short in handling strict URLLC requirements if not wisely used. This is because:

- prior contextual information might be difficult to exploit;
- it can be hard to obtain large training data sets in case of URLLC applications with sporadic (rare) error events (cf. Section IV);
- the accuracy of most ML algorithms may not match the stringent reliability requirements;
- the required time for (re)training can violate the strict latency constraints.

Fig. 21 illustrates the suitability of ML vs. conventional mathematics in solving different problems. For instance, RL adapts well to dynamic behaviours through a reward function, and leverages gradient methods to find efficient policies online, thus, it may be appealing for solving dynamic problems. Meanwhile, deep Q-learning is able to deal with the curse of dimensionality by sampling the state and action spaces and reducing the problem complexity. On the other hand, typical convex and near-convex problems may be easily solved using well-known methods [182]. For URLLC applications, the recent advances in ML algorithms can be harnessed by adopting a model based learning framework which promotes integrating domain knowledge with learning [33]. Here, certain aspects of the system can be assumed to operate under a known model, of which some parameters may be learned by applying ML algorithms.

A. Large-Scale Optimization

Conventional convex/non-convex optimization approaches do not scale well with the number of non-linear parameters, making them computationally prohibitive for solving large-scale/high-dimensional problems. Given this, the recent few years have witnessed a growing trend towards applying ML tools to solve such problems, including those related to wireless communications.

TABLE X
SUMMARY OF ML APPLICATIONS IN URLLC

URLLC challenge	Technology enablers	ML solutions	Use cases
Extreme low latency	Traffic prediction Predictive resource allocation FBL communication	Long short term memory (LSTM) and Support vector machines [183] Attention-based methods [184]	Vehicular networks Virtual reality
Massive networks with URLLC requirements	Dense networksDistributed massive MIMO	Multi-agent RL Combinatorial neural networks	• UAV swarms • Large-scale MTC
Fast uplink scheduling	• Traffic prediction	• Deep RL	• Mixed MBB & URLLC scheduling • Fast uplink grant
Channel modeling	• Fast channel estimation	Meta-learning [185], [186]LSTM [187]	Adaptive demodulation
Communication control co-design	Age and outage analysis [188]MTTFF analysis	• Deep RL	 Unmanned aerial vehicle (UAV) remote control Machine mobility control Remote surgery
Enhanced user experience	• QoS prediction	• Convolutional/deep neural networks • LSTM [189]	Service recommendation [190]
Cloud / Fog networks	Edge communication & computing	• FL	Internet of vehicles

Decentralized ML approaches such as FL and multiagent RL are attractive candidates for solving large-scale problems with high dimensional action and state spaces. For instance, Choi in [191] proposed a distributed stochastic gradient approach for large-scale MTC scenarios without CSI, which seems favourable for distributed URLLC applications. Moreover, such a distributed approach does not require user specific information because only the gradients are transmitted over the air and hence, data privacy is preserved.

Deep RL can be applied to reduce the state space in extremely high dimensional problems. A typical example is the large-scale UAV trajectory planning problem for serving massive MTC deployment with URLLC requirements, which has been recently addressed in works such as [192], where the authors applied combinatorial neural networks in order to optimize the user scheduling and AoI, and [193], where deep RL and device clustering are used to facilitate trajectory planning for multiple UAVs with the target of reducing the AoI and energy consumption of MTC networks. These works imposed maximum thresholds for AoI to guarantee minimum level of reliability.

B. Learning with Limited Data Samples

In many URLLC scenarios, it is not feasible to obtain large data sets due to the transmission overhead involved, while a large number of trials are required to witness rare events. Unfortunately, conventional supervised learning schemes are not adequate in such cases as they require large number of data points. Instead, meta-learning seems to be a more appealing tool as illustrated in [186]. Meta-learning refers to "learning to learn" and aims at solving many tasks that are different but related to each other through acquiring a common parameter θ called the "prior" among the learning

model. This would assist learning new tasks faster than learning them from scratch.

EXAMPLE 17 (ML-ASSISTED CSI ACQUISITION [194]).

Consider a channel estimation scenario, where URLLC devices sporadically transmit their uplink data to the base station using short packets with a few pilot symbols. In the context of channel estimation, meta learning could be applied to estimate a channel using only few pilot symbols. As shown in Fig. 22, the target is to estimate the channel and find an efficient demodulator for the meta-test device. Meta-learning would utilize the channel estimation of other meta-training devices to facilitate the channel learning of the meta-test device. Herein, the base station can make use of the channel estimation of meta-training devices in order to facilitate the channel learning of a meta-test device transmitting a few number of pilot symbols. A demodulator consisting of multi-layer neural network is constructed. Then the shared learning parameter θ and the task specific parameter ϕ are jointly and iteratively updated using a model-agnostic meta learning algorithm [194], which depends mainly on the following two gradient update equations for each device k

$$\phi_k = \theta - \alpha \nabla L_{tr}(\theta), \tag{91}$$

$$\theta = \theta - \beta \sum_{k=1}^{K} \nabla L_{test}(\phi_k), \tag{92}$$

where $\nabla(\cdot)$ is the gradient operator, and α , and β are the step sizes. For an input vector **s** and output vector **y**, L is the cross entropy loss-function given by

$$L(x) = -\sum_{s \in \mathbf{s}, y \in \mathbf{y}} \log p_x(s|y). \tag{93}$$

The algorithm details and the results can be consulted in [186]. Therein, it is shown that the meta-learning assisted

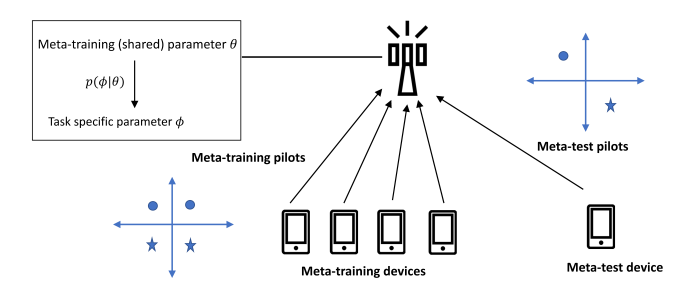


Fig. 22. Meta-learning based channel estimation and demodulation with few pilot symbols. The algorithm works by maximizing $p(\phi|\theta)$ as in [186]. We assume QPSK modulation with 4 meta training pilots at each device, where 2 pilots are used for meta training to estimate ϕ and 2 pilots are used for meta testing to estimate θ . The meta test device uses only 2 pilots to estimate and demodulate the signal using the shared parameter θ .

demodulator significantly outperforms the conventional and joint learning techniques in terms of bit error rate using only 4 pilot symbols.

Notice that, meta-learning can be leveraged in many other scenarios that include learning different but related tasks. An example of this is any learning problem that involve different network topologies. Learning to solve the problem in one topology would facilitate solving the same problem in other topologies using the "prior" shared parameter instead of learning from scratch on the new topology.

C. Predictive time series

Ensuring high reliability and low latency mandates a departure from the conventional reactive radio resource management practices to a framework incorporating predictive solutions. There are many sources of randomness in wireless systems, such as the traffic arrival at a transmitter, the interference experienced by a receiver, and the channel fading. The randomness can be reduced to a certain extent by leveraging predictive approaches, resulting in a higher degree of determinism as mandated by URLLC. Accurate prediction of the traffic arrival can be achieved by considering the contextual information such as the nature of the device/link (e.g., sensor-actuator loop), the traffic type (periodic or event-driven), and the correlation among the devices (temporally and/or spatially). Similarly, considering the correlation in the interference variation across time and space by characterizing the interference distribution can lead to better interference prediction. The observed pattern (e.g., the traffic arrival, interference variation, etc.) over time can be considered to be a time series that can be used as the basis of the prediction. One can resort to model-based or data-based approaches to draw inference from the observed samples.

In a model-based approach, each of the observed sample is assumed to be the realization of a certain RV, which follows a known hypothetical probability model [195]. The goal is then to estimate the parameters of the model from the observed data. A complete probabilistic time series model for the sequence of RVs corresponding to the

observed samples would specify all of the joint distributions of the underlying RVs. In general, such a specification will contain far too many parameters to be estimated. Hence, usually only the first- and second-order moments of the joint distributions are specified. The general approach to time series modeling involves the following steps:

- Processing the data to get a stationary series¹⁴. The processed stationary series is known as the residual.
- Choose a model to fit the residual, making use of various (first and second-order) sample statistics including the sample autocorrelation function.

Commonly used models in the literature include the autoregressive moving average (and its variants) [196], Markov chains [197], [198], Bayesian network [199], and Kalman filter [200].

Next, we present an example of a simple model-based interference prediction scheme enabling efficient allocation of resources for URLLC applications [197]. Specifically, the interference variation is modeled as a discrete-time Markov chain, while the state transition probability matrix, obtained by observing the history of state transitions, is used to predict future interference states and allocate resources accordingly.

EXAMPLE 18 (MODEL-DRIVEN RESOURCE ALLOCATION [197]). Consider the downlink of a wireless network where the URLLC link of interest operates in the presence of N interferers. Single shot [201] transmissions are considered for the sake of low latency transmissions, i.e., there are no retransmissions.

The sketch of the interference prediction algorithm is pictorially outlined in Fig. 23. First, we discretize the interference space \mathcal{I} into the state space $\mathcal{L} \triangleq \{\mathcal{L}_1, \dots, \mathcal{L}_L\}$ where the state \mathcal{L}_1 corresponds to the interference values in the range $[I_{l-1}, I_l)$. Besides, we define $\tilde{\mathcal{I}} \triangleq \{\mathcal{L}^0, \mathcal{L}^1, \dots\}$ as the set of observed interference states at time index $t = 0, 1, \dots$. For example, $\mathcal{L}^t = S_i$ implies that the interference state at time t is \mathcal{L}_i . Next, we compute the entries of the transition matrix \mathcal{L} which describes the transition probabilities of the states in \mathcal{L} as

$$p_{ij} = \frac{\sum_{t} \mathbb{I}\{\mathcal{S}^{t+1} \in \mathcal{S}_{j} \& \mathcal{S}^{t} \in \mathcal{S}_{i}\}}{\sum_{t} \mathbb{I}\{\mathcal{S}^{t} \in \mathcal{S}_{i}\}} \quad \forall i, j \in \{1, 2, \dots, L\}, \quad (94)$$

where $p_{i,j}$ is the probability of transition from state \mathcal{S}_i to \mathcal{S}_j .

Now, we introduce the confidence level parameter $\eta < 1$ to utilize the tail statistics of the interference distribution. We aim to ensure that the predicted interference at time t+1, \hat{I}^{t+1} , is greater than the actual interference, I^{t+1} , with probability greater than or equal to η , i.e., $\Pr[I^{t+1} \leq \hat{I}^{t+1}] \geq \eta$. For this, we first predict the next state $\hat{\mathcal{F}}^{t+1}$ to be \mathcal{F}_i , where

 $^{^{14}\}mathrm{A}$ time series is said to be (weakly) stationary if its mean and the variance are independent of the time observation, i.e., the joint probability distribution does not change when shifted in time

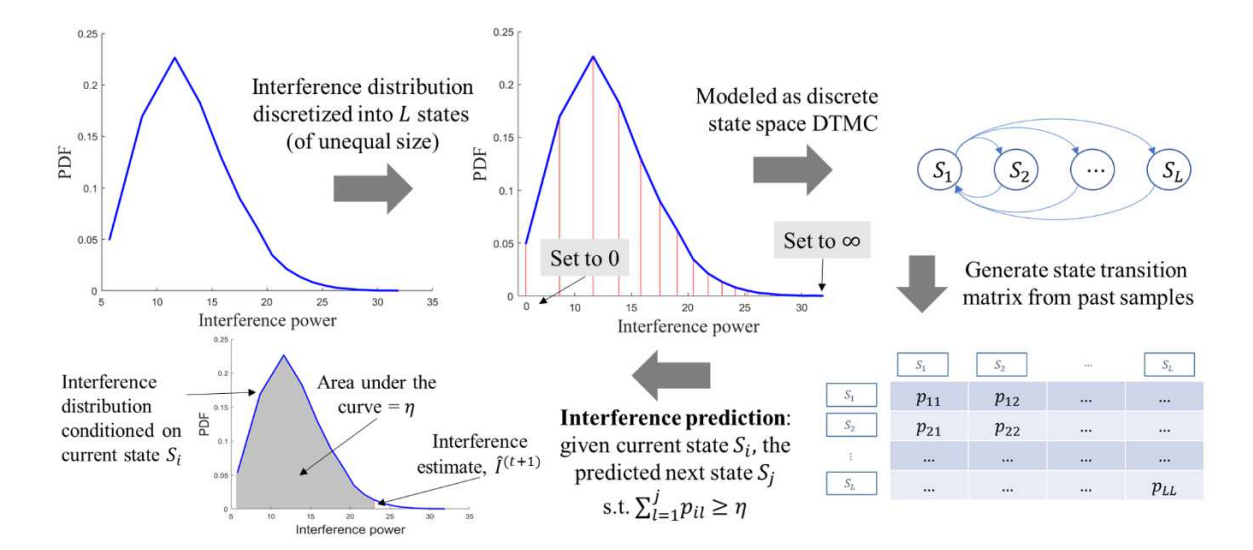


Fig. 23. Sketch of the model-based interference prediction algorithm.

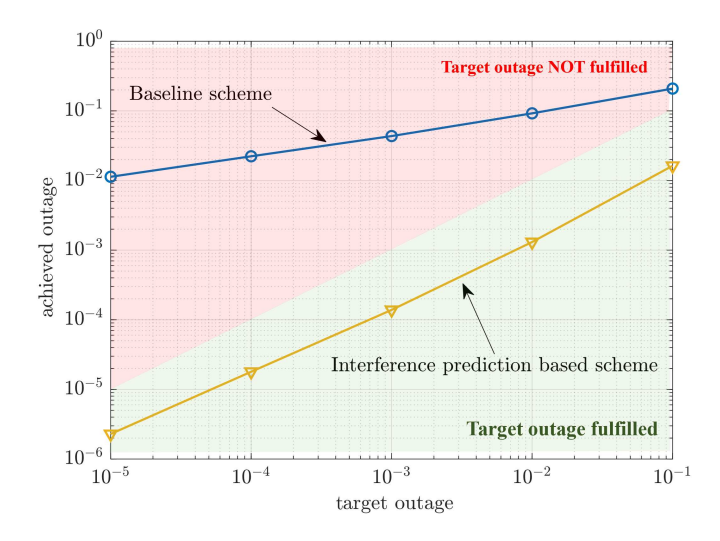


Fig. 24. Achieved outage as a function of the target outage probability with correlated traffic and $\eta=0.95$.

j is the smallest integer such that $\sum_{l=1}^{j} p_{il} \ge \eta$. The predicted interference level at time index t+1 is then

$$\hat{I}^{t+1} = \begin{cases} I_j & \text{if } j \neq L \\ 2I_{L-1} - I_{L-2} & \text{if } j = L \end{cases}$$
 (95)

where I_j is the right-endpoint of state \mathcal{S}_j . Lastly, once a transition is made from state \mathcal{S}_i to state \mathcal{S}_j , the transition matrix \mathcal{P} is updated as

step 1:
$$p_{ij} \leftarrow p_{ij} + \omega_{ij}$$
 for each i, j ,

step 2: normalize
$$i$$
-th row such that $\sum_{j=1}^{L} p_{ij} = 1$,

where $0 \le \omega_{ij} \ll 1$ is the learning rate.

Let $\hat{\gamma} = SNR/\hat{I}$ be the predicted SINR, where the SNR of the desired transmission is assumed to be known using CSI estimates. Using the FBL theory results detailed in Section V-A, one can obtain the channel uses that need to

be allocated for a given number of information bits and a target outage probability. After the transmission takes place, the achieved outage can be calculated using Eq. (54), where $\hat{\gamma}$ is replaced by the actual SINR.

The outage probability performance attained with the outlined interference prediction based resource management algorithm vs. the target outage for $\eta=0.95$ is illustrated in Fig. 24. The conventional weighted average based interference estimator adopted as an estimator in link adaptation for conventional MBB services [202] is considered as the baseline scheme. The proposed interference estimate based resource management scheme is found to always fulfill the target outage. On the other hand, the baseline scheme is only able to meet a BLER target of about 10%, which is the usual BLER target in MBB applications. Conversely, the number of information bits that can be transmitted with a desired decoding error probability for a given FBL size can be obtained using the FBL theory outlined in Section V, where γ is set to be the predicted SINR value.

On the other hand, a data-based approach advocates learning the dependence structure from past data without the need to consider the underlying structure. Data-driven methods employ ML tools to predict future instances of the observed data. These include applying DL schemes like deep belief network [203], convolutional neural network [204], recurrent neural network [205], LSTM networks [206], [207], and the novel "transformer" architecture [208]. The latter may provide unprecedented support to tackle sophisticated and high dimensional time series problems, but much research is still needed for a comprehensive assessment of its potentialities.

Observe that model-based approaches have several advantages over data-based approaches, namely, *i*) they allow easily taking advantage of prior information; *ii*) they can be easily adapted to different environments even in the absence of training data; and *iii*) it can be gradually improved using training information. However, they are built on some

underlying assumptions, such as the stationarity of the residual and the validity of the assumed model. In contrast, a data-driven approach can capture the nonlinearity and randomness of actual time series, albeit usually at the cost of large training overhead and complexity. Nonetheless, the advantages of both approaches can be harnessed by integrating domain knowledge in data-based approaches [33].

IX. CONCLUSIONS & FUTURE DIRECTIONS

URLLC is about taming the tail of reliability and latency under the uncertainty arising from the stochastic nature of wireless communications. Moreover, most URLLC use cases are very different from conventional human-type communications as characterized by traffic with smaller payloads and sporadic arrivals, large device density, and heterogeneous service demands. Thus, designing and/or analyzing URLLC systems mandates adopting a vastly different set of statistical tools and methodologies. Aiming to fulfill the corresponding gap in existing surveys and overview papers on URLLC, this article presented a unified framework for designing and/or analyzing URLLC. Specifically, several relevant statistical tools and methodologies were introduced, and their applications to URLLC were highlighted together with thorough discussions on how these tools can be used interdependently towards designing/analyzing URLLC systems. As a unique feature of the tutorial-like nature of this article, each of the introduced tools and methodologies was further elaborated through concrete numerical examples and selected applications. This article is targeted toward graduate students, early-stage researchers, and professionals interested in getting a comprehensive overview of the statistical tools and methodologies relevant to URLLC, and will help foster more research in URLLC and its evolution towards next-generation wireless systems. In what follows, we present some potential future research directions for each of the discussed tools and methodologies.

1) From URLLC to dependable communications: Current 5G approaches for meeting URLLC requirements based on tweaking the system design is not scalable nor efficient. This is specially evident for use cases related to emerging sophisticated cyber-physical systems, which rely on embedded, decentralized, real-time computations and interactions, where physical and software components are deeply intertwined [209]. The design and analysis of such systems mandate a departure from link-specific URLLC to holistic dependability. For this, there is a series of associated challenges, which are mainly related to i) the scalable modeling of the different kinds of adverse events, e.g., errors, faults, failures (refer to [210]), and their cross-correlation, ii) the extrapolation of dependability concepts and tools as those overviewed in Section II, which are originally conceived for systems engineering, to wireless communications engineering in different domains/layers, and iii) the development of data-driven dependable mechanisms. Moreover, notice that a thorough joint optimization of the communication, control, computing, and sensing processes is fundamental for resource-efficient truly-dependable systems. Therefore, communication and control co-design,

quantum computing and communication, and joint communication and sensing, are instrumental for this and may continue receiving dedicated research in the coming years. All in all, the notion of dependability is expected to play a more dominant role in beyond 5G wireless systems to provide a richer performance measure of critical systems [6], [7].

2) Statistical bounds, inequalities, approximations, and risk measures on small sample sizes: The bounds, approximations, and risk-assessment tools discussed in Section III inherently rely on a statistical pre-processing of data samples. For instance, applying Markov's inequality (28) mandates computing the expected value of a certain random process, the GPD fitting of the conditional CDF (35) is data-driven, and the evaluation of the VaR (39) and CVar (40) risk metrics leverages the distribution and conditional expectation of an underlying random process, respectively. Therefore, the confidence in such approaches increases with the sample size. However, the number of samples corresponding to a certain relevant random process may be strictly limited in many URLLC use cases, which calls for novel probabilistic bounds/approximations/risk-metrics with accompanied confidence guarantees. As commented in Example 5, they may be designed using the same tools and approaches outlined in Section III but enriched with additional procedures considering the data finitude, e.g., exploiting the central limit theorem. Finally, the risk metrics discussed in Section III-C, i.e., VaR (39) and CVar (40), are by no means the only ones within the risk management theory [74], and further research is needed to identify and link more risk-related metrics to the design/analysis of URLLC systems.

3) Ultra-efficient sampling for rare event simulations: The methods discussed in Section IV rely on statistical models, including some underlying prior knowledge, for proper sampling. Therefore, efficient approximations/upper bounds and optimization of target distributions are needed to reduce computational complexity and/or increase accuracy. In addition, many URLLC use cases require efficient sampling to assess novel probabilistic metrics with a significant number of samples from the probability space where the URLLC event exists. Therefore, further research is needed to properly link efficient sampling algorithms and URLLC research. One direction may be using Hamiltonian Monte Carlo methods, particularly for use cases with large dimensions, as it is a non-Markovian-based method able to explore the probability space efficiently by avoiding the dependencies of the Markov chain [211], [212]. Similarly, variational Bayes methods [80], [81], poorly explored in the URLLC literature, deserve more attention.

4) Fixed to variable length coding: The FBL channel codes considered in Section V are fixed-length codes where each codeword has the same number of bits. Variable-length codes, on the other hand, encodes message symbols to codewords with a variable number of bits. This has the advantage that the coding rate can be adjusted to the channel conditions leading to enhanced resource efficiency, albeit requiring a feedback channel [213]. The involvement

of the feedback loop incurs extra latency and an additional error-source (as illustrated through the example in Section V-B). A recent study has shown that noise in the feedback link can cause a significant increase in the minimum average latency when applying variable-length codes to URLLC use cases [214]. This raises the question whether variable-length coding scheme are suitable for URLLC, or alternately how to design variable-length codes for URLLC applications with FBL transmissions?

5) FBL queuing and dependable AoI: Notably, SNC may help identify and define new delay-bounded QoS metrics incorporating the channel's and the arrival and service processes' stochasticity. However, the relationship between SNC and FBL theory/coding still requires further investigation, especially the characterization of the tail distribution and the delay bounds in extreme URLLC [111]. Meanwhile, open challenges in the context of information freshness include the characterization of AoI tail distributions for different network models, part of which were characterized in [118]. Moreover, future research should focus on critical decision making in inter-disciplinary problems such as communication control co-design, which demands timely and reliable fresh information. In such cases, the link between AoI and dependability metrics, such as mean time to first failure, deserves particular attention [188].

6) Strengthening the large-scale URLLC design/analysis: In Section VII-B, we only referred to hard-clustering, where a point can only belong to exactly one cluster. However, soft (or fuzzy) clustering [215], [216], where a point can potentially belong to multiple clusters, may be more appealing for assessing the inherent complexity/heterogeneity of wireless networks, specially URLLC. Meanwhile, tools and methodologies related to the meta distribution, compressed sensing, and MF games rely heavily on underlying models and assumptions. Since ultimately "all models are wrong" (quote from George Box), say imperfect, they must be investigated considering modeling imperfections/uncertainties. Finally, regarding Example 16 in Section VII-C and the discussions that followed it, we would like to emphasize that multi-user detection in grant-free URLLC systems can be assisted by a preliminary sparsity level estimation phase as discussed in [162]. However, there are numerous associated research directions yet to explore, including i) sparsity level estimators exploiting prior traffic history knowledge and/or optimized for MIMO operation, and ii) a joint optimization of the sparsity level estimation and multi-user detection phases since the total number of symbols for these tasks might be very limited and accuracy of the sparsity level estimation is intrinsically imperfect.

7) Towards Intelligent URLLC: The learning process in multi-agent RL depends only on the states and actions observed by each agent without or with partial information about the states and actions of the whole environment. Therefore, its application in large-scale systems may significantly reduce the action-state space and complexity, thus, the incurred latency, which is beneficial for URLLC. However, how to reduce the state and action spaces through either partial or no information sharing between the learn-

ing agents remains an open question. Further research is still needed to characterize the performance degradation resulting from the limited information of states and actions, the accuracy of distributed approaches, and the factors affecting their performance. Meanwhile, in another direction, accurate and intelligent prediction techniques that integrate model-driven approaches with ML/AI tools via deep unfolding principles must be developed, together with efficient resource management schemes that utilize the prediction information to enable URLLC without overprovisioning the system redundancy.

REFERENCES

- M. A. Lema, A. Laya, T. Mahmoodi, M. Cuevas, J. Sachs, J. Markendahl, and M. Dohler, "Business case and technology analysis for 5G low latency applications," *IEEE Access*, vol. 5, pp. 5917–5935, 2017.
- [2] H. Chen, R. Abbas, P. Cheng, M. Shirvanimoghaddam, W. Hard-jawana, W. Bao, Y. Li, and B. Vucetic, "Ultra-reliable low latency cellular networks: Use cases, challenges and approaches," *IEEE Communications Magazine*, vol. 56, no. 12, pp. 119–125, 2018.
- [3] M. Angjelichinoski, K. F. Trillingsgaard, and P. Popovski, "A statistical learning approach to ultra-reliable low latency communication," *IEEE Transactions on Communications*, vol. 67, no. 7, pp. 5153–5166, 2019.
- [4] P. Popovski, C. Stefanović, J. J. Nielsen, E. De Carvalho, M. Angjelichinoski, K. F. Trillingsgaard, and A.-S. Bana, "Wireless access in ultrareliable low-latency communication (URLLC)," *IEEE Transactions on Communications*, vol. 67, no. 8, pp. 5783–5801, Aug. 2019.
- [5] G. J. Sutton, J. Zeng, R. P. Liu, W. Ni, D. N. Nguyen, B. A. Jayawickrama, X. Huang, M. Abolhasan, Z. Zhang, E. Dutkiewicz, and T. Lv, "Enabling technologies for ultra-reliable and low latency communications: From PHY and MAC layer perspectives," *IEEE Communications Surveys & Tutorials*, vol. 21, no. 3, pp. 2488–2524, 2019.
- [6] N. H. Mahmood, H. Alves, O. L. A. López, M. Shehab, D. P. M. Osorio, and M. Latva-Aho, "Six key features of machine type communication in 6G," in 2nd 6G Wireless Summit (6G SUMMIT), 2020, pp. 1–5.
- [7] N. Mahmood, O. López, O. Park, I. Moerman, K. Mikhaylov, E. Mercier, A. Munari, F. Clazzer, S. Böcker, and H. Bartz (Eds.), "White paper on critical and massive machine type communication towards 6G [white paper]," 6G Research Visions, vol. 11, 2020. [Online]. Available: http://urn.fi/urn:isbn:9789526226781
- [8] N. H. Mahmood, S. Boecker, I. Moerman, O. A. Lopez, A. Munari, K. Mikhaylov, F. Clazzer, H. Bartz, O.-S. Park, E. Mercier et al., "Machine type communications: key drivers and enablers towards the 6G era," EURASIP Journal on Wireless Communications and Networking, vol. 2021, no. 1, pp. 1–25, 2021.
- [9] 3GPP TS 22.261 v.16.0.0, Service Requirements for the 5G System. [Online]. Available: https://portal.3gpp.org/desktopmodules/Specifications/SpecificationDetails.aspx?s
- [10] H. Ji, S. Park, J. Yeo, Y. Kim, J. Lee, and B. Shim, "Ultra-reliable and low-latency communications in 5G downlink: Physical layer aspects," *IEEE Wireless Communications*, vol. 25, no. 3, pp. 124–130, 2018.
- [11] R. E. Barlow and F. Proschan, *Mathematical theory of reliability*. Wiley, 1965.
- [12] M. Bennis, M. Debbah, and H. V. Poor, "Ultrareliable and low-latency wireless communication: Tail, risk, and scale," *Proceedings of the IEEE*, vol. 106, no. 10, pp. 1834–1853, 2018.
- [13] M. Shirvanimoghaddam, M. S. Mohammadi, R. Abbas, A. Minja, C. Yue, B. Matuz, G. Han, Z. Lin, W. Liu, Y. Li, S. Johnson, and B. Vucetic, "Short block-length codes for ultra-reliable low latency communications," *IEEE Communications Magazine*, vol. 57, no. 2, pp. 130–137, Feb. 2019.
- [14] G. Durisi, T. Koch, and P. Popovski, "Toward massive, ultrareliable, and low-latency wireless communication with short packets," *Proceedings of the IEEE*, vol. 104, no. 9, pp. 1711–1726, Sep. 2016.
- [15] M. Alsenwi, N. H. Tran, M. Bennis, A. Kumar Bairagi, and C. S. Hong, "eMBB-URLLC resource slicing: A risk-sensitive approach," *IEEE Communications Letters*, vol. 23, no. 4, pp. 740–743, 2019.

- [16] O. L. A. Lopez, N. H. Mahmood, H. Alves, C. M. Lima, and M. Latvaaho, "Ultra-low latency, low energy, and massiveness in the 6G era via efficient CSIT-limited scheme," *IEEE Communications Magazine*, vol. 58, no. 11, pp. 56–61, 2020.
- [17] R. Kotaba, C. N. Manchón, and P. Popovski, "Enhancing performance of uplink URLLC systems via shared diversity transmissions and multiple antenna processing," in 53rd Asilomar Conference on Signals, Systems, and Computers, 2019, pp. 1409–1415.
- [18] O. L. A. López, N. H. Mahmood, and H. Alves, "Enabling URLLC for low-cost IoT devices via diversity combining schemes," in *IEEE International Conference on Communications Workshops (ICC Workshops)*, 2020, pp. 1–6.
- [19] O. L. A. López, H. Alves, and M. Latva-Aho, "Distributed rate control in downlink NOMA networks with reliability constraints," *IEEE Transactions on Wireless Communications*, vol. 18, no. 11, pp. 5410–5423, 2019.
- [20] E. N. Tominaga, H. Alves, O. L. A. López, R. D. Souza, J. L. Rebelatto, and M. Latva-aho, "Network slicing for eMBB and mMTC with NOMA and space diversity reception," in 2021 IEEE 93rd Vehicular Technology Conference (VTC2021-Spring), 2021, pp. 1–6.
- [21] J. Khan and L. Jacob, "Learning based CoMP clustering for URLLC in millimeter wave 5G networks with blockages," in *IEEE International Conference on Advanced Networks and Telecommunications Systems* (ANTS), 2019, pp. 1–6.
- [22] B. Kharel, O. L. A. López, H. Alves, and M. Latvaaho, "Ultra-reliable communication for critical machine type communication via CRAN-enabled multi-connectivity diversity schemes," Sensors, vol. 21, no. 23, 2021. [Online]. Available: https://www.mdpi.com/1424-8220/21/23/8064
- [23] I. Muhammad, H. Alves, N. H. Mahmood, O. L. A. López, and M. Latva-aho, "Mission effective capacity—a novel dependability metric: A study case of multiconnectivity-enabled URLLC for IIoT," *IEEE Transactions on Industrial Informatics*, vol. 18, no. 6, pp. 4180– 4188, 2022.
- [24] B. Kharel, O. L. A. López, N. H. Mahmood, H. Alves, and M. Latva-Aho, "Fog-RAN enabled multi-connectivity and multi-cell scheduling framework for ultra-reliable low latency communication," *IEEE Access*, vol. 10, pp. 7059–7072, 2022.
- [25] F. B. Dihn, A. A. Razzac, A. El Falou, and S. E. Elayoubi, "Adaptive data replication for URLLC in cooperative 4G/5G networks," in IEEE 32nd Annual International Symposium on Personal, Indoor and Mobile Radio Communications (PIMRC), 2021, pp. 1376–1381.
- [26] P. Wu and N. Jindal, "Coding versus ARQ in fading channels: How reliable should the PHY be?" *IEEE Transactions on Communications*, vol. 59, no. 12, pp. 3363–3374, Dec. 2011.
- [27] S. R. Panigrahi, N. Bjorsell, and M. Bengtsson, "Feasibility of large antenna arrays towards low latency ultra reliable communication," in *IEEE International Conference on Industrial Technology (ICIT)*, 2017, pp. 1289–1294.
- [28] O. L. A. López, E. M. G. Fernández, R. D. Souza, and H. Alves, "Ultrareliable cooperative short-packet communications with wireless energy transfer," *IEEE Sensors Journal*, vol. 18, no. 5, pp. 2161–2177, 2018.
- [29] S. Paris, P. Kela, D. Laselva, and Q. Zhao, "Addressing reliability needs of industrial applications in 5G NR with network coding," in 2020 IEEE 91st Vehicular Technology Conference (VTC2020-Spring), 2020, pp. 1–6.
- [30] P. Nouri, H. Alves, M. A. Uusitalo, O. A. López, and M. Latva-aho, "Machine-type wireless communications enablers for beyond 5G: Enabling URLLC via diversity under hard deadlines," Computer Networks, vol. 174, p. 107227, 2020. [Online]. Available: https://www.sciencedirect.com/science/article/pii/S1389128619315361
- [31] Y. Zhang, Y. Xiang, L. Y. Zhang, Y. Rong, and S. Guo, "Secure wireless communications based on compressive sensing: A survey," *IEEE Communications Surveys & Tutorials*, vol. 21, no. 2, pp. 1093–1111, 2019
- [32] H. Yang, K. Zheng, K. Zhang, J. Mei, and Y. Qian, "Ultra-reliable and low-latency communications for connected vehicles: Challenges and solutions," *IEEE Network*, vol. 34, no. 3, pp. 92–100, 2020.
- [33] C. She, C. Sun, Z. Gu, Y. Li, C. Yang, H. V. Poor, and B. Vucetic, "A tutorial on ultrareliable and low-latency communications in 6G: Integrating domain knowledge into deep learning," *Proceedings of the IEEE*, vol. 109, no. 3, pp. 204–246, 2021.
- [34] I. Eusgeld and F. C. Freiling, Introduction to Dependability Metrics. Berlin, Heidelberg: Springer Berlin Heidelberg, 2008, pp. 1–4. [Online]. Available: https://doi.org/10.1007/978-3-540-68947-8_1

- [35] A. Birolini, Reliability engineering: theory and practice. Springer Science & Business Media, 2013.
- [36] A. Hoyland and M. Rausand, System reliability theory: models and statistical methods. John Wiley & Sons, 2009.
- [37] K. S. Trivedi, Probability & statistics with reliability, queuing and computer science applications. John Wiley & Sons, 2008.
- [38] R. Sattiraju and H. D. Schotten, "Reliability modeling, analysis and prediction of wireless mobile communications," in *IEEE 79th Vehicular Technology Conference (VTC Spring)*, 2014, pp. 1–6.
- [39] S. M. Ross, Introduction to probability models. Academic press, 2014.
- [40] W. S. Lee, D. L. Grosh, F. A. Tillman, and C. H. Lie, "Fault tree analysis, methods, and applications - a review," *IEEE Transactions* on *Reliability*, vol. R-34, no. 3, pp. 194–203, 1985.
- [41] L. Xing and S. V. Amari, "Fault tree analysis," Handbook of performability engineering, pp. 595–620, 2008.
- [42] W. Kuo and M. J. Zuo, Optimal reliability modeling: principles and applications. John Wiley & Sons, 2003.
- [43] D. Colombo, D. T. Abreu, and M. R. Martins, "Application of markovian models in reliability and availability analysis: advanced topics," in *Safety and Reliability Modeling and its Applications*. Elsevier, 2021, pp. 91–160.
- [44] R. A. Howard, *Dynamic probabilistic systems: Markov models*. Courier Corporation, 2012, vol. 1.
- [45] M. A. Boyd and S. Lau, "An introduction to markov modeling: Concepts and uses," in *Annual Reliability and Maintainability Symposium*, 1998.
- [46] E. N. Gilbert, "Capacity of a burst-noise channel," *Bell system technical journal*, vol. 39, no. 5, pp. 1253–1265, 1960.
- [47] M. Zorzi, R. Rao, and L. Milstein, "On the accuracy of a first-order Markov model for data transmission on fading channels," in Proceedings of the 4th IEEE International Conference on Universal Personal Communications (ICUPC), 1995, pp. 211–215.
- [48] D. Öhmann and G. P. Fettweis, "Minimum duration outage of wireless Rayleigh-fading links using selection combining," in *IEEE Wireless Communications and Networking Conference (WCNC)*, 2015, pp. 681–686.
- [49] T. S. Rappaport et al., Wireless communications: principles and practice. New Jersey, USA: Prentice Hall PTR, 1996, vol. 2.
- [50] T. Hößler, M. Simsek, and G. P. Fettweis, "Joint analysis of channel availability and time-based reliability metrics for wireless URLLC," in *IEEE Global Communications Conference (GLOBECOM)*, 2018, pp. 206–212.
- [51] ——, "Dependability theory for selection-combined channels with Rician fading and interference," in *IEEE 2nd 5G World Forum* (5GWF), 2019, pp. 440–445.
- [52] N. Mandayam, P.-C. Chen, and J. Holtzman, "Minimum duration outage for cellular systems: a level crossing analysis," in *Proceedings* of Vehicular Technology Conference - VTC, vol. 2, 1996, pp. 879–883 vol.2.
- [53] S. O. Rice, "Distribution of the duration of fades in radio transmission: Gaussian noise model," *The Bell System Technical Journal*, vol. 37, no. 3, pp. 581–635, 1958.
- [54] O. L. A. López, H. Alves, and M. Latva-Aho, "Rate control under finite blocklength for downlink cellular networks with reliability constraints," in 15th International Symposium on Wireless Communication Systems (ISWCS), 2018, pp. 1–6.
- [55] O. L. A. López, H. Alves, and M. Latva-aho, "Joint power control and rate allocation enabling ultra-reliability and energy efficiency in SIMO wireless networks," *IEEE Transactions on Communications*, vol. 67, no. 8, pp. 5768–5782, 2019.
- [56] B. K. Ghosh, "Probability inequalities related to Markov's theorem," The American Statistician, vol. 56, no. 3, pp. 186–190, 2002.
- [57] D. Echevarría, O. L. A. López, and H. Alves, "Robust downlink multiantenna beamforming with heterogenous CSI: Enabling eMBB and URLLC coexistence," *IEEE Transactions on Wireless Communications* (submitted).
- [58] R. Paley and A. Zygmund, "On some series of functions,(1)," in Mathematical Proceedings of the Cambridge Philosophical Society, vol. 26, no. 3. Cambridge University Press, 1930, pp. 337–357.
- [59] W. Hoeffding, "Probability inequalities for sums of bounded random variables," in *The collected works of Wassily Hoeffding*. Springer, 1994, pp. 409–426.
- [60] D. Vysochanskij and Y. I. Petunin, "Justification of the 3σ rule for unimodal distributions," *Theory of Probability and Mathematical Statistics*, vol. 21, no. 25-36, 1980.

- [61] F. P. Cantelli, "Sui confini della probabilita," in Atti del Congresso Internazionale dei Matematici: Bologna del 3 al 10 de settembre di 1928, 1929, pp. 47–60.
- [62] S. W. Dharmadhikari and K. Joag-Dev, "The Gauss-Tchebyshev inequality for unimodal distributions," *Theory of Probability & Its Applications*, vol. 30, no. 4, pp. 867–871, 1986.
- [63] P. Massart, "The tight constant in the Dvoretzky-Kiefer-Wolfowitz inequality," The annals of Probability, pp. 1269–1283, 1990.
- [64] M. Kountouris and A. Avranas, "Delay performance of multi-antenna multicasting in wireless networks," in *IEEE 19th International Work-shop on Signal Processing Advances in Wireless Communications* (SPAWC), 2018, pp. 1–5.
- [65] J. Choi, "On error rate analysis for URLLC over multiple fading channels," in *IEEE Wireless Communications and Networking Conference* (WCNC), 2020, pp. 1–5.
- [66] M. Haenggi, "The meta distribution of the SIR in Poisson bipolar and cellular networks," *IEEE Transactions on Wireless Communications*, vol. 15, no. 4, pp. 2577–2589, 2016.
- [67] S. Coles, J. Bawa, L. Trenner, and P. Dorazio, An introduction to statistical modeling of extreme values. Springer, 2001, vol. 208.
- [68] S. Samarakoon, M. Bennis, W. Saad, and M. Debbah, "Federated learning for ultra-reliable low-latency V2V communications," in *IEEE Global Communications Conference (GLOBECOM)*, 2018, pp. 1–7.
- [69] N. Mehrnia and S. Coleri, "Wireless channel modeling based on extreme value theory for ultra-reliable communications," *IEEE Trans*actions on Wireless Communications, pp. 1–1, 2021.
- [70] M. Falk, J. Hüsler, and R.-D. Reiss, Laws of small numbers: extremes and rare events. Springer Science & Business Media, 2010.
- [71] J. Pickands III, "Statistical inference using extreme order statistics," the Annals of Statistics, pp. 119–131, 1975.
- [72] A. L. Dekkers, J. H. Einmahl, and L. De Haan, "A moment estimator for the index of an extreme-value distribution," *The Annals of Statistics*, pp. 1833–1855, 1989.
- [73] B. M. Hill, "A simple general approach to inference about the tail of a distribution," *The annals of statistics*, pp. 1163–1174, 1975.
- [74] A. J. A. J. McNeil, R. Frey, and P. Embrechts, "Quantitative risk management: Concepts, techniques and tools," *Risk Manag.*, vol. 101, no. 476, p. 30, 2005.
- [75] J. Park, S. Samarakoon, H. Shiri, M. K. Abdel-Aziz, T. Nishio, A. El-gabli, and M. Bennis, "Extreme URLLC: Vision, challenges, and key enablers," 2020.
- [76] R. Karasik, O. Simeone, H. Jang, and S. Shamai, "Learning to broadcast for ultra-reliable communication with differential quality of service via the conditional value at risk," arXiv preprint arXiv:2112.02007, 2021.
- [77] O. L. A. López, H. Alves, R. D. Souza, and M. Latva-Aho, "Finite blocklength error probability distribution for designing ultra reliable low latency systems," *IEEE Access*, vol. 8, pp. 107353–107363, 2020.
- [78] M. F. Bugallo, V. Elvira, L. Martino, D. Luengo, J. Miguez, and P. M. Djuric, "Adaptive importance sampling: the past, the present, and the future," *IEEE Signal Processing Magazine*, vol. 34, no. 4, pp. 60–79, 2017. [Online]. Available: http://dx.doi.org/10.1109/MSP.2017.2699226
- [79] R. Y. Rubinstein and D. P. Kroese, Simulation and the Monte Carlo Method, ser. Wiley Series in Probability and Statistics. Hoboken, NJ, USA: John Wiley & Sons, Inc., nov 2016. [Online]. Available: http://doi.wiley.com/10.1002/9781118631980
- [80] C. W. Fox and S. J. Roberts, "A tutorial on variational Bayesian inference," Artificial Intelligence Review, vol. 38, no. 2, pp. 85–95, Aug. 2012. [Online]. Available: https://doi.org/10.1007/s10462-011-9236-8
- [81] M.-N. Tran, T.-N. Nguyen, and V.-H. Dao, "A practical tutorial on variational Bayes." 2021.
- [82] V. N. Swamy, N. Naderializadeh, V. N. Ekambaram, S. Talwar, and A. Sahai, "Monitoring under-modeled rare events for URLLC," in 2019 IEEE 20th Int. Work. Signal Process. Adv. Wirel. Commun., vol. 2019-July. IEEE, jul 2019, pp. 1–5. [Online]. Available: https://ieeexplore.ieee.org/document/8815583/
- [83] D. Kroese, T. Taimre, and Z. Botev, Handbook of Monte Carlo Methods. John Wiley and Sons, New York: Wiley Applied Probability & Statistics, 2011.
- [84] K. M. Zuev, "Subset simulation method for rare event estimation: An introduction," in *Encyclopedia of Earthquake Engineering*, M. Beer, I. A. Kougioumtzoglou, E. Patelli, and I. S.-K. Au, Eds. Berlin, Heidelberg: Springer, 2021, pp. 1–25. [Online]. Available: https://doi.org/10.1007/978-3-642-36197-5_165-1

- [85] M.-T. Suer, C. Thein, H. Tchouankem, and L. Wolf, "Multi-connectivity as an enabler for reliable low latency communications—an overview," *IEEE Communications Surveys & Tutorials*, vol. 22, no. 1, pp. 156–169, 2020.
- [86] A. Goldsmith, Wireless Communications. New York, USA: Cambridge University Press, 2005.
- [87] R. W. Hamming, "Error detecting and error correcting codes," The Bell System Technical Journal, vol. 29, no. 2, pp. 147–160, Apr. 1950.
- [88] Y. Polyanskiy, H. V. Poor, and S. Verdu, "Channel coding rate in the finite blocklength regime," *IEEE Transactions on Information Theory*, vol. 56, no. 5, pp. 2307–2359, May 2010.
- [89] J. Park, "Rate analysis of ultra-reliable low-latency communications in random wireless networks," Oct. 2019.
- [90] P. Mary, J.-M. Gorce, A. Unsal, and H. V. Poor, "Finite blocklength information theory: What is the practical impact on wireless communications?" in *IEEE Globecom Workshops (GC Wkshps)*, 2016, pp. 1–6
- [91] O. L. Alcaraz López, H. Alves, R. D. Souza, S. Montejo-Sánchez, and E. M. García Fernández, "Rate control for wireless-powered communication network with reliability and delay constraints," *IEEE Transactions on Wireless Communications*, vol. 18, no. 12, pp. 5791– 5805, 2019
- [92] O. L. A. López, E. M. G. Fernández, R. D. Souza, and H. Alves, "Wireless powered communications with finite battery and finite blocklength," *IEEE Transactions on Communications*, vol. 66, no. 4, pp. 1803–1816, 2018.
- [93] P. C. F. Eggers, M. Angjelichinoski, and P. Popovski, "Wireless channel modeling perspectives for ultra-reliable communications," *IEEE Transactions on Wireless Communications*, vol. 18, no. 4, pp. 2229–2243, Apr. 2019.
- [94] E. Arikan, "Channel polarization: A method for constructing capacity-achieving codes for symmetric binary-input memoryless channels," *IEEE Transactions on Information Theory*, vol. 55, no. 7, pp. 3051–3073, Jul. 2009.
- [95] N. Doan, S. A. Hashemi, F. Ercan, and W. J. Gross, "Fast SC-Flip decoding of polar codes with reinforcement learning," in *IEEE International Conference on Communications (ICC)*, Montreal, Canada, Jun. 2021, pp. 1–6.
- [96] A. Alamdar-Yazdi and F. R. Kschischang, "A simplified successivecancellation decoder for polar codes," *IEEE Communications Letters*, vol. 15, no. 12, pp. 1378–1380, 2011.
- [97] H. Zheng, S. A. Hashemi, A. Balatsoukas-Stimming, Z. Cao, T. Koonen, J. M. Cioffi, and A. Goldsmith, "Threshold-based fast successive-cancellation decoding of polar codes," *IEEE Transactions* on Communications, vol. 69, no. 6, pp. 3541–3555, Jun. 2021.
- [98] O. Dizdar and E. Arıkan, "A high-throughput energy-efficient implementation of successive cancellation decoder for polar codes using combinational logic," *IEEE Transactions on Circuits and Systems I: Regular Papers*, vol. 63, no. 3, pp. 436–447, Mar. 2016.
- [99] F. Ercan, C. Condo, and W. J. Gross, "Reduced-memory highthroughput fast-SSC polar code decoder architecture," in *IEEE In*ternational Workshop on Signal Processing Systems (SiPS), Lorient, France, Oct. 2017.
- [100] K. R. Duffy, J. Li, and M. Médard, "Capacity-achieving guessing random additive noise decoding," *IEEE Transactions on Information Theory*, vol. 65, no. 7, pp. 4023–4040, Jul. 2019.
- [101] K. R. Duffy, M. Médard, and W. An, "Guessing random additive noise decoding with symbol reliability information (SRGRAND)," *IEEE Transactions on Communications*, vol. 70, no. 1, pp. 3–18, Jan. 2022.
- [102] K. R. Duffy, A. Solomon, K. M. Konwar, and M. Médard, "5G NR CA-polar maximum likelihood decoding by GRAND," in 2020 54th Annual Conference on Information Sciences and Systems (CISS), Virtual, Mar. 2020, pp. 1–5.
- [103] M. Shehab, H. Alves, and M. Latva-aho, "Effective capacity and power allocation for machine-type communication," *IEEE Transac*tions on Vehicular Technology, vol. 68, no. 4, pp. 4098–4102, April 2019.
- [104] M. Fidler and A. Rizk, "A guide to the stochastic network calculus," IEEE Communications Surveys & Tutorials, vol. 17, no. 1, pp. 92–105, 2015.
- [105] H. Al-Zubaidy, J. Liebeherr, and A. Burchard, "Network-layer performance analysis of multihop fading channels," *IEEE/ACM Trans*actions on Networking, vol. 24, no. 1, pp. 204–217, Feb. 2016.
- [106] C. Xiao, J. Zeng, W. Ni, X. Su, R. P. Liu, T. Lv, and J. Wang, "Downlink MIMO-NOMA for ultra-reliable low-latency communications," *IEEE*

- Journal on Selected Areas in Communications, vol. 37, no. 4, pp. 780–794, Apr. 2019.
- [107] M. Kountouris, N. Pappas, and A. Avranas, "QoS provisioning in large wireless networks," in 2018 16th International Symposium on Modeling and Optimization in Mobile, Ad Hoc, and Wireless Networks (WiOpt), May 2018, pp. 1–6.
- [108] M. Shehab, H. Alves, E. A. Jorswieck, E. Dosti, and M. Latva-Aho, "Effective energy efficiency of ultrareliable low-latency communication," *IEEE Internet of Things Journal*, vol. 8, no. 14, pp. 11135– 11149, Jul. 2021.
- [109] J. Zhang, X. Xu, S. Han, K. Zhang, P. Zhang, and T. Q. S. Quek, "Intelligent ultra-reliable and low latency communications: Flexibility and adaptation," *IEEE Internet of Things Journal*, pp. 1–1, 2022.
- [110] X. Zhao, W. Chen, and H. Vincent Poor, "Queue-aware finite-blocklength coding for ultra-reliable and low-latency communications: A cross-layer approach," *IEEE Transactions on Wireless Communications*, pp. 1–1, 2022.
- [111] X. Zhang, J. Wang, and H. V. Poor, "Statistical delay and error-rate bounded qos control for urllc in the non-asymptotic regime," in 2022 IEEE International Symposium on Information Theory (ISIT), 2022, pp. 2112–2117.
- [112] F. Qasmi, M. Shehab, H. Alves, and M. Latva-aho, "Effective energy efficiency and statistical QoS provisioning under Markovian arrivals and finite blocklength regime," *IEEE Internet of Things Journal*, pp. 1–1, 2022.
- [113] I. Muhammad, H. Alves, O. A. López, and M. Latvaaho, "Secure Rate Control and Statistical QoS Provisioning for Cloud-Based IoT Networks," Security and Communication Networks, vol. 2021, p. 8650272, Oct. 2021. [Online]. Available: https://doi.org/10.1155/2021/8650272
- [114] S. Kaul, M. Gruteser, V. Rai, and J. Kenney, "Minimizing age of information in vehicular networks," in 8th Annual IEEE Communications Society Conference on Sensor, Mesh and Ad Hoc Communications and Networks, 2011, pp. 350–358.
- [115] P. Popovski, F. Chiariotti, K. Huang, A. E. Kalør, M. Kountouris, N. Pappas, and B. Soret, "A perspective on time toward wireless 6G," *Proceedings of the IEEE*, vol. 110, no. 8, pp. 1116–1146, 2022.
- [116] A. Kosta, N. Pappas, and V. Angelakis, "Age of information: A new concept, metric, and tool," Foundations and Trends in Networking, Now Publishers, Inc., 2017.
- [117] M. A. Abd-Elmagid and H. S. Dhillon, "Average peak age-ofinformation minimization in UAV-assisted IoT networks," *IEEE Transactions on Vehicular Technology*, vol. 68, no. 2, pp. 2003–2008, 2019.
- [118] A. Franco, B. Landfeldt, and U. Körner, "Extended analysis of age of information threshold violations," *Computer Communications*, vol. 161, pp. 191–201, 2020. [Online]. Available: https://www.sciencedirect.com/science/article/pii/S0140366420318508
- [119] M. Haenggi, Stochastic geometry for wireless networks. Cambridge University Press, 2012.
- [120] —, "On distances in uniformly random networks," *IEEE Transactions on Information Theory*, vol. 51, no. 10, pp. 3584–3586, 2005.
- [121] H. A. Ammar, Y. Nasser, and H. Artail, "Closed form expressions for the probability density function of the interference power in PPP networks," in *IEEE International Conference on Communications (ICC)*, 2018, pp. 1–6.
- [122] J. Tang, G. Chen, and J. P. Coon, "Meta distribution of the secrecy rate in the presence of randomly located eavesdroppers," *IEEE Wireless Communications Letters*, vol. 7, no. 4, pp. 630–633, 2018.
- [123] S. Guruacharya and E. Hossain, "Approximation of meta distribution and its moments for Poisson cellular networks," *IEEE Wireless Communications Letters*, vol. 7, no. 6, pp. 1074–1077, 2018.
- [124] A. H. Sakr and E. Hossain, "Cognitive and energy harvesting-based D2D communication in cellular networks: Stochastic Geometry modeling and analysis," *IEEE Transactions on Communications*, vol. 63, no. 5, pp. 1867–1880, 2015.
- [125] H. Wei, N. Deng, W. Zhou, and M. Haenggi, "Approximate SIR analysis in general heterogeneous cellular networks," *IEEE Transactions on Communications*, vol. 64, no. 3, pp. 1259–1273, 2016.
- [126] O. L. A. López, H. Alves, P. H. Juliano Nardelli, and M. Latva-aho, "Aggregation and resource scheduling in machine-type communication networks: A Stochastic Geometry approach," *IEEE Transactions* on Wireless Communications, vol. 17, no. 7, pp. 4750–4765, 2018.
- [127] N. Deng and M. Haenggi, "The energy and rate meta distributions in wirelessly powered D2D networks," *IEEE Journal on Selected Areas* in Communications, vol. 37, no. 2, pp. 269–282, 2019.

- [128] M. M. Azari, G. Geraci, A. Garcia-Rodriguez, and S. Pollin, "UAV-to-UAV communications in cellular networks," *IEEE Transactions on Wireless Communications*, vol. 19, no. 9, pp. 6130–6144, 2020.
- [129] N. J. Mayedo Rodríguez, O. L. A. López, H. Alves, and M. Latvaaho, "On the SIR meta distribution in massive MTC networks with scheduling and data aggregation," in *IEEE 93rd Vehicular Technology Conference (VTC2021-Spring)*, 2021, pp. 1–6.
- [130] J. P. Jeyaraj and M. Haenggi, "Cox models for vehicular networks: SIR performance and equivalence," *IEEE Transactions on Wireless Communications*, vol. 20, no. 1, pp. 171–185, 2021.
- [131] A. Talgat, M. A. Kishk, and M.-S. Alouini, "Stochastic geometry-based analysis of LEO satellite communication systems," *IEEE Communi*cations Letters, vol. 25, no. 8, pp. 2458–2462, 2021.
- [132] I. S. Gradshteyn and I. M. Ryzhik, Table of integrals, series, and products. Academic press, 2014.
- [133] L. Kaufman and P. J. Rousseeuw, Finding groups in data: an introduction to cluster analysis. John Wiley & Sons, 2009, vol. 344.
- [134] A. Shahini and N. Ansari, "NOMA aided narrowband IoT for machine type communications with user clustering," *IEEE Internet of Things Journal*, vol. 6, no. 4, pp. 7183–7191, 2019.
- [135] H. Yin, D. Gesbert, M. Filippou, and Y. Liu, "A coordinated approach to channel estimation in large-scale multiple-antenna systems," *IEEE Journal on Selected Areas in Communications*, vol. 31, no. 2, pp. 264–273, 2013.
- [136] A. Adhikary, J. Nam, J.-Y. Ahn, and G. Caire, "Joint spatial division and multiplexing—the large-scale array regime," *IEEE Transactions* on *Information Theory*, vol. 59, no. 10, pp. 6441–6463, 2013.
- [137] C. Lin and M. Gerla, "Adaptive clustering for mobile wireless networks," *IEEE Journal on Selected Areas in Communications*, vol. 15, no. 7, pp. 1265–1275, 1997.
- [138] P. Kumarawadu, D. J. Dechene, M. Luccini, and A. Sauer, "Algorithms for node clustering in wireless sensor networks: A survey," in 4th International Conference on Information and Automation for Sustainability, 2008, pp. 295–300.
- [139] C. Zheng, F.-C. Zheng, J. Luo, and D. Feng, "Open-loop communications for up-link URLLC under clustered user distribution," *IEEE Transactions on Vehicular Technology*, vol. 70, no. 11, pp. 11509–11522, 2021.
- [140] O. M. Rosabal, O. L. A. López, H. Alves, R. D. Souza, and S. Montejo-Sánchez, "Massive wireless energy transfer with multiple power beacons for very large internet of things," arXiv preprint arXiv:2106.12968, 2021.
- [141] P. Orim, N. Ventura, and J. Mwangama, "Cluster-based random access scheme for 5G URLLC," in *IEEE International Conference on Advanced Networks and Telecommunications Systems (ANTS)*, 2019, pp. 1–6.
- [142] G. R. MacCartney, T. S. Rappaport, and A. Ghosh, "Base station diversity propagation measurements at 73 GHz millimeter-wave for 5G coordinated multipoint (CoMP) analysis," in *IEEE Globecom Workshops (GC Wkshps)*, 2017, pp. 1–7.
- [143] A. Lopusina, E. Kocan, and M. Pejanovic-Djurisic, "Macrodiversity for performance improvement of mmwave cellular communications," in 40th International Conference on Telecommunications and Signal Processing (TSP), 2017, pp. 174–177.
- [144] A. K. Gupta, J. G. Andrews, and R. W. Heath, "Macrodiversity in cellular networks with random blockages," *IEEE Transactions on Wireless Communications*, vol. 17, no. 2, pp. 996–1010, 2018.
- [145] A. E. Kalor, O. A. Hanna, and P. Popovski, "Random access schemes in wireless systems with correlated user activity," in 2018 IEEE 19th International Workshop on Signal Processing Advances in Wireless Communications (SPAWC), 2018, pp. 1–5.
- [146] C. Zheng, M. Egan, L. Clavier, A. E. Kalør, and P. Popovski, "Stochastic resource optimization of random access for transmitters with correlated activation," *IEEE Communications Letters*, vol. 25, no. 9, pp. 3055–3059, 2021.
- [147] J. W. Choi, B. Shim, Y. Ding, B. Rao, and D. I. Kim, "Compressed sensing for wireless communications: Useful tips and tricks," *IEEE Communications Surveys & Tutorials*, vol. 19, no. 3, pp. 1527–1550, 2017
- [148] D. Donoho, "Compressed sensing," IEEE Transactions on Information Theory, vol. 52, no. 4, pp. 1289–1306, 2006.
- [149] E. J. Candes and M. B. Wakin, "An introduction to compressive sampling," *IEEE Signal Processing Magazine*, vol. 25, no. 2, pp. 21–30, 2008.
- [150] H. Liu, B. Song, H. Qin, and Z. Qiu, "An adaptive-ADMM algorithm with support and signal value detection for compressed sensing," *IEEE Signal Processing Letters*, vol. 20, no. 4, pp. 315–318, 2013.

- [151] J. A. Tropp and A. C. Gilbert, "Signal recovery from random measurements via orthogonal matching pursuit," *IEEE Transactions on Information Theory*, vol. 53, no. 12, pp. 4655–4666, 2007.
- [152] D. L. Donoho, A. Maleki, and A. Montanari, "Message-passing algorithms for compressed sensing," PNAS, vol. 106, no. 45, pp. 18914–18919, 2009.
- [153] K. Senel and E. G. Larsson, "Grant-free massive MTC-enabled massive MIMO: A compressive sensing approach," *IEEE Transactions* on Communications, vol. 66, no. 12, pp. 6164–6175, 2018.
- [154] L. Marata, O. L. A. López, E. N. Tominaga, and H. Alves, "Joint channel estimation and device activity detection in heterogeneous networks," in 2021 29th European Signal Processing Conference (EUSIPCO), 2021, pp. 836–840.
- [155] L. Marata, O. L. A. López, H. Djelouat, M. Leinonen, H. Alves, and M. Juntti, "Joint coherent and non-coherent detection and decoding techniques for heterogeneous networks," *IEEE Transactions on Wireless Communications*, pp. 1–1, 2022.
- [156] H. Wang, A. Kosasih, C.-K. Wen, S. Jin, and W. Hardjawana, "Expectation propagation detector for extra-large scale massive MIMO," IEEE Transactions on Wireless Communications, vol. 19, no. 3, pp. 2036–2051, 2020.
- [157] C. Zhang, J. Bütepage, H. Kjellström, and S. Mandt, "Advances in variational inference," *IEEE transactions on pattern analysis and machine intelligence*, vol. 41, no. 8, pp. 2008–2026, 2018.
- [158] X. Meng, S. Wu, L. Kuang, and J. Lu, "An expectation propagation perspective on approximate message passing," *IEEE Signal Process-ing Letters*, vol. 22, no. 8, pp. 1194–1197, 2015.
- [159] J. Ahn, B. Shim, and K. B. Lee, "EP-based joint active user detection and channel estimation for massive machine-type communications," *IEEE Transactions on Communications*, vol. 67, no. 7, pp. 5178–5189, 2019.
- [160] K.-H. Ngo, M. Guillaud, A. Decurninge, S. Yang, and P. Schniter, "Multi-user detection based on expectation propagation for the non-coherent SIMO multiple access channel," *IEEE Transactions on Wireless Communications*, vol. 19, no. 9, pp. 6145–6161, 2020.
- [161] D. Zhang, X. Song, W. Wang, G. Fettweis, and X. Gao, "Unifying message passing algorithms under the framework of constrained bethe free energy minimization," *IEEE Transactions on Wireless Communications*, vol. 20, no. 7, pp. 4144–4158, 2021.
- [162] O. L. López, G. Brante, R. D. Souza, M. Juntti, and M. Latva-aho, "Coordinated pilot transmissions for detecting the signal sparsity level in a massive IoT network under Rayleigh fading," arXiv preprint arXiv:2205.00406, 2022.
- [163] H. Zhu and G. B. Giannakis, "Exploiting sparse user activity in multiuser detection," *IEEE Transactions on Communications*, vol. 59, no. 2, pp. 454–465, 2011.
- [164] B. Knoop, F. Monsees, C. Bockelmann, D. Wuebben, S. Paul, and A. Dekorsy, "Sparsity-aware successive interference cancellation with practical constraints," in 17th International ITG Workshop on Smart Antennas, 2013, pp. 1–8.
- [165] J. Ahn, B. Shim, and K. B. Lee, "Sparsity-aware ordered successive interference cancellation for massive machine-type communications," *IEEE Wireless Communications Letters*, vol. 7, no. 1, pp. 134–137, 2018.
- [166] R. B. Di Renna and R. C. d. Lamare, "Activity-aware multiple feedback SIC for massive machine-type communications," in 12th International ITG Conference on Systems, Communications and Coding, 2019, pp. 1–6.
- [167] H. Djelouat, M. Leinonen, L. Ribeiro, and M. Juntti, "Joint user identification and channel estimation via exploiting spatial channel covariance in mMTC," *IEEE Wireless Communications Letters*, vol. 10, no. 4, pp. 887–891, 2021.
- [168] O. Guéant, J.-M. Lasry, and P.-L. Lions, "Mean field games and applications," in *Paris-Princeton lectures on mathematical finance* 2010. Springer, 2011, pp. 205–266.
- [169] R. Carmona, F. Delarue et al., Probabilistic theory of mean field games with applications I-II. Springer, 2018.
- [170] M. Kamel, W. Hamouda, and A. Youssef, "Ultra-dense networks: A survey," *IEEE Communications Surveys & Tutorials*, vol. 18, no. 4, pp. 2522–2545, 2016.
- [171] S. Samarakoon, M. Bennis, W. Saad, M. Debbah, and M. Latvaaho, "Ultra dense small cell networks: Turning density into energy efficiency," *IEEE Journal on Selected Areas in Communications*, vol. 34, no. 5, pp. 1267–1280, 2016.
- [172] A. Vasiliadis, "An introduction to mean field games using probabilistic methods," arXiv preprint arXiv:1907.01411, 2019.

- [173] H. Shiri, J. Park, and M. Bennis, "Massive autonomous UAV path planning: A neural network based mean-field game theoretic approach," in *IEEE Global Communications Conference (GLOBECOM)*, 2019, pp. 1–6.
- [174] —, "Communication-efficient massive UAV online path control: Federated learning meets mean-field game theory," *IEEE Transactions on Communications*, vol. 68, no. 11, pp. 6840–6857, 2020.
- [175] Y. S. Abu-Mostafa, M. Magdon-Ismail, and H.-T. Lin, *Learning From Data*. USA: AMLbook.com, 2012.
- [176] D. E. Ruiz-Guirola, C. A. Rodríguez-López, S. Montejo-Sánchez, R. D. Souza, O. L. A. López, and H. Alves, "Energy-efficient wake-up signalling for machine-type devices based on traffic-aware long-short term memory prediction," *IEEE Internet of Things Journal*, pp. 1–1, 2022.
- [177] Y. Xu, F. Yin, W. Xu, J. Lin, and S. Cui, "Wireless traffic prediction with scalable Gaussian process: Framework, algorithms, and verification," *IEEE Journal on Selected Areas in Communications*, vol. 37, no. 6, pp. 1291–1306, Jun. 2019.
- [178] D. Ruiz-Guirola, O. L. A. López, S. Montejo-Sánchez, R. Demo Souza, and M. Bennis, "Performance analysis of ML-based MTC traffic pattern predictors," *IEEE Wireless Communications Letters (submitted)*.
- [179] T. Wang, C.-K. Wen, H. Wang, F. Gao, T. Jiang, and S. Jin, "Deep learning for wireless physical layer: Opportunities and challenges," *China Communications*, vol. 14, no. 11, pp. 92–111, Nov. 2017.
- [180] N. Kato, Z. M. Fadlullah, B. Mao, F. Tang, O. Akashi, T. Inoue, and K. Mizutani, "The deep learning vision for heterogeneous network traffic control: Proposal, challenges, and future perspective," *IEEE Wireless Communications*, vol. 24, no. 3, pp. 146–153, Jun. 2017.
- [181] J. Park, S. Samarakoon, M. Bennis, and M. Debbah, "Wireless network intelligence at the edge," *Proceedings of the IEEE*, vol. 107, no. 11, pp. 2204–2239, Nov. 2019.
- [182] S. Boyd and L. Vandenberghe, Convex Optimization. New York, NY, USA: Cambridge University Press, 2004.
- [183] E. Eldeeb, M. Shehab, and H. Alves, "A learning-based fast uplink grant for massive IoT via support vector machines and long shortterm memory," *IEEE Internet of Things Journal*, vol. 9, no. 5, pp. 3889–3898, 2022.
- [184] H. Shiri, H. Seo, J. Park, and M. Bennis, "Attention based communication and control for multi-UAV path planning," *CoRR*, vol. abs/2112.12584, 2021. [Online]. Available: https://arxiv.org/abs/2112.12584
- [185] S. Park, H. Jang, O. Simeone, and J. Kang, "Learning to demodulate from few pilots via offline and online meta-learning," *IEEE Trans*actions on Signal Processing, vol. 69, pp. 226–239, 2021.
- [186] —, "Learning how to demodulate from few pilots via metalearning," in 2019 IEEE 20th International Workshop on Signal Processing Advances in Wireless Communications (SPAWC), 2019, pp. 1–5.
- [187] J. D. Herath, A. Seetharam, and A. Ramesh, "A deep learning model for wireless channel quality prediction," in *IEEE International Conference on Communications (ICC)*, 2019, pp. 1–6.
- [188] B. Han, S. Yuan, Z. Jiang, Y. Zhu, and H. D. Schotten, "Robustness analysis of networked control systems with aging status," in *IEEE Conference on Computer Communications Workshops (INFOCOM WKSHPS)*, 2020, pp. 1360–1361.
- [189] G. White, A. Palade, and S. Clarke, "Forecasting QoS attributes using LSTM networks," in *International Joint Conference on Neural Networks (IJCNN)*, 2018, pp. 1–8.
- [190] T. Jirsik, S. Trcka, and P. Celeda, "Quality of service forecasting with LSTM neural network," in 2019 IFIP/IEEE Symposium on Integrated Network and Service Management (IM), 2019, pp. 251–260.
- [191] J. Choi, "Communication-efficient distributed SGD using preamble-based random access," CoRR, vol. abs/2105.09427, 2021. [Online]. Available: https://arxiv.org/abs/2105.09427
- [192] A. Ferdowsi, M. A. Abd-Elmagid, W. Saad, and H. S. Dhillon, "Neural combinatorial deep reinforcement learning for age-optimal joint trajectory and scheduling design in uav-assisted networks," *IEEE Journal on Selected Areas in Communications*, vol. 39, no. 5, pp. 1250–1265, 2021.
- [193] E. Eldeeb, J. D. S. Santana, D. E. Pérez, M. Shehab, H. Mahmood, Alves, "Multi-UAV and Η. Optimization Learning for Age and Power in IoT with UAV Battery Recharge," 5 2022. [Online]. Available: https://www.techrxiv.org/articles/preprint/Multi-UAV_Path_Learning_for_Age_and
- [194] C. Finn, P. Abbeel, and S. Levine, "Model-agnostic meta-learning for fast adaptation of deep networks," in *Proceedings of the 34th International Conference on Machine Learning*, ser. Proceedings

- of Machine Learning Research, D. Precup and Y. W. Teh, Eds., vol. 70. PMLR, 06–11 Aug 2017, pp. 1126–1135. [Online]. Available: https://proceedings.mlr.press/v70/finn17a.html
- [195] P. J. Brockwell and R. A. Davis, *Introduction to time series and forecasting*, 3rd ed. Switzerland: Springer, 2016.
- [196] X. Luo, L. Niu, and S. Zhang, "An algorithm for traffic flow prediction based on improved SARIMA and GA," KSCE Journal of Civil Engineering, vol. 22, no. 10, pp. 4107–4115, Oct. 2018.
- [197] N. H. Mahmood, O. L. A. López, H. Alves, and M. Latva-Aho, "A predictive interference management algorithm for URLLC in Beyond 5G networks," *IEEE Communications Letters*, vol. 25, no. 3, pp. 995– 999, Mar. 2021.
- [198] S. Zhang, Z. Kang, Z. Zhang, C. Lin, C. Wang, and J. Li, "A hybrid model for forecasting traffic flow: Using layerwise structure and markov transition matrix," *IEEE Access*, vol. 7, pp. 26002–26012, Feb. 2019.
- [199] Z. Li, S. Jiang, L. Li, and Y. Li, "Building sparse models for traffic flow prediction: an empirical comparison between statistical heuristics and geometric heuristics for Bayesian network approaches," *Trans*portmetrica B: Transport Dynamics, vol. 7, no. 1, pp. 107–123, 2019.
- [200] J. F. Schmidt, U. Schilcher, M. K. Atiq, and C. Bettstetter, "Interference prediction in wireless networks: Stochastic geometry meets recursive filtering," *IEEE Transactions on Vehicular Technology*, vol. 70, no. 3, pp. 2783–2793, Mar. 2021.
- [201] N. H. Mahmood, N. Pratas, T. H. Jacobsen, and P. E. Mogensen, "On the performance of one stage massive random access protocols in 5G systems," in *Proc. 9th International Symposium on Turbo Codes* and Iterative Information Processing, (ISTC), Brest, France, Sep. 2016, pp. 340–344.
- [202] G. Pocovi, B. Soret, K. I. Pedersen, and P. Mogensen, "MAC layer enhancements for ultra-reliable low-latency communications in cellular networks," in *IEEE International Conference on Communications Workshops (ICC Workshops)*, Paris, France, May 2017, pp. 1005–1010.
- [203] W. Huang, G. Song, H. Hong, and K. Xie, "Deep architecture for traffic flow prediction: Deep belief networks with multitask learning," *IEEE Transactions on Intelligent Transportation Systems*, vol. 15, no. 5, pp. 2191–2201, May 2014.
- [204] S. Sakib, T. Tazrin, M. M. Fouda, Z. M. Fadlullah, and N. Nasser, "A deep learning method for predictive channel assignment in beyond 5G networks," *IEEE Network*, vol. 35, no. 1, pp. 266–272, 2021.
- [205] W. Jiang and H. D. Schotten, "Neural network-based fading channel prediction: A comprehensive overview," *IEEE Access*, vol. 7, pp. 118112–118124, 2019.
- [206] L. Hu, Y. Miao, J. Yang, A. Ghoneim, M. S. Hossain, and M. Alrashoud, "IF-RANs: Intelligent traffic prediction and cognitive caching toward fog-computing-based radio access networks," *IEEE Wireless Commu*nications, vol. 27, no. 2, pp. 29–35, Apr. 2020.
- [207] W. Zhai, H. Han, L. Liu, and J. Zhao, "An LSTM-aided hybrid random access scheme for 6G machine type communication networks," 2020, arXiv:2012.13537v8.
- [208] H. Jiang, M. Cui, D. W. K. Ng, and L. Dai, "Accurate channel prediction based on transformer: Making mobility negligible," *IEEE Journal on Selected Areas in Communications*, vol. 40, no. 9, pp. 2717–2732, 2022.
- [209] Y. Wang, M. C. Vuran, and S. Goddard, "Cyber-physical systems in industrial process control," ACM Sigbed Review, vol. 5, no. 1, pp. 1–2, 2008.
- [210] W. Elghazel, J. Bahi, C. Guyeux, M. Hakem, K. Medjaher, and N. Zerhouni, "Dependability of wireless sensor networks for industrial prognostics and health management," *Computers in Industry*, vol. 68, pp. 1–15, 2015.
- [211] A. Mousavi, R. Monsefi, and V. Elvira, "Hamiltonian adaptive importance sampling," *IEEE Signal Processing Letters*, vol. 28, pp. 713–717, 2021.
- [212] Z. Wang, M. Broccardo, and J. Song, "Hamiltonian Monte Carlo methods for Subset Simulation in reliability analysis," *Structural Safety*, vol. 76, pp. 51–67, Jan. 2019.
- [213] T.-Y. Chen, N. Seshadri, and B.-Z. Shen, "Is feedback a performance equalizer of classic and modern codes?" in 2010 Information Theory and Applications Workshop (ITA), Texas, USA, Jun. 2010, pp. 1–5.
- [214] J. Östman, R. Devassy, G. Durisi, and E. G. Ström, "Short-packet transmission via variable-length codes in the presence of noisy stop feedback," *IEEE Transactions on Wireless Communications*, vol. 20, no. 1, pp. 214–227, 2021.
- [215] J. C. Dunn, "A fuzzy relative of the ISODATA process and its use in detecting compact well-separated clusters," 1973.

[216] J. C. Bezdek, Pattern recognition with fuzzy objective function algorithms. Springer Science & Business Media, 2013.